FIZIOLOGIA
physiology

ACCREDITED BY CNCSIS - B+CATEGORY ■ CODE 240
http://www.ebscohost.com/titleLists/a9h-journals.pdf

Fiziologia (Physiology) is issued quarterly
Printed at Editura **EUROSTAMPA**
www.eurostampa.ro
Bd. Revoluției din 1989 nr. 26, Timișoara
Tel/fax: 0256-204816
ISSN 1223-2076

Instructions to Authors

Submission: Only original papers in English are considered and should be sent to the following address: carmen.tatu@umft.ro

Manuscripts should be submitted by e-mail only, written in Microsoft Word 97 or later versions.

Conditions: AII manuscripts are subject to editorial review. Manuscripts are received with the explicit understanding that they are not under simultaneous consideration by any other publication. Submission of an article for publication implies the transfer of the Copyright from the author the publisher upon acceptance. Accepted papers become the permanent property of "Fiziologia" (Physiology) and may not be reproduced by any means, in-whole or in part, without the written consent of the publisher. It is the author's responsibility to obtain permission to reproduce illustrations, tables, etc. from other publications.

Arrangement:

Title page: The first of each paper should indicate the title, the authors' names and their affiliation(s). A short title for use as running head is also required.

Keywords: for indexing purposes, a list of 3-5 keywords in English and Romanian is essential.

Corresponding author: Indicate the full name, the email address and the phone number.

Abstract: Each paper needs abstract and title in Romanian and English language, fonts size 9, Arial Narrow.

Body text: fonts size 10, Arial Narrow.

Small type: Paragraphs which can or must be set in smaller type (case histories, test methods, etc.) should be indicated with a „p" (petit) in the margin on the left-hand side.

Footnotes: Avoid footnotes. When essential, they are numbered consecutively and typed at the foot of the appropriate page, fonts size 8, Arial Narrow.

Tables and illustrations: Tables (numbered in Roman numerals) and illustrations (numbered in Arabic numerals) should be prepared on separate sheets, fonts size 9, Arial Narrow. Tables require a heading, and figures a legend, also prepared on a separate sheet. For the reproduction of illustrations, only good drawings and original photographs can be accepted; negatives or photocopies cannot be used. When possible, group several illustrations on one block for reproduction (max. size 140x188 mm) or provide crop marks. On the back of each illustration indicate its number, the author's name, and article title.

References: In the text identify references by Arabic figures, (in brackets), fonts size 9, Arial Narrow. Material submitted for publication but not yet accepted should be noted as "unpublished data" and not be included in the reference list. The list of references should include only those publications which are cited in the text. The references should be numbered and arranged alphabetically by the authors' names. The surnames of the authors followed by initials should be given. There should be no punctuation signs other than a comma to separate the authors. When there are more than 3 authors, the names of the 3 only are used, followed by "et al" abbreviate journal names according to the Index Medicus system. (also see International Committee of Medical Journal Editors: Uniform Requirements for manuscripts submitted to biomedical journals. Ann Intern Med 1982; 96: 766-771).

Examples:

(a) Papers published in periodicals: Kauffman HF, van der Heide S, Beaumont F, et al: Class-specific antibody determination against Aspergillus fumigatus by mean of the enzyme-linked immunosorbent assay. III. Comparative study: IgG, IgA, IgM, ELISA titers, precipitating antibodies and IGE biding after fractionation of the antigen. Int Arch Allergy Appl Immunol 1986; 80:300 - 306.

(b) Monographs; Matthews DE, Farewell VT: *Using and Understanding Medical Statistics.* Basel, Karger, 1985.

(c) Edited books: Hardy WD Jr, Essex *M:.FeLV-inducted feline acquiredimmunedeficiencysyndrome:AmodelforhumanAIDS;* in Klein E(ed): Acquired Immunodeficiency Syndrome. Prag Allergy, Busel, Karger, 1986, vol 37,353 - 376.

Galley proofs: unless indicated otherwise, galley proofs are sent to the first-named author and should be returned with the least possible delay. Alternations made in galley proofs, other than the corrections of printer's errors, are charged to the author. No page proofs are supplied.

CUPRINS

CONTENTS

THE ROLES OF INSULIN IN GLUCOSE HOMEOSTASIS AT THE NEURONAL AND ASTROCYTARY LEVEL

MATEI DANIELA MARIANA
University of Oradea, Faculty of Medicine and Pharmacy, Department of Preclinical Disciplines

ABSTRACT

The identification of insulin receptors on the plasma membrane of brain cells is unequivocal evidence that insulin acts in the brain, performing functions related to brain energy metabolism, but not only. Insulin could facilitate the coupling of cerebral blood flow with the level of neuronal activity, the expression of some neuronal and astrocytic glucose transporters, the uptake of glucose and its storage as glycogen, and the normal functioning of mitochondria in these cells. The aim of this work is to analyze aspects regarding the crossing of the blood brain barrier by glucose and insulin, the energy substrate used by neurons and astrocytes in resting and activated conditions, the effect of blood glucose concentration on glucose transporters, insulin, the insulin receptor and energy metabolism of the brain. From this perspective, disturbances observed in diseases associated with brain insulin resistance, such as type 2 diabetes mellitus and Alzheimer`s disease, will be highlighted.

Keywords: glucose transporters, insulin, astrocytes, energy metabolism, diabetes mellitus.

INTRODUCTION

Glial cells (GCs) represent a heterogeneous cell population in the nervous system, which, in addition to the structural role of supporting nerve cells and fibers, influence their metabolism and functioning, creating a microenvironment that allows the normal development of neuronal activity. A type of GC is the astrocyte. It participates in the formation of the blood-brain barrier (BBB). This barrier consists of tightly connected endothelial cells, the basement membrane of cerebral capillaries, pericytes and the foot processes of astrocytes [1]. Being located between blood vessels and neurons, astrocytes couple the delivery of blood-supplied nutrients with the neurons' required energy level [2-5]. One of the nutrients is glucose, which is the principal fuel needed by the brain`s energy metabolism [2, 4, 6-8]. Additionally, the brain can use lactate [4, 6, 9-11], mainly when its blood level is elevated, as in strenuous exercise, ketone bodies [4, 6, 9-11] derived from fat catabolism, stimulated during long-term starvation, and fatty acids [9,11].

Under normal living conditions, the concentration of glucose in the blood is tightly regulated to enable neurons to be continuously supplied with an adequate amount of glucose per unit time. Too much glucose or depriving the nervous system of glucose adversely affects neurons and GCs [12]. Hyperglycemia causes glucose neurotoxicity [13-15], either directly damaging neurons or indirectly via GCs [13], whereas hypoglycemia ultimately leads to neuronal death.

ENDOTHELIAL, NEURONAL AND ASTROCYTIC GLUCOSE TRANSPORTERS

Meeting the energy demands of neurons requires the passage of glucose into the brain parenchyma and close cooperation between neurons and astrocytes [4, 11, 16, 17]. Glucose is absorbed from the bloodstream by the endothelial cells of the brain`s microvessels. Facilitated diffusion occurs via the glucose transporter (GLUT) 1 which has been identified in endothelial cells of the human BBB and other mammalian species [18-20]. GLUT1 has an essential role in providing glucose to the brain, even though it is not the only type of GLUT expressed by the endothelium [20-23]. GLUT1 is located both in the luminal and abluminal membrane of vascular endothelial cells and in intracellular vesicles [20, 22, 24]. The transporter is asymmetrically distributed between these compartments in a proportion that varies with the species analyzed and the method used for its identification [7, 20, 22]. GLUT1 from the intracellular pool could be recruited to the luminal surface of endothelial cells to increase glucose uptake when neuronal energy needs are high [24].

Normally, the concentration of glucose in the blood perfusing the brain is higher than its concentration in the brain`s interstitial fluid [22, 25]. This concentration gradient causes the movement of glucose to the brain cells [25]. It is assumed that the largest fraction of blood glucose is taken up by astrocytes and only a small amount reaches the interstitial space directly [22]. From the interstitial fluid of the brain, glucose is transported into neurons by GLUT3 [7, 21, 22, 24], the main GLUT expressed by these cells [22, 26, 27]. GLUT3 has a low Michaelis-Menten constant that facilitates neuronal glucose uptake even when the extracellular glucose concentration is reduced [7, 22]. Another isoform of GLUT, namely GLUT4, has been identified in neuronal populations associated with high energy expenditure [26, 27] and cognitive behavior [28]. Its distribution appears to be related to that of the insulin receptor (IR) [7, 22, 26, 29], suggesting that GLUT4 is an insulin-sensitive transporter [7, 28-30] that is regulated by insulin [7, 26, 28]. GLUT4 provides neurons with an extra amount of glucose during periods of high energy demand, supplementing the glucose taken up by GLUT3 [22, 26, 28], whose expression is considered not to be significantly influenced by neuronal activity [22, 31], although in a study [32] on cultured cortical and hippocampal neurons, synaptic activation was proven to increase GLUT3 translocation to the neuronal plasma membrane and glucose transport into neurons [32]. Increased synaptic transmission has also been shown to induce insertion of GLUT4 into the presynaptic plasma membrane [29, 31, 33], and ablation of GLUT4 resulted in cessation of synaptic vesicle recycling during sustained neuronal

firing [31]. GLUT4 has been identified in the rat hippocampus [26, 29, 31]. Impaired translocation of GLUT4 to the plasma membrane of neurons might be a consequence of hippocampal insulin resistance and a cause of cognitive dysfunctions in type 2 diabetes mellitus (DM) and Alzheimer`s disease (AD) [26, 28, 34].

GLUT1 and GLUT3 have a heterogeneous distribution in the rat brain [7]. A direct correlation has been found between resting blood flow in different brain areas, capillary density in those areas, and local density of GLUTs [7]. GLUT1 and GLUT3 density also positively correlates with local cerebral glucose utilization [7, 35] and conversely, glucose utilization in a particular part of the brain influences the density of the two GLUTs in that brain structure [7]. Local glucose utilization was unchanged in acute hyperglycemia, but increased in chronic hyperglycemia (3 weeks) experimentally induced in rats by intraperitoneal injection of streptozotocin compared with normoglycemic control animals [35].

In conditions of chronic hypoglycemia or hyperglycemia, GLUT density can change [7, 15]. Studies in rat brain evidenced an increase in GLUT3 density in hypoglycemia [7, 36], but no change in GLUT1 density [7], and a moderate downregulation of GLUT1 in hyperglycemia [7, 35]. Other studies observed an upregulation of GLUT1 and increased expression of GLUT1 mRNA in chronic hypoglycemia in rats [19, 37], without changing the level of GLUT3 mRNA or GLUT3 protein [19]. The level of glycemia may be the main factor determining the expression of GLUT1 mRNA and GLUT3 mRNA and the level of GLUT1 and GLUT3 proteins in the brain [15]. It was unveiled that the expression of GLUT1 and GLUT3 was more reduced in diabetic rats compared to normal control rats and this was not due to lower cerebral microvessel density in diabetic rats [15]. Decreasing blood glucose by insulin administration may correct and reverse abnormal GLUTs expression in the brain [15].

The downregulation of GLUT1 and GLUT3 expression in chronic hyperglycemia might be an adaptive and protective reaction of the BBB endothelium and neurons to prevent their damage by intracellular glucose accumulation [15, 21], while the stimulation of the gene expression of the two GLUTs in chronic hypoglycemia [21] and upregulation of GLUT1 and GLUT3 have the role to enhance glucose uptake, providing the energy substrate necessary for cell metabolism [15]. Although it has been stated in many studies that glucose transport via GLUT1 and GLUT3 is insulin-independent [13, 38-41] and the gene expression of these two brain GLUTs is not regulated by insulin [15], others consider that GLUT3 is an insulin-sensitive transporter whose activity is modulated by insulin [30, 42]. Clarification of this aspect through future research is crucial to understanding the role of insulin in glucose delivery to the brain cells.

Endothelial cells of the BBB directly transfer glucose to astrocytes. GLUTs expressed on the pericapillary processes of astrocytes carry glucose across the cell membrane. Morgello et al. [18] identified by immunoelectron microscopy the presence of GLUT1 in the foot processes of astrocytes surrounding gray matter blood vessels and synapses in the human brain [18]. As a peculiarity, GLUT1 of perivascular astrocytic endfeet is not structurally identical to GLUT1 of BBB endothelial cells. The latter is glycosylated and has a higher molecular weight (55 KDa versus 45 KDa) [7, 18-20]. GLUT1 is more expressed in astrocytes than in BBB endothelium [19, 43]. In addition to the high expression of GLUT1, human astrocytes significantly express GLUT3, very little GLUT2, and only traces of GLUT4 [22, 44]. GLUT1 and GLUT3 are insulin-independent transporters [39, 40, 44], whereas GLUT4 is insulin-dependent [22, 44]. However, in rats, immunoflourescence analysis of cortical astrocyte culture and astrocytes co-cultured with neurons obtained from the cerebellum and cerebral cortex did not identify GLUT3, but only GLUT1 [45].

When GLUT mRNA content was compared between human astrocytes, myotubes and adipocytes, the determination showed that the amount of GLUT1 mRNA and GLUT2 mRNA was higher in astrocytes than in myotubes or adipocytes, while GLUT3 mRNA content was found at comparable values to those in myotubes and adipocytes [44]. Human astrocytic GLUT3 has a high affinity for glucose and was detected by Heni and co-workers even under basal conditions [44]. Therefore, they considered that GLUT3 might have an important role in astrocytic glucose uptake [44].

While ablation of GLUT1 in BBB endothelial cells causes changes in brain vasculature and BBB integrity [46, 47], ablation of astrocyte GLUT1 in mice was not followed by altered vascular morphology nor leakage of serum proteins (Immunoglobulin G and fibrin) from blood vessels, suggesting preservation of BBB integrity [46]. Astrocytes with GLUT1 ablation present structural changes characterized by increased branching of the processes, but without their elongation [46]. Hyperglycemia can promote structural alterations in astrocytes as well. Exposure to high glucose concentration (25 mM) of primary cultured astrocytes was followed by irreversible inhibition of proliferation and modification of their morphology, with a flat appearance and fewer processes compared to astrocytes cultured in normal glucose medium [13]. Their viability was also significantly reduced by hyperglycemic conditions compared to culture in a normoglycemic medium (5.5 mM) [13]. As a consequence, in DM, inhibition of astrocyte proliferation is a disadvantage in the reconstruction process after brain damage [13]. Insulin was proved to stimulate the proliferation of cultured human astrocytes [44].

Research in mice overexpressing amyloid β-peptide (Aβ) precursor protein showed that GLUT1 deletion in the endothelium results in diminished BBB glucose transport, BBB disruption, capillary degeneration, reduced cerebral microvasculature and perfusion, and Aβ accumulation that contributed to neuronal dysfunction and neuronal loss [47]. Reduced expression of GLUT1 and GLUT3 in the cerebral cortex and other brain regions has been observed in AD patients, leading to lower glucose uptake and brain energy metabolism [22, 23, 30, 48] and, eventually, to neuronal degeneration [27, 30]. The decrease in the concentration of GLUT3 in the cortex of these subjects was greater than that of GLUT1 and than the loss of

synapses [48].

ENDOTHELIAL, NEURONAL AND ASTROCYTIC INSULIN RECEPTOR

In addition to GLUTs, the cell membrane of astrocytes and neurons exhibits IR [39]. Expression of IR on mouse astrocytes was demonstrated by Fernandez et al. [3], who, using IR immunogold labeling combined with electron microscopy, located them in astrocytic endfeet ensheating the endothelial cells of the BBB [3]. The authors also uncovered that the interaction of insulin with its receptor in astrocytes is responsible for coupling brain glucose uptake with blood flow to sustain brain activity and that brain insulin resistance uncouples this process [3]. Immunoreactive IR deposits were also found in the endothelial cells of BBB capillaries [3]. Leclerc et al. [49] revealed that in humans and animals (murines), cerebral IRs, especially the isoform B of IR, are more concentrated in microvessels than in the brain parenchyma [49].

Human astrocytes express IRs as well, quantitatively similar to myotubes [44]. Approximately two-thirds of human astrocyte IR is in the isoform A and one-third in the isoform B [44]. According to other determinations, the predominant isoform of human astrocytic IR is isoform B [39, 50, 51]. Studies in mice with astrocyte IR ablation (GFAP-IR KO mice) highlighted the role of astrocyte IR and insulin signaling for adequate glucose and insulin transport into the brain [43]. Neurons express only the isoform A of IR [28, 39, 50-52], characterized by a high binding affinity for insulin and the ability to be stimulated by low concentrations of insulin-like growth factor II (IGF-II) [28, 52]. Neurons have a higher IR density compared to astrocytes [52, 53]. Immunochemical methods demonstrated that in the rat brain, neuronal IRs are concentrated at synapses [54], both in presynaptic and postsynaptic plasma membranes [51], and IR is a component of postsynaptic density fractions [54]. IR is also localized in nonsynaptic areas of dendrites [54].

Although there are still uncertainties regarding the pathway through which circulating insulin reaches the brain interstitial fluid, probably either crossing the BBB or via the cerebrospinal fluid [38-40, 55], Gray and co-workers [56] showed that the passage of insulin from the bloodstream to astrocytes occurs by crossing the endothelial cells of the BBB [56]. The process of transcytosis has been evidenced in cultured human and rat brain endothelial cells, uncovering that at physiological concentrations of insulin, its uptake is an IR-specific, vesicle-mediated transport [56]. Anyway, tight junctions between BBB endothelial cells prohibit paracellular transport of insulin [38], except in non-BBB zones of the brain with fenestrated capillaries, such as those in the circumventricular organs [39, 55]. Furthermore, the authors [56] observed that insulin transcytosis increased when astrocytes were stimulated with L-glutamate and decreased by inhibiting nitric oxide synthase (NOS), from which it follows that astrocytes could regulate the passage of insulin across the BBB [56]. In IR-deficient astrocyte mice, injection of digoxigenin-labeled insulin into the carotid artery was not followed by its passage into the brain parenchyma, but was retained in the BBB endothelium [3].

A previous study on microvessels obtained from autopsied brains showed that microvessels bind insulin with high affinity, internalize it, and transport it into the medium [57]. However, it has been demonstrated in two models, one genetic (mice with endothelial-specific loss of the signaling-related IR) and one pharmacological (utilization of a selective antagonist of IR – S961), that insulin can also be transported across the BBB *in vivo,* independent of endothelial cell signaling-related IRs, albeit the amount of insulin bound to the endothelium was lower [58]. This research [58] indicates that there might be other protein or proteins involved in the transport of insulin across the BBB and suggests that signaling-related IR is not the only mechanism for insulin to pass through the BBB into the brain interstitium [58]. Consequently, it is incompletely understood whether IR at the BBB endothelium only binds insulin and acts as a receptor, or whether it also mediates insulin transport through the cytoplasm of endothelial cells [49, 58]. Nonetheless, an animal study provided evidence that IR at the BBB acts as a receptor, not as a transporter, and circulating insulin interacts with IR at the luminal membrane of BBB vessels [49].

The source of insulin in the brain is most likely peripheral insulin secreted by the pancreas [39, 40, 56, 59]. Recently, it has been indicated that insulin is also produced by the brain [22, 40, 60, 61]. Insulin influences the BBB transport of other molecules, as well as its own transport rate [25, 59]. There are differences in insulin uptake between brain regions and between the brain and spinal cord [25]. The rate of insulin transport across the BBB is influenced by many factors, including blood glucose level [25].

The rate of insulin transport into the brain is altered in DM [59, 62] and AD [25, 49, 59]. Studies on the brain of patients who died of AD revealed that, compared to age-matched controls, IR and IGF-I receptor expression was decreased in several brain structures [39, 63, 64]. Moreover, this abnormality has been associated with impaired insulin and IGF-I and IGF-II signaling mechanism, decreased IR substrate mRNA level, and expression of genes encoding insulin, IGF-I and IGF-II [63]. Research in human and animal models of AD showed that there is an alteration in vascular IR-mediated response in this disease and that defects and low level of endothelial IR contribute to insulin resistance in AD [49].

GLYCATION OF INSULIN AND THE INSULIN RECEPTOR

Under hyperglycemic conditions, both insulin [65, 66] and IR can be glycated [65]. This interferes with the binding of insulin to its receptor and may lead to insulin resistance [65-68]. IR shares identical amino acid sequences with insulin and binds glucose like insulin [65]. Several glucose binding sites have been identified, located on both the A and B chains of insulin [65, 67]. The experiment conducted by Rhinesmith et al. [65], showed that insulin glycation is a two-step process, with an initial,

very rapid glycation in the first few hours after exposure to high glucose levels (above 20 mM), followed by a slower glycation over several days [65]. The same authors [65], working on IR-derived peptides, uncovered their rapid glycation [65]. Interestingly, the process was not observed for lower (5 mM) glucose concentrations, but only for hyperglycemic levels [65].

High glucose is associated with glycation of the insulin-binding insulin-like regions of the IR, and this, in addition to glycation of insulin itself, can cause *in vivo* a decrease in the binding affinity of insulin to its receptor and a significant reduction in IR activation [65], effects that have also been observed in other research [67, 68]. The molecular dynamics study of glycated insulin showed that the glycation process of insulin results in conformational changes of the insulin B-chain, with the transition from the open to the close conformation, the alteration in the secondary structure of insulin, the impairment of its binding to the IR and signaling transduction [66]. IR glycation might have long-term consequences because the turnover of glycated IR is slower, of weeks or months [65]. Aside from insulin and IR, enzymes [68] and plasma proteins can be glycated [65, 67].

The presence of glycated insulin has been evidenced in human plasma from patients with type 2 DM and that glycated insulin has a much lower ability to decrease glycemia in normal subjects compared to physiological concentrations of native insulin [68]. The study carried out by Walke et al. [67], which aimed to evaluate the effect of insulin and glycated insulin on both IR and receptor for advanced glycation end-products (RAGE) signaling in Chinese hamster ovary cells (CHO-IR-GLUT4) showed that treatment of these cells with glycated insulin had several consequences, such as impaired insulin signaling and translocation of GLUT4 to the cell membrane, reduced binding affinity of insulin to IR but increased binding affinity to RAGE, activation of RAGE signaling, increased production of reactive oxygen species (ROS) and a higher level of cell death compared to cells treated with nonglycated insulin [67]. These changes can ultimately determine increased insulin resistance, decreased glucose uptake by cells, and cytotoxicity [67].

By stimulating ROS production and apoptosis, glycated insulin causes BBB damage, leading to a reduction in the number of astrocytes and alteration of tight junctions [67]. On the other hand, there is evidence that AGEs promote cerebral small vessel dysfunction that affects cerebral perfusion and causes neuronal disturbances and cognitive alterations in type 2 DM patients [69, 70]. Hyperglycemia is associated with overproduction of AGEs which in turn stimulate ROS production by increasing NADPH oxidase activity [71]. This enzyme is a considerable source of ROS (superoxide) in cerebral blood vessels, neurons and GCs [72].

Brain insulin resistance has been shown in type 2 DM and AD [30, 39, 64, 73]. Type 2 DM is widely recognized as a risk factor for AD [14, 64, 73-75]. Peripheral insulin resistance in type 2 DM is also implicated in impaired BBB functionality [71]. Hyperinsulinemia causes downregulation of endothelial IR and decreased BBB permeability to insulin [71]. However, increased BBB permeability was evidenced in a study of type 2 DM patients compared to age-matched healthy controls [74]. BBB dysfunction was assessed by gadolinium magnetic resonance imaging [74].

Another element that is affected in type 2 DM and AD is the brain insulin-phosphoinositide 3-kinase (PI3K)-protein kinase B (Akt) signaling pathway [63, 71, 75]. The level and activity of the components of this signaling pathway were investigated in samples of frontal cortices obtained postmortem from patients with these diseases and controls [75]. They were significantly reduced in both type 2 DM and AD brains compared to the age-matched control brains [75]. In most cases, the decrease was greater in brain samples from patients with type 2 DM than in those from patients with AD, and the greatest reduction was noticed in the brains of patients who had both type 2 DM and AD [75]. Downregulation of components of the insulin-PI3K-AKT signaling pathway in the brain of individuals with type 2 DM is a finding that supports the existence of brain insulin resistance and that type 2 DM, through this alteration, may increase the risk of AD [64, 75].

NEUROVASCULAR COUPLING AND THE EFFECT OF INSULIN ON THIS PROCESS

Astrocytes have a very important role in coupling the level of neuronal activity with focal cerebral blood flow, the so-called neurovascular coupling or functional hyperemia [3-5, 12, 76, 77]. The aim of this process is to ensure that the brain regions that are highly functionally active will receive a commensurate amount of oxygen and fuel when activated [77-79]. Neurovascular coupling requires precise coordination between neurons, astrocytes, and vascular wall cells [69, 79]. This process is subject to change during development, correlated with the maturation of the anatomical elements that make up the neurovascular unit of the brain [76].

Several explanations have been proposed to decipher the underlying mechanism of neurovascular coupling [5, 76, 80]. It was initially thought that the decrease in energy substrate and oxygen supply to the brain or the accumulation of waste products derived from neuronal metabolism causes vasodilation to improve blood flow and to compensate for the lack of ATP and to remove byproducts and heat, but these mechanisms could not entirely explain the response of the vasculature to the change in neuronal activity [5, 12, 76, 78]. Lin et al. [81], in research investigating activation-induced hyperemia by visual stimulation in healthy human subjects, showed that the increase in cerebral blood flow triggered by neuronal activation was large and negatively correlated with the percentage change in cerebral metabolic rate of oxygen, instead, neuronal activation caused a small increase in ATP production [81]. The authors found that there is a disproportion between the hyperemic response and energy demand, the latter increasing much less than the hyperemic response, leading them to infer that the augmentation in cerebral blood flow secondary to neuronal activation is not mediated by oxygen demand [81]. This observation may also support the idea that neurovascular coupling could be regulated by a feedforward neurotransmitter-mediated mechanism [12], not by a negative feedback mechanism driven by energy demand, because in the case of negative feedback

regulation, the increase in energy supply does not exceed the increase in energy consumption [12].

Information from studies investigating this issue has found that neurovascular coupling is very rapid, with the change in blood flow occurring within less than a second [80, 82] or within a few seconds [77, 78, 83] of the onset of neuronal activation, too early to allow the accumulation of byproducts, and encompassing areas from hundreds of microns to millimeters away from the center of the activated focus [80]. Since activation of both excitatory and inhibitory neurons in the brain causes increased local blood flow [12, 69, 84, 85], it has been challenging to establish which type of neurons can trigger neurovascular coupling and whether neurons signal directly to smooth muscle cells in the arteriolar wall to dilate or do so indirectly through other cell types [12, 80]. One possibility is that neurons first signal to astrocytes and then these cells signal to smooth muscle cells to relax and alter blood flow [12, 78-80, 83, 86]. The other scenario is that neurons signal directly to microvessels [12, 70, 87]. There is evidence that, at least in the hippocampus, the connection between neurons and blood vessels is made directly by NO, released from active glutamatergic neurons, which diffuses into the blood vessels and causes them to dilate [70, 87].

The outer surface of capillaries and arterioles in the BBB is almost completely covered by perivascular astrocytic endfeet, while the perisynaptic processes of astrocytes enwrap neuronal synapses. This architectural organization makes astrocytes an ideal relay for transmitting signals related to changes in neuronal activity to blood vessels [5, 11, 76-78, 80]. *In vivo* and *in vitro* studies have shown that increase in astrocyte Ca^{2+} concentration as a result of neuronal activation determines the release of a variety of astrocytic vasoactive agents that can trigger arteriolar relaxation and enhance cerebral blood flow [4, 12, 78, 79]. In support of this observation is a study [86] performed on rat cortical slices showing that inhibition of the astrocytic increase in Ca^{2+} concentration mediated by glutamate release causes a decrease in activity-induced hyperemia [86].

Takano et al. [83] observed that cortical astrocytes in the somatosensory cortex of adult mice respond to photolysis of caged Ca^{2+} in astrocytic processes covering the blood vessel wall by a marked increase in blood flow [83]. The latency of this response was only 1 - 2 seconds, and vasodilation was blocked by indomethacin and a cyclooxygenase-1 inhibitor SC-560 [83]. Another *in vivo* study [82] turned out that in the primary somatosensory cortex of mice there is a subset of astrocytes that present short-latency Ca^{2+} responses to sensory stimulation [82]. The peak of Ca^{2+} elevation was recorded within 0.5 seconds after stimulation [82]. This short latency is consistent with astrocyte modulation of the hyperemic response to neuronal activation [82]. However, other experimental data collected from awake mice showed that functional hyperemia is a bimodal phenomenon, with an early and a late phase [79]. The authors considered that astrocyte Ca^{2+} does not initiate or mediate functional hyperemia when neuronal activation is of short-lived (less than 5 seconds), but amplifies it when neuronal activation is prolonged (30 seconds) [79]. Therefore, astrocytic Ca^{2+} might be involved in augmenting cerebral blood flow when neuronal activation is sustained [79].

One hypothesis regarding local blood flow regulation by astrocytes posits that this occurs through activation of metabotropic glutamate receptors on astrocyte foot processes ensheating synapses [4, 5, 69, 86]. These receptors bind glutamate released into the synaptic cleft during neuronal firing and cause an increase in intraastrocytic Ca^{2+} concentration, followed by stimulation of cytosolic phospholipase A2 and release of arachidonic acid [4, 5, 12, 86, 88]. Further, from this compound, vasodilator agents are generated, either via the cyclooxygenase pathway, such as prostaglandin E2 (PGE2), or via the epoxygenase pathway, such as epoxyeicosatrienoic acids (EETs), which cause smooth muscle relaxation in the wall of arterioles located near the active neurons [4, 5, 12, 76, 86, 88].

The level of neuronal activity and oxygen tension influence the tone of cerebral blood vessels [12, 88]. Studies in rat brain slices have shown that neuronal activation causes relaxation of blood vessels when oxygen tension is low and vasoconstriction when the oxygen level is high [4, 88]. It is hypothesized that when oxygen supply is increased or when it is not consumed quickly because neurons are not activated in certain regions of the brain, arachidonic acid from astrocytes diffuses into arteriolar smooth muscle cells where it is converted to a vasoconstrictor metabolite, 20-hydroxyeicosatetraenoic acid (20-HETE), reducing cerebral blood flow in less active foci [4, 5, 12, 76, 88]. Under low oxygen conditions, increased astrocyte glycolysis results in increased production of lactate [88, 89, 90] and adenosine [88]. Lactate causes vasodilation by inhibiting the prostaglandin transporter in astrocytes and thereby increases the local level of PGE_2 [4, 88], while adenosine inhibits the vasoconstrictor effect of 20-HETE on smooth muscle in the arteriolar wall [4, 88].

Apart from metabotropic receptor activation, glutamate in the synaptic cleft is co-transported with Na^+ into astrocyte foot processes [89, 91] where it stimulates glucose uptake and utilization and production of lactate [5, 77, 88, 89, 91]. Glutamate release from active synapses and its uptake by astrocytes may represent a signaling mechanism that couples neuronal activity to the stimulation of astrocytic glycolysis, as demonstrated in primary culture of mouse cerebral cortical astrocytes [89].

Another vasoactive substance that participates in the regulation of neurovascular coupling is NO [12, 70, 87]. This compound is synthesized and released by neurons in the hippocampus and acts on vascular smooth muscle, having an important role in regulation of blood flow in this structure [70, 87]. Glutamate released by active neurons binds to the postsynaptic N-methyl-D-aspartate (NMDA)-glutamate receptor, elevates intracellular Ca^{2+} concentration and activates neuronal NOS (nNOS), which catalyzes the convertion of L-Arginine to NO [12, 87]. NO diffuses through the interstitial fluid to the smooth muscle cells in the microvessel wall, where it stimulates guanylate cyclase to convert GTP to cGMP, thereby increasing local blood flow and oxygen amount [12, 87]. A transient increase in NO concentration induced by glutamate release

causes a synergistic transient increase in time, space, and amplitude with local cerebral blood flow in the rat hippocampus seconds later [87]. Administration of the NOS inhibitor (N^G-monomethyl-l-arginine) in humans substantially reduced the neurovascular coupling response, demonstrating that NO is a key messenger involved in this process [92].

Increased intracellular Ca^{2+} concentration in neurons can also activate phospholipase A2 and release arachidonic acid, which is subsequently converted to a vasodilator prostaglandin (PG) by cyclooxygenase 2 [12]. Thus, through the convergent action of NO and PG, blood vessel tone decreases [12]. It is possible that *in vivo,* both neurons and astrocytes intervene in the control of cerebral blood flow by releasing different vasoactive compounds through various pathways, between which could be interactions, but the importance of these agents in mediating neurovascular coupling may be variable from a region to another of the brain [12].

The role of insulin and IR in the regulation of neurovascular coupling [3, 8] and the fact that this process might be altered in type 2 DM [69, 70, 93] is beginning to be increasingly investigated. Ablation of astrocytic IR in mice results in mitochondrial dysfunction and elevated ROS that trigger hypoxia-inducible factor-1α activation and angiogenesis [3]. These disturbances were corrected by treatment with N-acetylcysteine, an antioxidant substance [3]. Astrocyte IR can regulate neurovascular coupling by influencing glucose uptake and brain vascularity [3]. Disruption of neurovascular coupling in patients with type 2 DM was demonstrated by functional magnetic resonance imaging [93]. Compared to healthy controls, type 2 DM patients showed lower neurovascular coupling in several brain regions (hippocampus, putamen, amygdala), related to memory, emotions and movements [93].

Impairment of neurovascular coupling in type 2 DM is the result of reduced bioavailability of NO secondary to oxidative stress in the brain microvasculature [70]. Altered neurovascular coupling in the hippocampus, a potential causative element of cognitive disturbance in type 2 diabetic rats was tested in a study using a rat model (Goto-Kakizaki rats) that spontaneously develops DM [70]. Measurement of NO concentration and change in cerebral blood flow in the hippocampus in response to glutamatergic stimulation of diabetic and control animals evidenced that in both groups stimulation caused a transient increase in NO concentration coupled in time and space to a transient increase in cerebral blood flow, but in diabetic animals, the amount of NO and the hemodynamic response to the same stimulus were lower compared to controls [70].

Maladjustment of cerebral perfusion to brain activity, particularly in the hippocampus, contributes to neuronal disturbances and cognitive alterations in type 2 DM [69, 70] and AD [5, 12, 94]. Increased levels of ROS and reactive nitrogen species (RNS) alter nNOS activity and function [95] and inhibit the production of vasodilator messengers [12, 85, 95]. This leads to brain hypoperfusion in patients with type 2 DM [69] and AD [12, 85, 94]. The reduction of functional hyperemia is probably the result of ROS production by the cerebral microvessels that occurs from the early stages of AD [94]. The correlation was demonstrated in mice overexpressing amyloid precursor protein [85, 94]. These animals developed oxidative stress in cerebral blood vessels long before the appearance of oxidative stress in neurons and GCs [94]. The effect of reducing cerebral blood flow in response to activation of the somatosensory cortex by whisker stimulation was prevented by ROS scavengers, indicating that oxidative stress contributes to the decrease in functional hyperemia [94]. AGEs impair neurovascular coupling and promote cognitive alterations in type 2 DM [93]. Neurovascular uncoupling in type 2 DM may occur as a result of microvessel dysfunction driven by hyperglycemia-induced oxidative stress [96].

THE INFLUENCE OF INSULIN AND GLUCOSE CONCENTRATION ON GLUCOSE UPTAKE BY ASTROCYTES AND NEURONS

The role of insulin in glucose uptake by astrocytes and neurons is not fully established. The results, sometimes divergent, of the studies that have focused on this issue could be explained by the fact that the studies were not carried out under the same conditions, being either *in vivo* or *in vitro* studies on different animal species or cell cultures, with a different density and distribution of GLUTs, using glucose or glucose analogs in different concentrations and under stimulation of neural activity or under resting conditions. Besides, there might be regional differences in insulin sensitivity on glucose uptake, and some structures in the brain might be able to use different energy substrates, especially during starvation [55]. These factors can influence the measured value of parameters related to brain energy metabolism.

The view that brain glucose uptake is insulin-independent stems from studies showing that hyperinsulinemia did not cause an increase in glucose transport across the BBB [55]. However, a study using a fluorescent glucose analog (18-fluorodeoxyglucose) and positron emission tomography (PET) to evaluate the effect of basal insulin on global and regional brain glucose uptake revealed that in healthy male subjects the global rate of brain glucose utilization was significantly higher with insulin than without insulin, concluding that basal insulin influences glucose uptake in the human brain [55]. Regional differences were demonstrated, with glucose uptake in the cerebral cortex being most influenced by insulin and significantly less in the cerebellum [55]. It appeared that metabolic effects of insulin on the brain are greatest at basal (fasting) blood insulin concentrations and brain glucose uptake could be partially insulin sensitive [55].

A research [44], which had as one of its objectives to evaluate the influence of insulin on glucose uptake by cultured human astrocytes, did not prove an increase in glucose uptake after insulin stimulation, probably because the main GLUTs in human astrocytes, GLUT1 and GLUT3, are considered insulin-independent transporters [44]. However, another study on cultured rat GCs showed that insulin, aside from being bound to GCs (astrocytes) by a specific IR, stimulated 2-deoxy-D-

glucose uptake [97].

The effect of insulin on glucose uptake was also assessed indirectly by using genetically modified astrocytes without IR [8, 43]. Lack of astrocyte IR causes a decrease in GLUT1 expression, which is considered partially sensitive to insulin [8, 55], and thereby a reduction in astrocyte glucose uptake, glycolytic rate and L-lactate efflux compared to control animals with IR [43], and an increase in astrocyte fatty acid metabolism to compensate for the reduction in glucose supply [8, 43]. Ablation of astrocyte IR leads to decreased glucose transport across the BBB [43].

Deletion of astrocyte IR results in insulin resistance [3, 43] and uncoupling of blood flow with glucose uptake [3], altered metabolism and energy production [8]. Consistent with the lack of astrocyte IR, deletion of GLUT1 has an analogous effect. Glucose uptake was markedly decreased in primary cultured astrocytes obtained from mice in which deletion of GLUT1 was induced, compared to control astrocytes with GLUT1, which proves that GLUT1 is required for glucose uptake by astrocytes [46]. Additionally, these astrocytes showed increased IR expression compared to controls [46], and upregulation of IGF-I receptor [8].

Regarding the effect of insulin on glucose uptake by neurons, an *in vitro* experiment on hippocampal neuronal culture showed that insulin did not increase their glucose uptake [42]. In other studies on neuronal culture exposed to high concentrations of insulin, increased glucose uptake by neurons could not be demonstrated either [51, 97]. Instead, insulin stimulated the translocation of GLUT3 to the plasma membrane of neurons without causing the fusion of GLUT3 with the plasma membrane [42]. However, in neurons pre-exposed to insulin, depolarization with KCl determined increased fusion of GLUT3 with the cell membrane and glucose uptake [42]. Contrary to the initial conception that neuronal glucose uptake is an insulin-independent process, it appears that insulin influences neuronal glucose uptake, at least *in vitro,* in conditions of neuronal stimulation, by inducing GLUT3 translocation [42]. Further research in this direction is needed to obtain a better understanding of the influence of insulin on the process of glucose uptake by neurons.

The amount of glucose taken up by astrocytes is variable, depending on the concentration of glucose in their environment [2]. When neonatal rat astrocytes are exposed to a medium containing a high concentration of fluorescent glucose analog, they take up more glucose and store more glycogen compared to astrocytes exposed to a medium with a normal concentration of glucose analog [2]. But, as a consequence of exposure to excess glucose, astrocytes showed an altered metabolism with decrease in maximal mitochondrial respiration and glycolytic capacity and broke down much more glycogen than normal glucose astrocytes [2]. Another study on primary cultured astrocytes exposed to high glucose (25 mM) compared to normal glucose (5 mM) reached the same conclusion regarding glycogen content and glucose uptake [13]. A similar effect could not be evidenced in neurons [98]. If primary neurons in culture were incubated with increasing concentrations of glucose, their glycogen content did not vary with glucose concentration, indicating that neurons compared to astrocytes may have some mechanisms that maintain intracellular glycogen at a low level [98]. Accumulation of glycogen in neurons above a certain threshold is harmful and can cause their degeneration [99] and apoptosis [100, 101]. The mechanism by which intracellular glycogen is detrimental to neurons is not clearly understood [101].

The uptake of glucose and its analogs appears to be related to the state of activity and the part of the brain evaluated. An *in vivo* experiment on male rats that assessed the uptake of a nonmetabolizable fluorescent glucose analog 6-deoxy-N-(7-nitrobenz-2-oxa-1,3-diazol-4-yl)-aminoglucose (6-NBDG) by astrocytes and neurons uncovered that during resting conditions, both astrocytes and neurons in the rat barrel cortex took up 6-NBDG at the same rate, but during intense sensory neuronal activation, astrocytes increased their uptake more, while neuronal uptake remained almost unchanged [102]. It shows that glucose is primarily taken up by astrocytes [102]. But when the uptake of glucose and 6-NBDG was assessed by cultured neurons and astrocytes from mouse hippocampus and cerebellum, it was observed that cultured astrocytes took up glucose faster than neurons, whereas uptake of the glucose analog was faster in neurons than in astrocytes [103]. The result could be due to the different affinities and kinetics of GLUTs expressed by the two cell types in the evaluated structures [103].

In AD, the uptake of D-glucose [22, 41] and its analogs [30, 41] in specific parts of the brain (hippocampus and cortex) [41] is reduced, as a result of decreased cerebral blood flow and expression of GLUTs in BBB [22, 41]. This predisposes the brain to insufficient glucose supply, functional impairment and deterioration of cognitive capacity [41]. Accumulation of amyloid-β may be responsible for the depletion of GLUT1 and GLUT3 in the hippocampus and cerebral cortex in AD subjects [41]. Altered glucose transport and metabolism precedes the onset of cognitive impairment in AD by several years [41].

GLYCOGEN STORAGE IN NEURONS AND ATROCYTES

In both astrocytes and neurons, glucose is phosphorylated and irreversibly converted to glucose-6-phosphate [2, 4]. Further, this compound can follow several metabolic pathways, being either stored in the form of glycogen or metabolized through glycolysis [2, 4, 91, 104] and the pentose phosphate pathway [4, 91]. Glycogen is stored mainly in astrocytes [11, 16, 98, 105] and in very small amounts in neurons [98, 105]. Stimulation of human astrocytes in culture with insulin was followed by increased glucose incorporation into glycogen [44]. Glycogen is the only form in which energy is stored in the brain [6], and glucose can be rapidly released from this form without consuming adenosine triphosphate (ATP) [4]. The amount of glycogen in the brain is low compared to that deposited in the liver and muscle [44, 106]. For this reason, the brain depends on a continuous supply of blood-born energy substrate to support its intense energy metabolism [4].

Based on the intravenous infusion of [1-^{13}C] glucose combined with ^{13}C nuclear magnetic resonance spectroscopy, measurement of glycogen content and turnover in the human brain was carried out [106]. It was found that the amount of metabolically active glycogen in the brain was quite low (3 - 4 µmol/g) compared to other organs (liver and muscle), but much higher compared to the concentration of free glucose in the brain under normoglycemic conditions [106]. Brain glycogen turnover was very low, complete turnover taking 3 - 5 days [106]. Prolonged visual stimulation did not cause a change in the glycogen content of the visual cortex in human subjects, nor a significant increase in its turnover [106]. On the contrary, in studies on rat brains, the researchers indicated that the concentration of cerebral cortical glycogen in the unstimulated animals was higher (11 - 12 µmol/g), but the measured value was variable with the method used for its extraction [107]. Glycogen level decreased significantly after a brief sensory stimulation, and chronic inhibition of NOS substantially reduced resting glycogen content of the rat brain [107].

It was previously thought that glycogen is not stored in neurons but only in astrocytes, and neurons either do not possess glycogen phosphorylase to metabolize it or express this enzyme [98]. Nonetheless, Saez et al. [98], using a more sensitive method, demonstrated the presence of small but measurable amounts of glycogen in primary cultured neurons [98]. These cells express an isoform of glycogen synthase that is also expressed by muscle, called muscle glycogen synthase [98]. They also express the brain isoform of glycogen phosphorylase [98]. Neuronal glycogen protects cultured neurons from hypoxia-induced death [98, 105]. On the other hand, a decrease in brain glycogen phosphorylase activity may result in an abnormal accumulation of glycogen in neurons, followed by various brain diseases [99]. Primary mouse neurons in culture have the ability to synthesize and accumulate glycogen under basal conditions and at the same time to degrade it [98]. It was observed that in normoxemia neuronal glycogen turnover is decreased, whereas in hypoxia it is increased, when both glycogen synthase and glycogen phosphorylase activity were increased [98]. Glycogen could protect neurons *in vivo* against hypoxic stress [98].

Astrocytes express brain and muscle glycogen phosphorylase isoforms that degrade stored glycogen in response to extracellular signals and their metabolic needs [98, 99]. The release of neurotransmitters during intense neuronal activity induces the mobilization of glycogen stored in astrocytes [44]. Astrocytic glycogen protects neurons against lack of energy substrate, as can occur in hypoglycemia [4, 44, 99, 108] and ischemia [99, 106]. It has been demonstrated experimentally that if rats are subjected to moderate hypoglycemia by insulin administration, their brain glycogen content gradually decreases, and when plasma and brain glucose concentrations rise again, brain glycogen concentration begins to increase, exceeding several times pre-hypoglycemic level [108]. Brain glycogen metabolism changes with variations in insulinemia [108]. Astrocyte glycogen content is higher when cells are cultured under high glucose conditions compared to normal glucose levels [2, 13].

Because astrocytes lack glucose-6-phosphatase [105] to catalyze the release of glucose from glucose-6-phosphate for export to neurons, astrocytic glycogen can be metabolized to lactate and supplied to neighboring neurons. This mechanism probably operates when neurons have to deal with a glucose deficiency [2, 16, 105, 108]. At the same time, astrocytes themselves could use their own glycogen for energy production to facilitate the utilization of interstitial fluid glucose by neurons in situations of high energy requirements [17, 104, 105]. Other roles of astrocytic glycogen are related to providing energy to sustain glutamate synthesis, release and uptake [11, 108]. This prevents glutamate excitotoxicity [108]. By stimulating glycogen storage in astrocytes [108], insulin might indirectly contribute to sustaining neuronal activity [44], providing neuroprotection [108].

ENERGY SOURCE IN NEURONS AND ASTROCYTES UNDER RESTING AND NEURONAL ACTIVATION CONDITIONS

The release of neurotransmitters, the restoration of neuronal transmembrane potential differences, and the recycling of synaptic vesicles consume a large portion of neuronal energy [4, 30, 91]. Thus, it is important to understand which pathway and substrate the brain uses to rapidly produce ATP when the firing rate of neurons suddenly increases [33, 91]. Questions still persist regarding the importance of neuronal glycolysis *in vivo* in energy production and glucose metabolism through this pathway, as neurons are thought to derive most of their energy from oxidative phosphorylation [13, 91], and under physiological conditions rely less on glycolysis [11, 27, 30, 91], while astrocytes obtain energy mainly through glycolysis [4, 11, 30, 39, 91] and acid β oxidation [39]. The preference for a certain metabolic pathway of these cells is related to the different expression of genes related to energy metabolism [4, 13]. When glycolysis is increased in neurons, less glucose will be metabolized through the pentose-phosphate pathway [30].

Li et al. [27], investigated *in vitro* and *in vivo* glucose uptake by neurons and their glycolytic capacity using cellular and mouse models, in which either the GLUT3 or pyruvate kinase were deleted [27]. They showed that human neurons can take up glucose and metabolize it through glycolysis and use this pathway to produce most of the metabolites of the tricarboxylic acid cycle [27]. In addition, glucose uptake is required to maintain ATP level at the synapses and for normal neuronal function *in vivo* [27]. Glucose uptake was reduced in neurons lacking GLUT3, and cells were less responsive to variations in extracellular glucose [27]. Impaired glucose uptake was compensated by increased galactose metabolism [27].

On the other hand, contrary to the conclusion of the study by Diaz-Garcia et al. [109], Pellerin and Magistretti [89] considered that neuronal activation is associated with the stimulation of aerobic glycolysis in astrocytes, and the lactate derived

from this process is transferred to neurons where is converted into pyruvate that enters the mitochondria to be further metabolized by oxidative phosphorylation [89]. Inhibition of glycolysis caused a marked decrease in glutamate uptake by astrocytes, while hypoxia had less influence on this process [89, 110]. According to this model (ANLS – Astrocyte-Neuron Lactate Shuttle), lactate provided by astrocytes is the energy substrate for ATP production in firing neurons, not glucose, and the metabolic pathway is oxidative phosphorylation and less glycolysis [33]. Consistent with this hypothesis is the study [90] performed on rat cortical neurons showing that lactate is preferred by active neurons to glucose for producing energy, and ATP produced by cortical neurons derived mainly from oxidative phosphorylation and insignificantly from glycolysis [90]. Lactate and pyruvate, but not glucose, increase the activity of cortical neurons [90].

Glutamate released in the synaptic cleft is taken by astrocytes via the Na^+-glutamate transporter. Accumulation of Na^+ in astrocytes stimulates the Na^+/K^+-ATPase, increases ATP consumption [91], while decreasing the ATP/(ADP + AMP) ratio [22] and increasing GLUT1 activity [22, 30]. This, in turn, activates glucose uptake and glycolysis in astrocytes, followed by lactate production that is delivered to neurons [22, 30]. Upregulation of GLUT1 in astrocytes secondary to neuronal activation occurs within seconds and is mediated by increasing in cytosolic Ca^{2+}concentration as a result of Na^+-glutamate co-transport [22]. Experimental deletion of GLUT1 in mouse astrocytes results in significantly reduced glucose uptake and glycolytic rate, lower extracellular lactate concentration, and reduced lactate release upon glucose stimulation after starvation compared with control astrocytes [46].

In mixed cultures of hippocampal neurons and astrocytes, glutamate was observed to inhibit glucose transport into neurons but stimulate its entry into astrocytes, causing within seconds a large increase in the ratio of astrocyte-to-neuron glucose uptake rate [111]. This experiment showed that glutamate diverts glucose to astrocytes and indicates that activated neurons reduce their glucose uptake in favor of astrocytes and cause them preferentially use lactate, provided by neighboring astrocytes [111]. To determine the rate of glucose uptake by neurons and astrocytes, Jakoby et al. [103] assessed the transport and metabolism of two fluorescent glucose analogs in mouse hippocampal and cerebellar slices [103]. They found that, in both structures, glucose uptake and metabolism were faster in the astrocyte-rich compartment than in the nearby neuronal compartment [103]. This showed preferential glucose transport and metabolism by GCs than by neurons and may indirectly support the ANLS hypothesis at rest [103].

There are biochemical arguments for the preference for glycolysis by astrocytes over neurons. Compared to neurons, where some glycolytic enzymes are inhibited [30], astrocytes express glycolytic enzymes and an isoform of lactic dehydrogenase (LDH), type 5, which catalyzes the conversion of pyruvate, the product of glycolysis, to lactate [30]. Moreover, the higher NADH to NAD^+ ratio in astrocytes than in neurons stimulates the reduction of pyruvate to lactate [30], which can be delivered to nearby neurons. Neurons have another isoform of LDH, LDH1, which catalyzes the conversion of lactate to pyruvate [30] that will be further metabolized in mitochondrion. Neurons also express monocarboxylate transporter (MCT) type 2, with high affinity for lactate whereas astrocytes express lower affinity MCTs, type 1 and 4 [30]. This favors the movement of lactate from producing cells (astrocytes) to consuming cells (neurons) in the direction of the lactate concentration gradient [30].

However, as mentioned, Diaz-Garcia et al. [109], in research on hippocampal slices and brains of awake mice, evidenced that increased neuronal energy demand is supported by the direct increase in glucose consumption by neurons and not by the uptake of lactate released by astrocytes when stimulated by glutamate [109]. According to this view, neuronal glycolysis provides rapid energy supply when neurons are stimulated whereas astrocyte derived lactate can be used at rest, not during neuronal activation [109]. During stimulation, neurons might export lactate rather than import it from astrocytes [109]. Although oxidative phosphorylation can produce more ATP than glycolysis, this pathway takes longer to release energy, making it less efficient when there is an abrupt increase in energy requirement [109].

Glycolytic enzymes accumulate at the presynaptic ending of neurons in response to energy stress [112]. This location has the role of metabolizing glucose to provide the energy needed for vesicle recycling [33]. Neuronal glycolysis has an essential role in supplying neurons with ATP, as its blockade was followed by a slow reduction in ATP level when assessed in resting neurons, but the reduction was accelerated when glycolysis was blocked during activity [113]. Decreased ATP availability leads to impaired synaptic transmission [112, 113].

A study based on a theoretical model to assess changes in stored glycogen and the effect of glycogenolysis in sustaining the energy demand associated with 360-seconds of brain stimulation showed that astrocytic glycogen has the role of sparing extracellular glucose for neuronal use when stimulated, rather than as o source of lactate that is delivered from astrocytes to active neurons [17]. Astrocytic glycogen is primarily broken down and used by these cells, decreasing their needs for extracellular glucose [17]. In this way, more interstitial glucose can be taken by neurons. Therefore, there would be no need for glucose to be released from astrocytic glycogen and subsequently converted to lactate, and this exported to neurons [17]. Activation of glycogen phosphorylase leads to rapid formation of glucose-6-phosphate which inhibits hexokinase during stimulation, resulting in decreased glucose uptake and consumption by astrocytes during activation, but not during resting conditions [17]. A small amount of astrocytic cytosolic glucose can pass into the interstitium and be taken up by neurons [17].

Another analysis based on the concentration and kinetic properties of GLUT1, GLUT3 and MCTs in BBB endothelial cells, astrocytes and neurons allowed the development of a model for determining brain glucose and lactate levels during neuronal stimulation [24]. Simulations using this model suggest that during neuronal activation, glucose is primarily taken up

and metabolized by neurons, which release lactate that may be taken up by astrocytes [24]. Calculations have demonstrated that neurons are the primary site of glucose uptake and utilization, both in rest and activation state [24].

In conditions of hyperglycemia (25 mM), astrocytes have reduced maximal oxygen consumption rate and glycolytic activity compared to normoglycemic conditioned astrocytes (5.5 mM), and due to this to be unable to deliver lactate to neurons when energy requirements increase [2]. It was shown that the rate of oxygen consumption was variable depending on the time the cultured astrocytes were exposed to high levels of glucose (25 mM) [13]. After 6 hours of exposure, no significant change in oxygen consumption rate or extracellular acidification rate was observed compared to cells expose to normal glucose level [13]. Instead, the rate of extracellular acidification increased significantly after 24-hour of high glucose exposure, that signifies an activation of glycolysis and lactate production [13]. Hyperglycemic environment also resulted in increased expression of MCT1 mRNA and hexokinase mRNA levels in cultured astrocytes compared to exposure to normal glucose level [13].

Experiments on rodent models of streptozotocin-induced DM showed that glycolysis and lactate concentration were increased in hippocampal extracts of diabetic rats compared to control rats [14]. The researchers hypothesized that in the early stages of diabetes in rats, the elevated amount of lactate can be used by surrounding neurons, while in the later stages of the disease the use of lactate by neurons is reduced due to mitochondrial dysfunction and thus lactate accumulates in the extracellular fluid of the brain, which over time induces impairment of neuronal function and cognitive decline in rats [14]. The same authors working on primary cell culture exposed to high glucose concentrations found increased lactate levels in astrocytes but not in neurons [14].

The normal functioning of the brain`s energy metabolism requires insulin. Both glucose uptake and normal mitochondrial function have been shown to be dependent on astrocyte IR [3]. As mentioned, ablation of IR in hypothalamic mice astrocytes resulted in decreased glucose uptake and glycolytic rate compared with controls, but higher basal mitochondrial respiration and expression of the enzyme necessary for long-chain fatty acid transport in mitochondria (carnitine palmitoyltransferase 1C) [43]. Since most of the energy required for neuronal function is produced in the mitochondria by oxidative phosphorylation [64, 91, 114], mitochondrial dysfunction will result in impaired oxidative phosphorylation, decreased ATP synthesis, and abnormal neuronal metabolism, contributing to neurodegeneration [64]. Lack of astrocyte IR was also associated with fewer and smaller mitochondria and increased autophagosomes in response to hyperglycemia compared to controls [43].

Increased energy demand due to neurotransmission enhances mitochondrial ROS production [91, 114]. At the same time, it activates the transcription of antioxidant genes in astrocytes and the synthesis of glutathione, which confers neuroprotection and facilitates neuron survival [91, 114]. Neurons have their intrinsic capacity to defend against oxidative stress, but they are also assisted by astrocytes (astrocyte-neuronal glutathione shuttle) [91].

The binding of glutamate to its receptor in astrocytes activates a cascade of reactions that ultimately lead to the phosphorylarion of nuclear factor-erythroid 2-related factor-2 (Nrf2) which translocates to the astrocytic nucleus where interacts with antioxidant responsive elements and causes the expression of genes related to antioxidant compounds, including glutathione [91, 114]. In response to enhanced production of ROS, astrocytes synthesize and release reduced glutathione (GSH) into the extracellular fluid. GSH is degraded and the resulted compounds could be taken by nearby neurons to resynthesize GSH [114]. Astrocytes have a key role in supporting adjacent neurons to fight against oxidative stress, as the antioxidant capacity of neurons is less efficient [114].

In a study on cultured cortical neurons subjected to ascorbate/Fe^{2+} to induce oxidative stress, Duarte et al. [61], demonstrated that insulin inhibited lipid and protein oxidation, including GLUT3 oxidation and decrease in neuronal viability, reduced cell death by necrosis and apoptosis, and exerted a neuroprotective action against oxidative insult [61]. Also, the hormone preserved the antioxidant defense capacity of neurons subjected to oxidative stress by stimulating glutathione reductase and inhibiting glutathione peroxidase activities, thus maintaining the ratio between reduced (GSH) and oxidized (GSSG) forms of glutathione (GSH/GSSG) [61]. The decrease in intracellular uric acid level was also inhibited by insulin [61]. A lower level of cerebral GSH associated with increased GSSG was evidenced in conditions of brain insulin resistance and AD [71]. Insulin exerts a protective effect against oxidative injury of primary cortical neurons experimentally subjected to oxidative stress by stimulating the neuronal uptake of glucose and its glycolysis to pyruvate, increasing the intracellular concentration of macroergic compounds, ATP and phosphocreatine, and the level of adenosine [60]. Through several steps, adenosine is converted to uric acid [60].

Type 2 DM and AD are conditions with a complex pathogenetic mechanism. Altered insulin responsiveness [115], impaired brain glucose metabolism, mitochondrial dysfunction and oxidative stress have been evidenced in both diseases [30, 64, 73, 115, 116]. It has been hypothesized that neuronal oxidative stress may be causally related to peripheral or brain insulin resistance [71]. Due to the fact neurons are cells with high energy consumption, any changes in the number, motility, structure and function of mitochondria can increase the production of ROS and cause oxidative stress and neurodegeneration, and this may contribute to cognitive impairment in diabetic and AD patients [64].

CONCLUSIONS

Uncertainties persist regarding the metabolic peculiarities of neurons and astrocytes, the cooperation between

these cells in normal and pathological circumstances, the effect of variation in blood glucose concentration on the function and structure of brain cells, and the importance of insulin in modulating these aspects. Knowledge of brain energy metabolism and the role of insulin in supporting this process are critical, as impaired glucose metabolism is associated with neurodegenerative diseases. Insulin may fulfill several roles related to glucose homeostasis in the brain. Studies have shown that insulin could stimulate glucose uptake by neurons and astrocytes, especially under conditions of increased neuronal activity and the expression of some GLUTs that might be sensitive to insulin. It could also enhance the storage of glucose in astrocytes in the form of glycogen and its use as an energy resource, mainly in case of cerebral ischemia and hypoglycemia, having a neuroprotective role. Astrocyte IR is required for coupling glucose uptake to cerebral blood flow. This ensures an adequate supply of energy substrate in proportion to the metabolic demands of the brain. The normal activity and structure of brain cell mitochondria could be influenced by insulin as well, including antioxidant protection against ROS.

A number of mechanisms might account for impaired activity of insulin in the brain: decreased in the number of IR in brain cells, decreased in the rate of insulin transport in the brain parenchyma, glycation of insulin and IR in a high glucose environment, alteration of components of the insulin signaling pathways, and oxidative stress. The effects of altered insulin actions can lead to reduced brain glucose uptake, especially when energy requirements are high, decreased astrocytic glycogen stores, uncoupling of neuronal activity with glucose and oxygen demand, and overproduction of ROS. These factors may underlie brain cell degeneration in patients with type 2 DM and AD.

Future studies will shed light on the complexity of insulin`s actions in the brain, the link between brain insulin resistance and cognitive impairment in DM and AD, uncovering its therapeutic benefits, particularly in AD.

REFERENCES

1. Serlin Y, Shelef I, Knyazer B, Friedman A. Anatomy and physiology of the blood-brain barrier. Semin Cell Dev Biol. 2015 Feb;38:2-6. doi: 10.1016/j.semcdb.2015.01.002. Epub 2015 Feb 11. PMID: 25681530; PMCID: PMC4397166.
2. Staricha K, Meyers N, Garvin J, Liu Q, Rarick K, Harder D, Cohen S. Effect of high glucose condition on glucose metabolism in primary astrocytes. Brain Res. 2020 Apr 1;1732:146702. doi: 10.1016/j.brainres.2020.146702. Epub 2020 Feb 4. PMID: 32032612; PMCID: PMC7106974.
3. Fernandez AM, Martinez-Rachadell L, Navarrete M, Pose-Utrilla J, Davila JC, Pignatelli J, Diaz-Pacheco S, Guerra-Cantera S, Viedma-Moreno E, Palenzuela R, Ruiz de Martin Esteban S, Mostany R, Garcia-Caceres C, Tschöp M, Iglesias T, de Ceballos ML, Gutierrez A, Torres Aleman I. Insulin regulates neurovascular coupling through astrocytes. Proc Natl Acad Sci U S A. 2022 Jul 19; 119(29):e2204527119. doi: 10.1073/pnas.2204527119. Epub 2022 Jul 14. PMID: 35858325; PMCID: PMC9304019.
4. Bélanger M, Allaman I, Magistretti PJ, Brain Energy Metabolism: Focus on Astrocyte-Neuron Metabolic Cooperation, Cell Metabolism, Volume 14, Issue 6, 2011, P724-738, ISSN 1550-4131, https://doi.org/10.1016/j.cmet.2011.08.016.
5. Petzold GC, Murthy VN. Role of astrocytes in neurovascular coupling. Neuron. 2011 Sep 8;71(5):782-97. doi: 10.1016/j.neuron.2011.08.009. PMID: 21903073.
6. Mergenthaler P, Lindauer U, Dienel GA, Meisel A. Sugar for the brain: the role of glucose in physiological and pathological brain function. Trends Neurosci. 2013 Oct;36(10):587-97. doi: 10.1016/j.tins.2013.07.001. Epub 2013 Aug 20. PMID: 23968694; PMCID: PMC3900881.
7. Duelli R, Kuschinsky W. Brain Glucose Transporters: Relationship to Local Energy Demand. Physiology. 2001. 16:2,71-76
8. González-García I, Gruber T, García-Cáceres C. Insulin action on astrocytes: From energy homeostasis to behaviour. J Neuroendocrinol. 2021 Apr; 33(4):e12953. doi: 10.1111/jne.12953. Epub 2021 Mar 16. PMID: 33724579.
9. García-Cáceres C, Fuente-Martín E, Argente J, Chowen JA. Emerging role of glial cells in the control of body weight. Mol Metab. 2012 Aug 9;1(1-2):37-46. doi: 10.1016/j.molmet.2012.07.001. PMID: 24024117; PMCID: PMC3757650.
10. Jensen NJ, Wodshow HZ, Nilsson M, Rungby J. Effects of Ketone Bodies on Brain Metabolism and Function in Neurodegenerative Diseases. Int J Mol Sci. 2020 Nov 20;21(22):8767. doi: 10.3390/ijms21228767. PMID: 33233502; PMCID: PMC7699472.
11. Sonnay S, Gruetter R and Duarte JMN (2017) How Energy Metabolism Supports Cerebral Function: Insights from ^{13}C Magnetic Resonance Studies In vivo. Front. Neurosci. 11:288. doi: 10.3389/fnins.2017.00288
12. Attwell D, Buchan AM, Charpak S, Lauritzen M, Macvicar BA, Newman EA. Glial and neuronal control of brain blood flow. Nature. 2010 Nov 11;468(7321):232-43. doi: 10.1038/nature09613. PMID: 21068832; PMCID: PMC3206737.
13. Li W, Roy Choudhury G, Winters A, Prah J, Lin W, Liu R, Yang SH. Hyperglycemia Alters Astrocyte Metabolism and Inhibits Astrocyte Proliferation. Aging Dis. 2018 Aug 1;9(4):674-684. doi: 10.14336/AD.2017.1208. PMID: 30090655; PMCID: PMC6065301.
14. Zhao L, Dong M, Ren M, Li C, Zheng H, Gao H. Metabolomic Analysis Identifies Lactate as an Important Pathogenic Factor in Diabetes-associated Cognitive Decline Rats. Mol Cell Proteomics. 2018 Dec;17(12):2335-2346. doi: 10.1074/mcp.RA118.000690. Epub 2018 Aug 31. PMID: 30171160; PMCID: PMC6283288.
15. Hou WK, Xian YX, Zhang L, Lai H, Hou XG, Xu YX, Yu T, Xu FY, Song J, Fu CL, Zhang WW, Chen L. Influence of blood glucose on the expression of glucose transporter proteins 1 and 3 in the brain of diabetic rats. Chin Med J (Engl). 2007 Oct 5;120(19):1704-9. PMID: 17935675.
16. Falkowska A, Gutowska I, Goschorska M, Nowacki P, Chlubek D, Baranowska-Bosiacka I. Energy Metabolism of the Brain, Including the Cooperation between Astrocytes and Neurons, Especially in the Context of Glycogen Metabolism. Int J Mol Sci. 2015 Oct 29;16(11):25959-81. doi: 10.3390/ijms161125939. PMID: 26528968; PMCID: PMC4661798.

17. DiNuzzo M, Mangia S, Maraviglia B, Giove F. Glycogenolysis in Astrocytes Supports Blood-Borne Glucose Channeling Not Glycogen-Derived Lactate Shuttling to Neurons: Evidence from Mathematical Modeling. Journal of Cerebral Blood Flow & Metabolism. 2010;30(12):1895-1904. doi:10.1038/jcbfm.2010.151
18. Morgello S, Uson RR, Schwartz EJ, Haber RS. The human blood-brain barrier glucose transporter (GLUT1) is a glucose transporter of gray matter astrocytes. Glia. 1995 May; 14(1):43-54. doi: 10.1002/glia.440140107. PMID: 7615345.
19. Simpson IA, Appel NM, Hokari M, Oki J, Holman GD, Maher F, Koehler-Stec EM, Vannucci SJ, Smith QR. Blood-brain barrier glucose transporter: effects of hypo- and hyperglycemia revisited. J Neurochem. 1999 Jan;72(1):238-47. doi: 10.1046/j.1471-4159.1999.0720238.x. PMID: 9886075.
20. Simpson IA, Vannucci SJ, DeJoseph MR, Hawkins RA. Glucose transporter asymmetries in the bovine blood-brain barrier. J Biol Chem. 2001 Apr 20;276(16):12725-9. doi: 10.1074/jbc.M010897200. Epub 2001 Jan 12. PMID: 11278779.
21. Leão LL, Tangen G, Barca ML, Engedal K, Santos SHS, Machado FSM, de Paula AMB, Monteiro-Junior RS. Does hyperglycemia downregulate glucose transporters in the brain? Med Hypotheses. 2020 Jun;139:109614. doi: 10.1016/j.mehy.2020.109614. Epub 2020 Feb 6. PMID: 32087490.
22. Koepsell H. Glucose transporters in brain in health and disease. Pflugers Arch. 2020 Sep;472(9):1299-1343. doi: 10.1007/s00424-020-02441-x. Epub 2020 Aug 13. PMID: 32789766; PMCID: PMC7462931.
23. Shah K, Desilva S, Abbruscato T. The role of glucose transporters in brain disease: diabetes and Alzheimer's Disease. Int J Mol Sci. 2012 Oct 3;13(10):12629-55. doi: 10.3390/ijms131012629. PMID: 23202918; PMCID: PMC3497292.
24. Simpson IA, Carruthers A, Vannucci SJ. Supply and demand in cerebral energy metabolism: the role of nutrient transporters. J Cereb Blood Flow Metab. 2007 Nov;27(11):1766-91. doi: 10.1038/sj.jcbfm.9600521. Epub 2007 Jun 20. PMID: 17579656; PMCID: PMC2094104.
25. Banks WA, Owen JB, Erickson MA. Insulin in the brain: there and back again. Pharmacol Ther. 2012 Oct;136(1):82-93. doi: 10.1016/j.pharmthera.2012.07.006. Epub 2012 Jul 17. PMID: 22820012; PMCID: PMC4134675.
26. McNay EC, Pearson-Leary J. GluT4: A central player in hippocampal memory and brain insulin resistance. Exp Neurol. 2020 Jan;323:113076. doi: 10.1016/j.expneurol.2019.113076. Epub 2019 Oct 12. PMID: 31614121; PMCID: PMC6936336.
27. Li H, Guglielmetti C, Sei YJ, Zilberter M, Le Page LM, Shields L, Yang J, Nguyen K, Tiret B, Gao X, Bennett N, Lo I, Dayton TL, Kampmann M, Huang Y, Rathmell JC, Heiden MV, Chaumeil MM, Nakamura K. Neurons require glucose uptake and glycolysis in vivo. Cell Rep. 2023 Apr 6;42(4):112335. doi: 10.1016/j.celrep.2023.112335. Epub ahead of print. PMID: 37027294.
28. Pomytkin I, Pinelis V. Brain Insulin Resistance: Focus on Insulin Receptor-Mitochondria Interactions. Life (Basel). 2021 Mar 22;11(3):262. doi: 10.3390/life11030262. PMID: 33810179; PMCID: PMC8005009.
29. Grillo CA, Piroli GG, Hendry RM, Reagan LP. Insulin-stimulated translocation of GLUT4 to the plasma membrane in rat hippocampus is PI3-kinase dependent. Brain Res. 2009 Nov 3;1296:35-45. doi: 10.1016/j.brainres.2009.08.005. Epub 2009 Aug 11. PMID: 19679110; PMCID: PMC2997526.
30. Beard E, Lengacher S, Dias S, Magistretti PJ, Finsterwald C. Astrocytes as Key Regulators of Brain Energy Metabolism: New Therapeutic Perspectives. Front. Physiol. 12:825816. doi: 10.3389/fphys.2021.825816
31. Ashrafi G, Wu Z, Farrell RJ, Ryan TA. GLUT4 Mobilization Supports Energetic Demands of Active Synapses. Neuron. 2017 Feb 8;93(3):606-615.e3. doi: 10.1016/j.neuron.2016.12.020. Epub 2017 Jan 19. PMID: 28111082; PMCID: PMC5330257.
32. Ferreira JM, Burnett AL, Rameau GA. Activity-dependent regulation of surface glucose transporter-3. J Neurosci. 2011 Feb 9;31(6):1991-9. doi: 10.1523/JNEUROSCI.1850-09.2011. PMID: 21307237; PMCID: PMC3045034.
33. Ashrafi G, Ryan TA. Glucose metabolism in nerve terminals. Curr Opin Neurobiol. 2017 Aug;45:156-161. doi: 10.1016/j.conb.2017.03.007. Epub 2017 Jun 9. PMID: 28605677; PMCID: PMC5675126.
34. Pearson-Leary J, McNay EC. Novel Roles for the Insulin-Regulated Glucose Transporter-4 in Hippocampally Dependent Memory. J Neurosci. 2016 Nov 23;36(47):11851-11864. doi: 10.1523/JNEUROSCI.1700-16.2016. PMID: 27881773; PMCID: PMC5125244.
35. Duelli R, Maurer MH, Staudt R, Heiland S, Duembgen L, Kuschinsky W. Increased cerebral glucose utilization and decreased glucose transporter Glut1 during chronic hyperglycemia in rat brain. Brain Res. 2000 Mar 10;858(2):338-47. doi: 10.1016/s0006-8993(00)01942-9. PMID: 10708685.
36. Duelli R, Staudt R, Duembgen L, Kuschinsky W. Increase in glucose transporter densities of Glut3 and decrease of glucose utilization in rat brain after one week of hypoglycemia. Brain Res. 1999 Jun 12;831(1-2):254-62. doi: 10.1016/s0006-8993(99)01463-8. PMID: 10412004.
37. Kumagai AK, Kang YS, Boado RJ, Pardridge WM. Upregulation of blood-brain barrier GLUT1 glucose transporter protein and mRNA in experimental chronic hypoglycemia. Diabetes. 1995 Dec;44(12):1399-404. doi: 10.2337/diab.44.12.1399. PMID: 7589845.
38. Gray SM, Meijer RI, Barrett EJ. Insulin regulates brain function, but how does it get there? Diabetes. 2014 Dec;63(12):3992-7. doi: 10.2337/db14-0340. PMID: 25414013; PMCID: PMC4237995.
39. Milstein JL, Ferris HA. The brain as an insulin-sensitive metabolic organ. Mol Metab. 2021 Oct;52:101234. doi: 10.1016/j.molmet.2021.101234. Epub 2021 Apr 15. PMID: 33845179; PMCID: PMC8513144.
40. Csajbók ÉA, Tamás G. Cerebral cortex: a target and source of insulin? Diabetologia. 2016 Aug;59(8):1609-15. doi: 10.1007/s00125-016-3996-2. Epub 2016 May 20. PMID: 27207082.
41. Kyrtata N, Emsley HCA, Sparasci O, Parkes LM and Dickie BR (2021) A Systematic Review of Glucose Transport Alterations in Alzheimer's Disease. Front. Neurosci. 15:626636. doi: 10.3389/fnins.2021.626636
42. Uemura E, Greenlee HW. Insulin regulates neuronal glucose uptake by promoting translocation of glucose transporter GLUT3. Exp Neurol. 2006 Mar;198(1):48-53. doi: 10.1016/j.expneurol.2005.10.035. Epub 2005 Dec 9. PMID: 16337941.
43. García-Cáceres C, Quarta C, Varela L, Gao Y, Gruber T, Legutko B, Jastroch M, Johansson P, Ninkovic J, Yi CX, Le Thuc O, Szigeti-Buck K, Cai W, Meyer CW, Pfluger PT, Fernandez AM, Luquet S, Woods SC, Torres-Alemán I, Kahn CR, Götz M, Horvath

TL, Tschöp MH. Astrocytic Insulin Signaling Couples Brain Glucose Uptake with Nutrient Availability. Cell. 2016 Aug 11;166(4):867-880. doi: 10.1016/j.cell.2016.07.028. PMID: 27518562; PMCID: PMC8961449.
44. Heni M, Hennige AM, Peter A, Siegel-Axel D, Ordelheide AM, Krebs N, Machicao F, Fritsche A, Häring HU, Staiger H. Insulin promotes glycogen storage and cell proliferation in primary human astrocytes. PLoS One. 2011;6(6):e21594. doi: 10.1371/journal.pone.0021594. Epub 2011 Jun 27. PMID: 21738722; PMCID: PMC3124526.
45. Maher F. Immunolocalization of GLUT1 and GLUT3 glucose transporters in primary cultured neurons and glia. J Neurosci Res. 1995 Nov 1;42(4):459-69. doi: 10.1002/jnr.490420404. PMID: 8568932.
46. Ardanaz CG, de la Cruz A, Elizalde-Horcada M, Puerta E, Ramirez MJ, Ortega JE, Urbiola A, Ederra C, Ariz M, Ortiz-de-Solórzano C, Fernández-Irigoyen J, Santamaria E, Karsenty G, Brüning JC, Solas M. GLUTI ablation in atrocytes paradoxically improves central and peripheral glucose metabolism via enhanced insulin-stimulated ATP release. bioRxiv 2022.10.06.511112; doi: https://doi.org/10.1101/2022.10.06.511112
47. Winkler EA, Nishida Y, Sagare AP, Rege SV, Bell RD, Perlmutter D, Sengillo JD, Hillman S, Kong P, Nelson AR, Sullivan JS, Zhao Z, Meiselman HJ, Wendy RB, Soto J, Abel ED, Makshanoff J, Zuniga E, De Vivo DC, Zlokovic BV. GLUT1 reductions exacerbate Alzheimer's disease vasculo-neuronal dysfunction and degeneration. Nat Neurosci. 2015 Apr;18(4):521-530. doi: 10.1038/nn.3966. Epub 2015 Mar 2. PMID: 25730668; PMCID: PMC4734893.
48. Simpson IA, Chundu KR, Davies-Hill T, Honer WG, Davies P. Decreased concentrations of GLUT1 and GLUT3 glucose transporters in the brains of patients with Alzheimer's disease. Ann Neurol. 1994 May;35(5):546-51. doi: 10.1002/ana.410350507. PMID: 8179300.
49. Leclerc M, Bourassa P, Tremblay C, Caron V, Sugère C, Emond V, Bennett DA, Calon F. Cerebrovascular insulin receptors are defective in Alzheimer's disease, Brain, Volume 146, Issue 1, January 2023, Pages 75–90, https://doi.org/10.1093/brain/awac309
50. Garwood CJ, Ratcliffe LE, Morgan SV, Simpson JE, Owens H, Vazquez-Villaseñor I, Heath PR, Romero IA, Ince PG, Wharton SB. Insulin and IGF1 signalling pathways in human astrocytes in vitro and in vivo; characterisation, subcellular localisation and modulation of the receptors. Mol Brain. 2015 Aug 22;8:51. doi: 10.1186/s13041-015-0138-6. PMID: 26297026; PMCID: PMC4546315.
51. Gralle M. The neuronal insulin receptor in its environment. J Neurochem. 2017 Feb;140(3):359-367. doi: 10.1111/jnc.13909. Epub 2016 Dec 27. PMID: 27889917.
52. Pomytkin I, Costa-Nunes JP, Kasatkin V, Veniaminova E, Demchenko A, Lyundup A, Lesch KP, Ponomarev ED, Strekalova T. Insulin receptor in the brain: Mechanisms of activation and the role in the CNS pathology and treatment. CNS Neurosci Ther. 2018 Sep;24(9):763-774. doi: 10.1111/cns.12866. Epub 2018 Apr 24. PMID: 29691988; PMCID: PMC6489906.
53. Yanagita T, Nemoto T, Satoh S, Yoshikawa N, Maruta T, Shiraishi S, Sugita C, Murakami M. Neuronal Insulin Receptor Signaling: A Potential Target for the Treatment of Cognitive and Mood Disorders. Mood Disorders. Edited by Nese Kocabasoglu. Published: 23 January 2013. DOI: 10.5772/54389
54. Abbott MA, Wells DG, Fallon JR. The insulin receptor tyrosine kinase substrate p58/53 and the insulin receptor are components of CNS synapses. J Neurosci. 1999 Sep 1;19(17):7300-8. doi: 10.1523/JNEUROSCI.19-17-07300.1999. PMID: 10460236; PMCID: PMC6782521.
55. Bingham EM, Hopkins D, Smith D, Pernet A, Hallett W, Reed L, Marsden PK, Amiel SA. The role of insulin in human brain glucose metabolism: an 18fluoro-deoxyglucose positron emission tomography study. Diabetes. 2002 Dec;51(12):3384-90. doi: 10.2337/diabetes.51.12.3384. PMID: 12453890.
56. Gray SM, Aylor KW, Barrett EJ. Unravelling the regulation of insulin transport across the brain endothelial cell. Diabetologia. 2017 Aug;60(8):1512-1521. doi: 10.1007/s00125-017-4285-4. Epub 2017 Jun 11. PMID: 28601906; PMCID: PMC5534844.
57. Pardridge WM, Eisenberg J, Yang J. Human blood-brain barrier insulin receptor. J Neurochem. 1985 Jun;44(6):1771-8. doi: 10.1111/j.1471-4159.1985.tb07167.x. PMID: 2859355.
58. Rhea ME, Rask-Madsen C, Banks WA, Insulin transport across the blood-brain barrier can occur independently of the insulin receptor, J Physiol, 596.19 (2018) pp 4753-4765.
59. Banks WA. The source of cerebral insulin. Eur J Pharmacol. 2004 Apr 19;490(1-3):5-12. doi: 10.1016/j.ejphar.2004.02.040. PMID: 15094069.
60. Duarte AI, Proença T, Oliveira CR, Santos MS, Rego AC. Insulin restores metabolic function in cultured cortical neurons subjected to oxidative stress. Diabetes. 2006 Oct;55(10):2863-70. doi: 10.2337/db06-0030. PMID: 17003354.
61. Duarte AI, Santos MS, Oliveira CR, Rego AC. Insulin neuroprotection against oxidative stress in cortical neurons-involvement of uric acid and glutathione antioxidant defenses. Free Radic Biol Med. 2005 Oct 1;39(7):876-89. doi: 10.1016/j.freeradbiomed.2005.05.002. PMID: 16140208.
62. Banks WA, Jaspan JB, Kastin AJ. Effect of diabetes mellitus on the permeability of the blood-brain barrier to insulin. Peptides. 1997;18(10):1577-84. doi: 10.1016/s0196-9781(97)00238-6. PMID: 9437719.
63. Steen E, Terry BM, Rivera EJ, Cannon JL, Neely TR, Tavares R, Xu XJ, Wands JR, de la Monte SM. Impaired insulin and insulin-like growth factor expression and signaling mechanisms in Alzheimer's disease - is this type 3 diabetes? J Alzheimers Dis. 2005 Feb;7(1):63-80. doi: 10.3233/jad-2005-7107. PMID: 15750215.
64. Potenza MA, Sgarra L, Desantis V, Nacci C, Montagnani M. Diabetes and Alzheimer's Disease: Might Mitochondrial Dysfunction Help Deciphering the Common Path? Antioxidants (Basel). 2021 Aug 6;10(8):1257. doi: 10.3390/antiox10081257. PMID: 34439505; PMCID: PMC8389322.
65. Rhinesmith T, Turkette T, Root-Bernstein R. Rapid Non-Enzymatic Glycation of the Insulin Receptor under Hyperglycemic Conditions Inhibits Insulin Binding In Vitro: Implications for Insulin Resistance. Int J Mol Sci. 2017 Dec 2;18(12):2602. doi: 10.3390/ijms18122602. PMID: 29207492; PMCID: PMC5751205.
66. Jeevanandam J, Paramasivam E, Saraswathi NT. Glycation restrains open-closed conformation of Insulin. Comput Biol Chem. 2023 Feb;102:107803. doi: 10.1016/j.compbiolchem.2022.107803. Epub 2022 Dec 16. PMID: 36542957.

67. Walke PB, Bansode SB, More NP, Chaurasiya AH, Joshi RS, Kulkarni MJ. Molecular investigation of glycated insulin-induced insulin resistance via insulin signaling and AGE-RAGE axis, Biochimica et Biophysica Acta (BBA) - Molecular Basis of Disease, Volume 1867, Issue 2, 2021, 166029, ISSN 0925-4439, https://doi.org/10.1016/j.bbadis.2020.166029.
68. Hunter SJ, Boyd AC, O'Harte FP, McKillop AM, Wiggam MI, Mooney MH, McCluskey JT, Lindsay JR, Ennis CN, Gamble R, Sheridan B, Barnett CR, McNulty H, Bell PM, Flatt PR. Demonstration of glycated insulin in human diabetic plasma and decreased biological activity assessed by euglycemic-hyperinsulinemic clamp technique in humans. Diabetes. 2003 Feb;52(2):492-8. doi: 10.2337/diabetes.52.2.492. PMID: 12540626.
69. Barloese MCJ, Bauer C, Petersen ET, Hansen CS, Madsbad S, Siebner HR. Neurovascular Coupling in Type 2 Diabetes With Cognitive Decline. A Narrative Review of Neuroimaging Findings and Their Pathophysiological Implications. Front Endocrinol (Lausanne). 2022 Jul 4;13:874007. doi: 10.3389/fendo.2022.874007. PMID: 35860697; PMCID: PMC9289474.
70. Gonçalves JS, Seiça RM, Laranjinha J, Lourenço CF. Impairment of neurovascular coupling in the hippocampus due to decreased nitric oxide bioavailability supports early cognitive dysfunction in type 2 diabetic rats. Free Radic Biol Med. 2022 Nov 20;193(Pt 2):669-675. doi: 10.1016/j.freeradbiomed.2022.11.009. Epub 2022 Nov 11. PMID: 36372286.
71. Maciejczyk M, Żebrowska E, Chabowski A. Insulin Resistance and Oxidative Stress in the Brain: What's New? Int J Mol Sci. 2019 Feb 18;20(4):874. doi: 10.3390/ijms20040874. PMID: 30781611; PMCID: PMC6413037.
72. Park L, Anrather J, Girouard H, Zhou P, Iadecola C. Nox2-derived reactive oxygen species mediate neurovascular dysregulation in the aging mouse brain. J Cereb Blood Flow Metab. 2007 Dec;27(12):1908-18. doi: 10.1038/sj.jcbfm.9600491. Epub 2007 Apr 11. PMID: 17429347
73. Veselov IM, Vinogradova DV, Maltsev AV, Shevtsov PN, Spirkova EA, Bachurin SO, Shevtsova EF. Mitochondria and Oxidative Stress as a Link between Alzheimer's Disease and Diabetes Mellitus. Int J Mol Sci. 2023 Sep 22;24(19):14450. doi: 10.3390/ijms241914450. PMID: 37833898; PMCID: PMC10572926.
74. Starr JM, Wardlaw J, Ferguson K, MacLullich A, Deary IJ, Marshall I. Increased blood-brain barrier permeability in type II diabetes demonstrated by gadolinium magnetic resonance imaging. J Neurol Neurosurg Psychiatry. 2003 Jan;74(1):70-6. doi: 10.1136/jnnp.74.1.70. PMID: 12486269; PMCID: PMC1738177.
75. Liu Y, Liu F, Grundke-Iqbal I, Iqbal K, Gong CX. Deficient brain insulin signalling pathway in Alzheimer's disease and diabetes. J Pathol. 2011 Sep;225(1):54-62. doi: 10.1002/path.2912. Epub 2011 May 19. PMID: 21598254; PMCID: PMC4484598.
76. Stackhouse TL, Mishra A. Neurovascular Coupling in Development and Disease: Focus on Astrocytes. Front Cell Dev Biol. 2021 Jul 12;9:702832. doi: 10.3389/fcell.2021.702832. PMID: 34327206; PMCID: PMC8313501.
77. Jakovcevic D, Harder DR. Role of astrocytes in matching blood flow to neuronal activity. Curr Top Dev Biol. 2007;79:75-97. doi: 10.1016/S0070-2153(06)79004-4. PMID: 17498548.
78. Carmignoto G, Gómez-Gonzalo M. The contribution of astrocyte signalling to neurovascular coupling. Brain Res Rev. 2010 May;63(1-2):138-48. doi: 10.1016/j.brainresrev.2009.11.007. Epub 2009 Dec 4. PMID: 19948187.
79. Institoris A, Vandal M, Peringod G, Catalano C, Tran CH, Yu X, Visser F, Breiteneder C, Molina L, Khakh BS, Nguyen MD, Thompson RJ, Gordon GR. Astrocytes amplify neurovascular coupling to sustained activation of neocortex in awake mice. Nat Commun. 2022 Dec 22;13(1):7872. doi: 10.1038/s41467-022-35383-2. PMID: 36550102; PMCID: PMC9780254.
80. Kaplan L, Chow BW, Gu C. Neuronal regulation of the blood-brain barrier and neurovascular coupling. Nat Rev Neurosci. 2020 Aug;21(8):416-432. doi: 10.1038/s41583-020-0322-2. Epub 2020 Jul 7. PMID: 32636528; PMCID: PMC8934575.
81. Lin AL, Fox PT, Hardies J, Duong TQ, Gao JH. Nonlinear coupling between cerebral blood flow, oxygen consumption, and ATP production in human visual cortex. Proc Natl Acad Sci U S A. 2010 May 4;107(18):8446-51. doi: 10.1073/pnas.0909711107. Epub 2010 Apr 19. PMID: 20404151; PMCID: PMC2889577.
82. Winship IR, Plaa N, Murphy TH. Rapid astrocyte calcium signals correlate with neuronal activity and onset of the hemodynamic response in vivo. J Neurosci. 2007 Jun 6;27(23):6268-72. doi: 10.1523/JNEUROSCI.4801-06.2007. PMID: 17554000; PMCID: PMC6672142.
83. Takano T, Tian GF, Peng W, Lou N, Libionka W, Han X, Nedergaard M. Astrocyte-mediated control of cerebral blood flow. Nat Neurosci. 2006 Feb;9(2):260-7. doi: 10.1038/nn1623. Epub 2005 Dec 25. PMID: 16388306.
84. Kocharyan A, Fernandes P, Tong XK, Vaucher E, Hamel E. Specific subtypes of cortical GABA interneurons contribute to the neurovascular coupling response to basal forebrain stimulation. *J Cereb Blood Flow Metab.* 2008;28:221–231.
85. Phillips AA, Chan FH, Zheng MM, Krassioukov AV, Ainslie PN. Neurovascular coupling in humans: Physiology, methodological advances and clinical implications. J Cereb Blood Flow Metab. 2016 Apr;36(4):647-64. doi: 10.1177/0271678X15617954. Epub 2015 Nov 24. PMID: 26661243; PMCID: PMC4821024.
86. Zonta M, Angulo MC, Gobbo S, Rosengarten B, Hossmann KA, Pozzan T, Carmignoto G. Neuron-to-astrocyte signaling is central to the dynamic control of brain microcirculation. Nat Neurosci. 2003 Jan;6(1):43-50. doi: 10.1038/nn980. PMID: 12469126.
87. Lourenço CF, Santos RM, Barbosa RM, Cadenas E, Radi R, Laranjinha J. Neurovascular coupling in hippocampus is mediated via diffusion by neuronal-derived nitric oxide. Free Radic Biol Med. 2014 Aug;73:421-9. doi: 10.1016/j.freeradbiomed.2014.05.021. Epub 2014 Jun 2. PMID: 24887095.
88. Gordon GR, Choi HB, Rungta RL, Ellis-Davies GC, MacVicar BA. Brain metabolism dictates the polarity of astrocyte control over arterioles. Nature. 2008 Dec 11; 456(7223):745-9. doi: 10.1038/nature07525. Epub 2008 Oct 29. PMID: 18971930; PMCID: PMC4097022.
89. Pellerin L, Magistretti PJ. Glutamate uptake into astrocytes stimulates aerobic glycolysis: a mechanism coupling neuronal activity to glucose utilization. Proc Natl Acad Sci U S A. 1994 Oct 25;91(22):10625-9. doi: 10.1073/pnas.91.22.10625. PMID: 7938003; PMCID: PMC45074.
90. Karagiannis A, Gallopin T, Lacroix A, Plaisier F, Piquet J, Geoffroy H, Hepp R, Naudé J, Le Gac B, Egger R, Lambolez B, Li D, Rossier J, Staiger JF, Imamura H, Seino S, Roeper J, Cauli B. Lactate is an energy substrate for rodent cortical neurons and enhances their firing activity. Elife. 2021 Nov 12;10:e71424. doi: 10.7554/eLife.71424. PMID: 34766906; PMCID: PMC8651295.

91. Bolaños JP. Bioenergetics and redox adaptations of astrocytes to neuronal activity. J Neurochem. 2016 Oct;139 Suppl 2(Suppl Suppl 2):115-125. doi: 10.1111/jnc.13486. Epub 2016 Mar 10. PMID: 26968531; PMCID: PMC5018236.
92. Hoiland RL, Caldwell HG, Howe CA, Nowak-Flück D, Stacey BS, Bailey DM, Paton JFR, Green DJ, Sekhon MS, Macleod DB, Ainslie PN. Nitric oxide is fundamental to neurovascular coupling in humans. J Physiol. 2020 Nov;598(21):4927-4939. doi: 10.1113/JP280162. Epub 2020 Aug 31. PMID: 32785972.
93. Hu B, Yan LF, Sun Q, Yu Y, Zhang J, Dai YJ, Yang Y, Hu YC, Nan HY, Zhang X, Heng CN, Hou JF, Liu QQ, Shao CH, Li F, Zhou KX, Guo H, Cui GB, Wang W. Disturbed neurovascular coupling in type 2 diabetes mellitus patients: Evidence from a comprehensive fMRI analysis. Neuroimage Clin. 2019;22:101802. doi: 10.1016/j.nicl.2019.101802. Epub 2019 Mar 27. PMID: 30991623; PMCID: PMC6447740.
94. Park L, Anrather J, Forster C, Kazama K, Carlson GA, Iadecola C. Abeta-induced vascular oxidative stress and attenuation of functional hyperemia in mouse somatosensory cortex. J Cereb Blood Flow Metab. 2004 Mar;24(3):334-42. doi: 10.1097/01.WCB.0000105800.49957.1E. PMID: 15091114.
95. Sun J, Druhan LJ, Zweier JL. Dose dependent effects of reactive oxygen and nitrogen species on the function of neuronal nitric oxide synthase. Arch Biochem Biophys. 2008 Mar 15;471(2):126-33. doi: 10.1016/j.abb.2008.01.003. Epub 2008 Jan 11. PMID: 18201545; PMCID: PMC4073612.
96. Canna A, Esposito F, Tedeschi G, Trojsi F, Passaniti C, di Meo I, Polito R, Maiorino MI, Paolisso G, Cirillo M, Rizzo MR. Neurovascular coupling in patients with type 2 diabetes mellitus. Front Aging Neurosci. 2022 Sep 1;14:976340. doi: 10.3389/fnagi.2022.976340. PMID: 36118711; PMCID: PMC9476313.
97. Clarke DW, Boyd FT Jr, Kappy MS, Raizada MK. Insulin binds to specific receptors and stimulates 2-deoxy-D-glucose uptake in cultured glial cells from rat brain. J Biol Chem. 1984 Oct 10;259(19):11672-5. PMID: 6384211.
98. Saez I, Duran J, Sinadinos C, Beltran A, Yanes O, Tevy MF, Martínez-Pons C, Milán M, Guinovart JJ. Neurons have an active glycogen metabolism that contributes to tolerance to hypoxia. J Cereb Blood Flow Metab. 2014 Jun;34(6):945-55. doi: 10.1038/jcbfm.2014.33. Epub 2014 Feb 26. PMID: 24569689; PMCID: PMC4050236.
99. Mathieu C, Li de la Sierra-Gallay I, Duval R, Xu X, Cocaign A, Léger T, Woffendin G, Camadro JM, Etchebest C, Haouz A, Dupret JM, Rodrigues-Lima F. Insights into Brain Glycogen Metabolism: THE STRUCTURE OF HUMAN BRAIN GLYCOGEN PHOSPHORYLASE. J Biol Chem. 2016 Aug 26; 291(35):18072-83. doi: 10.1074/jbc.M116.738898. Epub 2016 Jul 8. PMID: 27402852; PMCID: PMC5000057.
100. Vilchez D, Ros S, Cifuentes D, Pujadas L, Vallès J, García-Fojeda B, Criado-García O, Fernández-Sánchez E, Medraño-Fernández I, Domínguez J, García-Rocha M, Soriano E, Rodríguez de Córdoba S, Guinovart JJ. Mechanism suppressing glycogen synthesis in neurons and its demise in progressive myoclonus epilepsy. Nat Neurosci. 2007 Nov;10(11):1407-13. doi: 10.1038/nn1998. Epub 2007 Oct 21. PMID: 17952067.
101. Ashcroft FM, Rohm M, Clark A, Brereton MF. Is Type 2 Diabetes a Glycogen Storage Disease of Pancreatic β Cells? Cell Metab. 2017 Jul 5;26(1):17-23. doi: 10.1016/j.cmet.2017.05.014. PMID: 28683284; PMCID: PMC5890904.
102. Chuquet J, Quilichini P, Nimchinsky EA, Buzsáki G. Predominant enhancement of glucose uptake in astrocytes versus neurons during activation of the somatosensory cortex. J Neurosci. 2010 Nov 10;30(45):15298-303. doi: 10.1523/JNEUROSCI.0762-10.2010. PMID: 21068334; PMCID: PMC2997269.
103. Jakoby P, Schmidt E, Ruminot I, Gutiérrez R, Barros LF, Deitmer JW. Higher transport and metabolism of glucose in astrocytes compared with neurons: a multiphoton study of hippocampal and cerebellar tissue slices. Cereb Cortex. 2014 Jan;24(1):222-31. doi: 10.1093/cercor/bhs309. Epub 2012 Oct 4. PMID: 23042735.
104. Waitt AE, Reed L, Ransom BR, Brown AM. Emerging Roles for Glycogen in the CNS. Front Mol Neurosci. 2017 Mar 16;10:73. doi: 10.3389/fnmol.2017.00073. PMID: 28360839; PMCID: PMC5352909.
105. Duran J, Gruart A, López-Ramos JC, Delgado-García JM, Guinovart JJ. Glycogen in Astrocytes and Neurons: Physiological and Pathological Aspects. Adv Neurobiol. 2019;23:311-329. doi: 10.1007/978-3-030-27480-1_10. PMID: 31667813; PMCID: PMC7315007.
106. Öz G, Seaquist ER, Kumar A, Criego AB, Benedict LE, Rao JP, Henry PG, Van De Moortele PF, Gruetter R. Human brain glycogen content and metabolism: implications on its role in brain energy metabolism. Am J Physiol Endocrinol Metab. 2007 Mar;292(3):E946-51. doi: 10.1152/ajpendo.00424.2006. Epub 2006 Nov 28. PMID: 17132822.
107. Cruz NF, Dienel GA. High glycogen levels in brains of rats with minimal environmental stimuli: implications for metabolic contributions of working astrocytes. J Cereb Blood Flow Metab. 2002 Dec; 22(12):1476-89. doi: 10.1097/01.WCB.0000034362.37277.C0. PMID: 12468892.
108. Choi IY, Seaquist ER, Gruetter R. Effect of hypoglycemia on brain glycogen metabolism in vivo. J Neurosci Res. 2003 Apr 1;72(1):25-32. doi: 10.1002/jnr.10574. PMID: 12645076; PMCID: PMC1471897.
109. Díaz-García CM, Mongeon R, Lahmann C, Koveal D, Zucker H, Yellen G. Neuronal Stimulation Triggers Neuronal Glycolysis and Not Lactate Uptake. Cell Metab. 2017 Aug 1;26(2):361-374.e4. doi: 10.1016/j.cmet.2017.06.021. PMID: 28768175; PMCID: PMC5559896.
110. Swanson RA. Astrocyte glutamate uptake during chemical hypoxia in vitro. Neurosci Lett. 1992 Dec 7;147(2):143-6. doi: 10.1016/0304-3940(92)90580-z. PMID: 1362805.
111. Porras OH, Loaiza A, Barros LF. Glutamate mediates acute glucose transport inhibition in hippocampal neurons. J Neurosci. 2004 Oct 27;24(43):9669-73. doi: 10.1523/JNEUROSCI.1882-04.2004. PMID: 15509754; PMCID: PMC6730152.
112. Jang S, Nelson JC, Bend EG, Rodríguez-Laureano L, Tueros FG, Cartagenova L, Underwood K, Jorgensen EM, Colón-Ramos DA. Glycolytic Enzymes Localize to Synapses under Energy Stress to Support Synaptic Function. Neuron. 2016 Apr 20;90(2):278-91. doi: 10.1016/j.neuron.2016.03.011. Epub 2016 Apr 7. PMID: 27068791; PMCID: PMC4840048.

113. Rangaraju V, Calloway N, Ryan TA. Activity-driven local ATP synthesis is required for synaptic function. Cell. 2014 Feb 13;156(4):825-35. doi: 10.1016/j.cell.2013.12.042. PMID: 24529383; PMCID: PMC3955179.
114. Baxter PS, Hardingham GE. Adaptive regulation of the brain's antioxidant defences by neurons and astrocytes. Free Radic Biol Med. 2016 Nov;100:147-152. doi: 10.1016/j.freeradbiomed.2016.06.027. Epub 2016 Jun 27. PMID: 27365123; PMCID: PMC5145800.
115. De Felice FG, Ferreira ST. Inflammation, defective insulin signaling, and mitochondrial dysfunction as common molecular denominators connecting type 2 diabetes to Alzheimer disease. Diabetes. 2014 Jul;63(7):2262-72. doi: 10.2337/db13-1954. Epub 2014 Jun 15. PMID: 24931033.
116. Belosludtsev KN, Belosludtseva NV, Dubinin MV. Diabetes Mellitus, Mitochondrial Dysfunction and Ca^{2+}-Dependent Permeability Transition Pore. Int J Mol Sci. 2020 Sep 8;21(18):6559. doi: 10.3390/ijms21186559. PMID: 32911736; PMCID: PMC7555889.

ROLURILE INSULINEI ÎN HOMEOSTAZIA GLUCOZEI LA NIVEL NEURONAL ȘI ASTROCITAR

REZUMAT

Identificarea receptorilor pentru insulină pe membrana plasmatică a celulelor creierului este o dovadă fără echivoc că insulina acționează în creier, îndeplinind funcții legate de metabolismul energetic al creierului, dar nu numai. Insulina ar putea facilita cuplarea fluxului sanguin cerebral cu nivelul activității neuronale, expresia unor transportori neuronali și astrocitari de glucoză, captarea glucozei și stocarea acesteia sub formă de glicogen și funcționarea normală a mitocondriilor din aceste celule. Scopul acestei lucrări este de a analiza aspecte privind traversarea barierei hematoencefalice de către glucoză și insulină, substratul energetic utilizat de neuroni și astrocite în condiții de repaus și activare, efectul concentrației sanguine a glucozei asupra transportorilor de glucoză, insulinei, receptorului pentru insulină și metabolismului energetic al creierului. Din această perspectivă, tulburările observate în bolile asociate cu rezistența la insulină a creierului, precum diabetul zaharat de tip 2 și boala Alzheimer, vor fi evidențiate.

Cuvinte cheie: transportori de glucoză, insulină, astrocite, metabolism energetic, diabet zaharat.

SIMPLE ALGORITHM IN MATLAB FOR THE INTERPRETATION OF ANTIBIOGRAMS – PRELIMINARY RESULTS

GABRIEL VINTER[1], DENISA ALEXANDRA VEREȘ[2], FLORIN MUSELIN[1*], BEATRICE ZEMBROD[3], DANIELA CRÎNSIC[3], ALBERT IOIART[3], ALEXANDRU TÎRZIU[3], MIHAI SĂRĂNDAN[4], DAMIAN OLEI[2], DANIEL BONCIOG[2] AND DAVID COMANICIU[3]

[1] University of Life Sciences „Regele Mihai I“ from Timișoara, Faculty of Veterinary Medicine, 119, Calea Aradului, 300645, Timișoara, Romania

[2] Politehnica University of Timișoara, 2 Victoriei Square, RO-300006, Timișoara, România

[3] University of Medicine and Pharmacy ”V. Babeș” Timișoara, 2 Eftimie Murgu Square, 300041, Timișoara, România

[4] Veterinary Sanitary and Food Safety Agency, Arad, 98C, Liviu Rebreanu Street, 310414, România

[*] Address for correspondence: Florin Muselin, PhD, University of Life Sciences „Regele Mihai I“ from Timișoara, Faculty of Veterinary Medicine, 119, Calea Aradului, 300645, Timișoara, Romania; e-mail: florinmuselin@usvt.ro

ABSTRACT

The purpose of this work was to test a simple MATLAB algorithm for the automatic analysis of Kirby-Bauer diffusion technique antibiograms. The experimental setup includes a digital camera connected to a computer for acquisition of the Petri dish images and an algorithm developed in MATLAB for the automatic interpretation of the image data. The workflow data required by this software includes patient identification, sample identification and the list of the antibiotics tested. The growth inhibition area corresponding to each of the antibiotics tested is identified, measured and interpreted automatically by the software which also calculates the results and returns data on the strain’s sensibility to an antibiotic. The results are also presented as a graphical chart ranking the antibiotics based on their efficiency, which simplifies the physician’s task of choosing the proper treatment for the patient. This algorithm represents another fast and cost-effective way for the interpretation of the laboratory bacterial antibiotic resistance test results.

Key words: Kirby-Bauer’s disk diffusion test, MATLAB, automated analysis of antibiogram, anti-microbial resistance

INTRODUCTION

The extensive and often unjustified use of antibiotic treatments in both human and veterinary medicine has led to the emergence of microbial strains resistant to common antibiotics. This evolution is worrisome in the long term because humanity could return to the pre-antibiotic era, when infectious diseases of bacterial etiology generated a significant part of morbidity and mortality in the general population [1]. In order to limit this phenomenon as much as possible, it is necessary to treat infectious diseases caused by bacteria using the antibiotics to which the respective germ is sensitive and of course taking into account the particularities of each patient. Also, the duration of the treatment must be adapted to each individual case, the intention being the sterilization of the infectious lesion.

The antibiogram or the antibiotic susceptibility test is widely used in all microbiology laboratories and completes the bacteriological diagnosis. The most frequently used procedure is the Kirby-Bauer

diffusion method. This method involves the cultivation of the microorganism isolated from the pathological product on the Mueller Hinton Agar medium, and the application of the antibiotics of interest on the Petri dish in the form of commercially available disks impregnated with antibiotics in standardized concentrations. The discs are positioned at equal distances, conveniently chosen so that the inhibition areas are well defined, without overlapping. Antibiotics diffuse freely in the culture medium, their concentration decreases as we move away from the respective disc, and when the minimum inhibitory concentration is reached, the microorganism develops on the rest of the culture medium. In this way, a series of clear, well-defined circular areas are formed, with a diameter proportional to the effectiveness of the respective antibiotic. The rest of the surface of the culture medium remains opaque due to the development of microorganisms.

The evaluation of sensitivity to antibiotics involves the measurement of these diameters and their comparison with standardized values for each individual antibiotic, either manually or with the computer through a data acquisition system. Currently, there are available software applications used for the automatic interpretation of antibiograms. An example is AntibiogramJ, open-source that offers good results, comparable to those given by experienced microbiologists [2,3]. The software application proposed by us has the advantage of being designed in a programming environment with great flexibility, widely accepted by the academic community and which offers the possibility of further development using the artificial intelligence and machine learning tools offered by MATLAB [4].

The potential of artificial intelligence in the field of microbiology is enormous, it will be possible to use genomic, proteomic and metabolomic data which, in association with the data provided by the usual antibiograms, will be able to generate much more accurate predictions regarding antibiotic resistance and certainly the development of effective health policies on long term regarding the management of bacterial infectious diseases [5,6].

EXPERIMENTAL DATA

The experimental device (Fig. 1) consists of a web camera (Selecline model PPW-10) fixed on a stand that allows photographing the Petri dish with the antibiogram on a black background and connected to a computer. The positioning of the plate is done so that one of the antibiotic disks that will be considered disk no. 1 to be positioned as precisely as possible at 9 o'clock on a fictitious clock face. This aspect is very important in the process of identifying antibiotics in the list to be entered in the software application.

Fig. 1. The experimental device for the automatic interpretation of the antibiogram using MATLAB

The raw image is acquired with the open-source YouCam 365 software and is saved in a directory created especially for this purpose, preferably on the computer's D drive. The name under which this image is saved is identical to the one that will be entered in the Sample ID field in the MATLAB application.

The actual application is structured in the form of a main program to which is added the use of some functions that ensure the interface with the user and proper function of software. Figure 2 shows the block diagram.

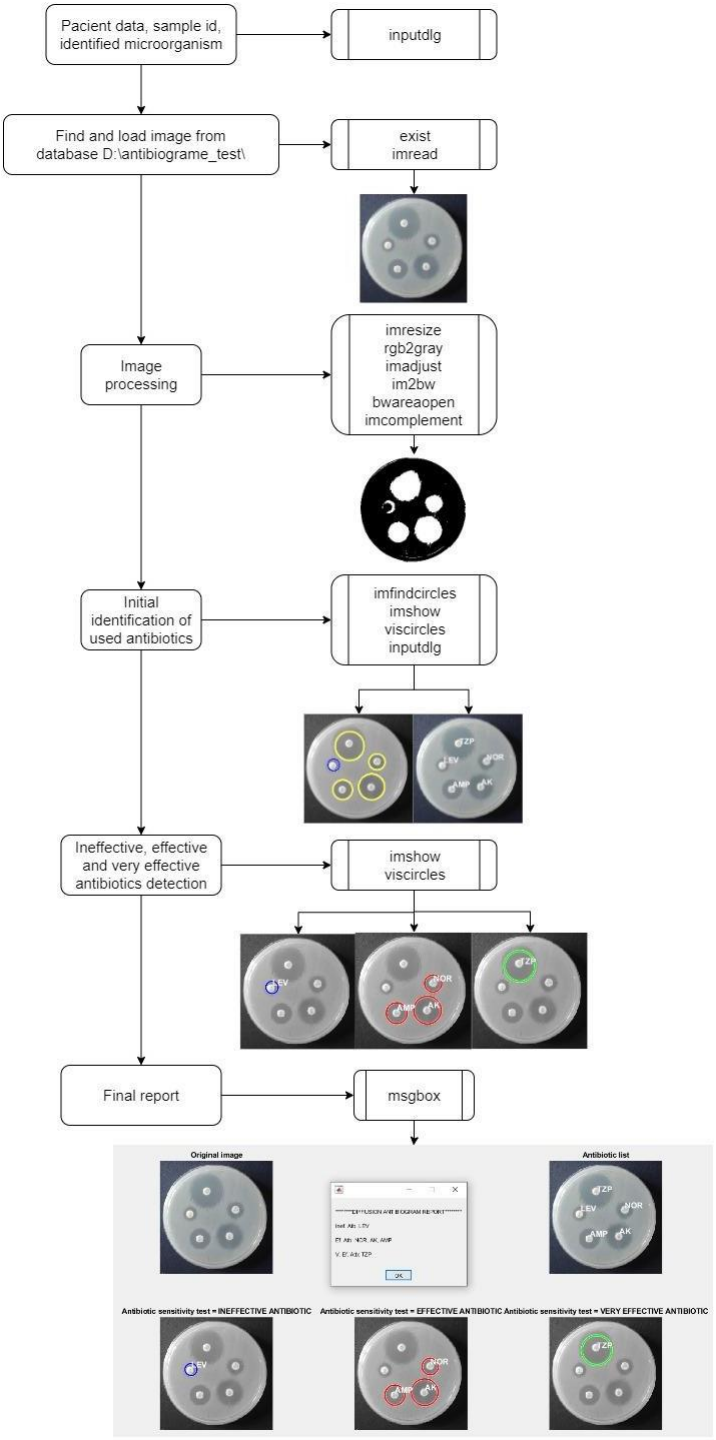

Fig. 2. Block diagram of the software application in MATLAB

In a first step (Fig.3), the identification data of the patient (surname and surname), the data related to the sample number and the pathological germ previously identified through specific microbiological tests (isolation in pure culture on specific media) are entered. The following formally presented instructions are used: userInput = inputdlg(prompt, dlgtitle, dims).

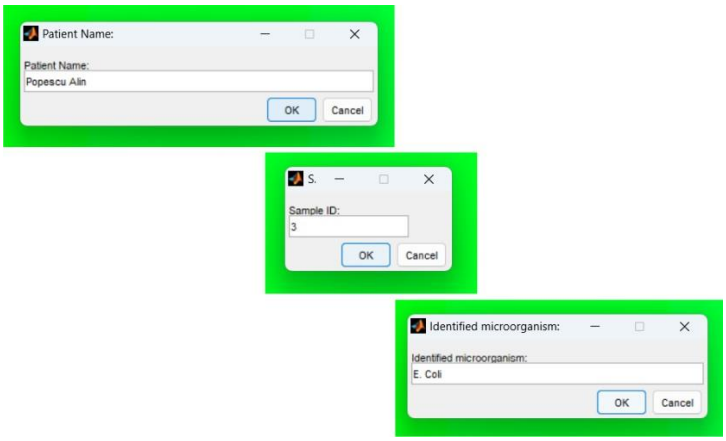

Fig.3. Entering input data into the software application

In order to be able to correctly identify each area of inhibition of the growth of microorganisms, an intermediate stage of processing the original image acquired by the web camera is necessary. The following formally presented instructions are used: imresize, rgb2gray, imadjust, im2bw, bwareaopen, imcomplement. The identification of all the antibiotics (Fig. 4) used will be done starting with the first disc positioned according to the previously mentioned. The following predefined instructions in MATLAB are used: imfindcircles (imag, [Rmin Rmax],'Object Polarity','bright', 'Sensitivity' value,'EdgeThreshold',value); reference Point; angles; [sortedAngles, sortedIndices]; sorted Centers; sortedRadi; viscircles (sorted Centers, sorted Radis,'Edge Color','...'); viscircles (sorted Centers,sorted Radis,'Edge Color','...'); userInput.

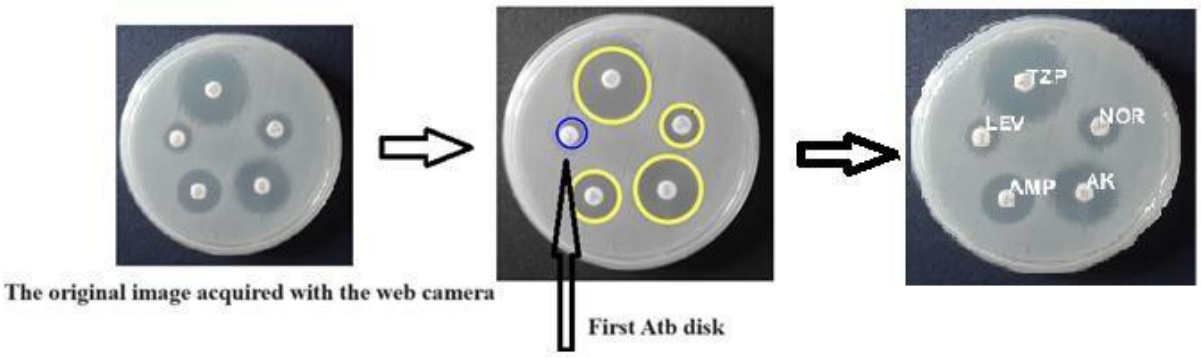

Fig. 4. Identifying the position of the microtablets with the antibiotics to be tested

The last step in the data analysis consists in determining and sorting the radius of the zone of inhibition of the growth zone of microorganisms. Thus, three categories of zones are obtained that correspond to the sensitivity of the microorganism involved to the set of antibiotics considered: ineffective, effective and very effective. The following predefined instructions in MATLAB are used: [Ctrs1,Radi1] = find_antibiotics(Rmin, Rmax, sortedRadi, sortedCenters); viscircles(Ctrs1,Radi1,'EdgeColor','b'); title(sprintf('Antibiotic sensitivity test = INEFFECTIVE ANTIBIOTIC',numel(Radi1))). The result of applying this algorithm is presented in the figure 5.

Fig. 5. The categories of microbial growth inhibition zones depending on their radius

RESULTS AND DISCUSSION

The result of the automatic interpretation of the antibiograms (Fig. 6.) with the proposed software is displayed in a very friendly way for the doctor in the form of an image and saved as a pdf file. The major advantage of this approach is the significant reduction of the time needed to analyze the antibiograms compared to the classic manual method of measuring the zones of inhibition of the growth of microorganisms. The limitations of this software are related to the possible confluence of inhibition areas, the existence of imprecisely delimited or inhomogeneous inhibition zones that raise the suspicion of the existence of several types of microorganisms with different sensitivity to antibiotics. The wider use of deep learning and machine learning methods will contribute decisively to the removal of these limitations.

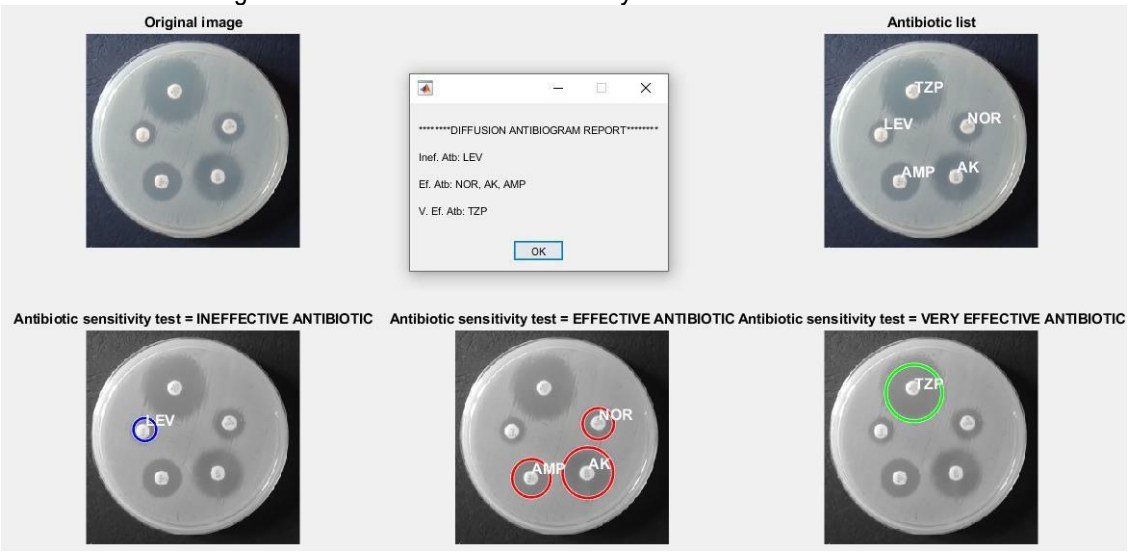

Fig. 6. Presentation of the result of the automatic analysis of antibiograms using the proposed MATLAB software

CONCLUSIONS

Manual analysis of antibiograms is generally a time-consuming process with a degree of subjectivity. The software proposed by us can bring improvements to this process, being useful both in the daily activity of microbiology laboratories and for didactic purposes, being flexible and easy to use and improve. The presentation of the results in a graphic way is more attractive and intuitive for the laboratory doctor and the clinician.

REFERENCES

1. Stamm W, Grayson ML, Nicolle L, Powell M: WHO Global Strategy for Containment of Antimicrobial Resistance (Document no: WHO/CDS/CSR/DRS/2001.2). Geneva, World Health Organization; 2001.
2. Alonso CA, Domínguez C, Heras J, Mata E, Pascual V, Torres C, Zarazaga M. Antibiogramj: A tool for analysing images from disk diffusion tests. Computer methods and programs in biomedicine. 2017 May 1;143:159-69.
3. Costa LF, da Silva ES, Noronha VT, Vaz-Moreira I, Nunes OC, de Andrade MM. Development of an automatic identification algorithm for antibiogram analysis. Computers in biology and medicine. 2015 Dec 1;67:104-15.
4. https://www.mathworks.com/products/matlab.html
5. Pascucci M, Royer G, Adamek J, Asmar MA, Aristizabal D, Blanche L, Bezzarga A, Boniface-Chang G, Brunner A, Curel C, Dulac-Arnold G. AI-based mobile application to fight antibiotic resistance. Nature communications. 2021 Feb 19;12(1):1-10.
6. Anahtar MN, Yang JH, Kanjilal S. Applications of machine learning to the problem of antimicrobial resistance: an emerging model for translational research. Journal of clinical microbiology. 2021 Jun 18;59(7):e01260-20.

ALGORITM SIMPLU ÎN MATLAB PENTRU INTERPRETAREA ANTIBIOGRAMELOR - REZULTATE PRELIMINARE

Rezumat

Scopul acestei lucrări a fost testarea unui algoritm simplu MATLAB pentru analiza automată a antibiogramelor realizate prin tehnica de difuzie Kirby-Bauer. Configurația experimentală include o cameră digitală conectată la un computer pentru achiziția imaginilor plăcilor Petri și un algoritm dezvoltat în MATLAB pentru interpretarea automată a datelor. Softul propus include identificarea pacientului, identificarea probei și lista antibioticelor testate. Zona de inhibare a creșterii microbiene corespunzătoare fiecărui antibiotic testat este identificată, măsurată și interpretată automat de software-ul care, de asemenea, calculează rezultatele și returnează date despre sensibilitatea tulpinii la un anumit antibiotic. Rezultatele sunt, de asemenea, prezentate sub forma unei diagrame grafice clasificând antibioticele în funcție de eficiența acestora, ceea ce simplifică sarcina medicului de a alege tratamentul adecvat pentru cazul respectiv. Acest algoritm reprezintă o altă modalitate rapidă și rentabilă de interpretare a rezultatelor testului de rezistență bacteriană la antibiotice prin tehnica difuziei.

Cuvinte cheie: test de difuziune Kirby-Bauer, MATLAB, antibiograma automată, rezistență antimicrobiană

POSSIBLE ELECTROPHYSIOLOGICAL CHANGES INDUCED BY THE PRACTICE OF PRAYER IN ORTHODOX CHRISTIAN TRADITION

ADRIAN SORIN MIHALACHE[1,2,5], ALEXANDRU PASLARU[1], MARIAN POBORONIUC[3], DĂNUȚ-CONSTANTIN IRIMIA[3], IULIAN STOLERIU[4], LEON ZĂGREAN[1]

[1] "Carol Davila" University of Medicine and Pharmacy, 050474 Bucharest, Romania

[2] Faculty of Orthodox Theology, "Alexandru Ioan Cuza" University of Iași, Romania

[3] Faculty of Electrical Engineering, "Gheorghe Asachi" Technical University of Iaşi, Romania

[4] Faculty of Mathematics, "Alexandru Ioan Cuza" University of Iași, Romania

[5] Medicine and Spirituality Research Center - Providența Hospital, Iași

ABSTRACT

The present study aims to highlight possible changes that the practice of prayer (in the Christian Orthodox Tradition) - PCOT - after a pattern of 30 minutes of daily practice, for 8 weeks - can induce in the electrical activity of the brain. The participants (n=33) were divided into two groups: Study Group (SG), n=16, with an average age of 39.2 years and Control Group (CG) n=17, with an average age of 38.6 years). The Study Group included Orthodox Christian faithful who do not pray daily, being trained in a 3-hour session on the psycho-emotional, behavioural and spiritual specifics of PCOT. No intervention was performed on the subjects of the Control Group. The study included, before and after the period of 8 weeks of daily practice of PCOT, EEG measurements according to a measurement protocol. Applying the Wilcoxon signed rank test revealed significant differences in median value in the case of SG subjects, pre/post-experience, in the alpha and gamma2 registers, but not in the beta and gamma1 registers. Further research and changes in the experimental design are needed so as to allow for more accurate assessments. Results are discussed in the context of similar studies, highlighting some specific limitations of studies that evaluate the physiological changes induced by spiritual/religious experiences, especially of those that use EEG, while also formulating some recommendations for increasing the methodological quality of future studies.

Keywords: Orthodox Christian prayer, EEG changes, alpha, gamma, beta frequency spectrum

1. GENERAL OBJECTIVE AND WORKING HYPOTHESES

In the present study we aimed to highlight possible changes in the electrical activity of the brain, in the case of some subjects who practice PCOT (prayer in the Christian Orthodox tradition). The research focused on three interconnected studies, which constitute the research section of the PhD paper The Neurosciences of Spiritual Life, defended at UMPCD in July 2023.

The general objective of the research was to highlight possible changes induced by the practice of Christian prayer, in the Christian Orthodox Tradition, through three different measurements (psychometric tests, the levels of some salivary markers and the inventory of changes in the electrical activity of the brain through EEG). In the first study, which inventoried the physiological changes in the table of some salivary markers, respectively [1]: Cortisol, Salivary Alpha Amylase (sAA), Immunoglobulin A (IgA), Oxytocin, Testosterone and cytokines interleukin 6 (IL-6) and interleukin 8 (IL-8), measurements showed a statistically significant decrease in Salivary Cortisol and an increase in IL-6 in Study Group (SG) subjects at post-testing relative to levels measured at pre-testing, suggesting that PCOT may ameliorate the physiological response to stress and the inflammatory response. No statistically significant results were obtained in other salivary markers. The second study, related to psychometric measurements [2], revealed significant results, regarding the subjects in SG at post-testing, regarding item a3 ("fears/phobias"), from the Hamilton scale and the change that appeared in SG at post-testing regarding item a14 ("appraisal of anxious mood at interview"), suggesting a possible influence of PCOT practice.

The general objective of the third research study was to highlight the possible changes in the alpha, beta and gamma register that appeared as a result of the PCOT practice. The general working hypothesis is that PCOT practice for 8 weeks (30 min./day) will produce changes in the electrical activity in these three registers.

The electroencephalogram (EEG) is a non-invasive evaluation that detects, enhances and records the bioelectrical activity of the brain. The study includes measurements of alpha, beta and gamma rhythms. The alpha (α) rhythm represents the background electrical activity of the brain in a normal subject during a state of wakefulness and psychosensory rest. The frequency of the alpha (α) rhythm ranges between 8 and 13 Hz. The beta (β) rhythm is the electrical expression of a brain in a state of activity. It has a fast frequency ranging between 14 and 30 Hz. Gamma (γ) waves are high-frequency neural oscillations typically associated with cognitive functions such as memory, attention, and perception. In terms of

electroencephalography (EEG), gamma waves generally have a frequency range of approximately 30 to 100 Hz. The presence and modulation of gamma activity in the EEG can provide insights into various cognitive processes and are often studied in the context of neuroscience and psychology. The Gamma1 (γ_1) sub-band is usually considered to have a frequency range of approximately 30 to 60 Hz. The Gamma2 (γ_2) sub-band typically covers frequencies above 60 Hz, extending up to 100 Hz or more.

To test this hypothesis, we formulated four working hypotheses, which we detail below.

PCOT practiced 30 min./day, for 8 weeks triggers:

- the increase in brain electrical activity in the alpha frequency spectrum in SG subjects, highlighted by the level measured in post-testing compared to the level measured in pre-testing (Hypothesis 2.1). Subsequently, we also formulate the hypothesis according to which the mean differences in the frequencies in the alpha register, between SG and Control Group (CG) (calculated by subtracting from the mean value obtained after the experience, the mean value before the experience, for each individual group), are statistically significant (Hypothesis 2.1. 1);

- an increase in cerebral electrical activity in the beta frequency spectrum in SG subjects, highlighted by the level measured post-testing compared to the level measured pre-testing (Hypothesis 2.2). Subsequently, we also formulate the hypothesis according to which the mean differences in the beta frequency spectrum, between SG and CG, are statistically significant (Hypothesis 2.2.1);

- increase in cerebral electrical activity in the gamma1 frequency spectrum in SG subjects, highlighted by the level measured post-testing compared to the level measured pre-testing. (Hypothesis 2.3). Subsequently, we formulate the hypothesis according to which the mean differences in the gamma1 frequency spectrum, between SG and CG, are statistically significant (Hypothesis 2.3.2);

- the increase of cerebral electrical activity in the gamma2 frequency spectrum in SG subjects, highlighted by the level measured post-testing compared to the level measured pre-testing (Hypothesis 2.4). Subsequently, we formulate the hypothesis according to which the mean frequency differences in the gamma2 frequency spectrum, between SG and CG, are statistically significant (Hypothesis 2.4.1).

Finally, the last two hypotheses concern possible changes induced by PCOT, 30 min. daily for 8 weeks in the electrical activity in the prefrontal region (Ch1 – FP1, Ch2 - FPz, Ch3 – FP3, see Fig. 1), in all four registers (alpha, beta, gamma1 and gamma2), among subjects from SG, compared to the evolution in the interval between the pre- and post-testing moments. For this, we follow a comparison between the median SG and that of CG, for the first three channels. For this, we formulate the following hypothesis:

- PCOT 30/8 triggers changes in electrical activity, in all registers, post-testing, compared to the time of pre-testing (Hypothesis 3.1);

- at the time of post-testing, the median of SG subjects is different among SG subjects (Hypothesis 3.2).

Implicitly, we shall also investigate the possible changes that appear in the interval between pre- and post-testing, among the subjects in the CG, in all four registers, in the first three channels (Ch1 – PF1, Ch2 – PFz, Ch3 – PF2).

2. PARTICIPANTS AND METHODS

In this study, subjects that had participated in the two previous studies were included [1,2].

EEG recordings were performed in two stages, pre- and post-testing, before and after the 8-week experimental interval (individual PCOT) intended for the subjects in SG.

Electrical brain (EEG) and cardiac activity was recorded using the g.USBamp biosignal amplifier and brain-computer interface system (g.tec medical engineering GmbH, Graz, Austria) with 16 channels of signals being simultaneously sampled at a maximum frequency of 37.4 kHz at 24-bit resolution.

12 EEG reference leads derivations were recorded with active electrodes in positions FP1, FP2, FPZ, FT7, FT8, FC3, FC4, Cz, P3, P4, O1, O2 and the reference on the left mastoid process (Fig. 1), using electrodes with g.LadyBird gel (g.tec medical engineering GmbH) and a bipolar ECG lead (D1 lead) using special wet electrodes for ECG recordings.

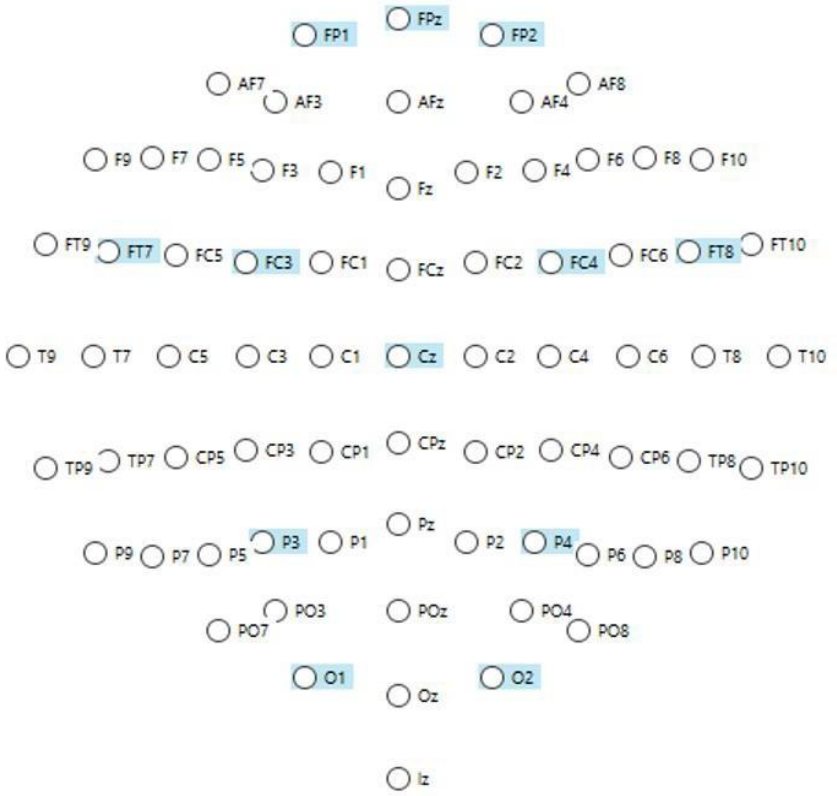

Fig. 1 The layout of the electrodes on the scalp of the subjects was done according to the international 10-20 system.

Electrophysiological recordings were performed in a quiet room without background noise, having a constant temperature of approx. 21℃. After attaching the electrodes, the subjects were placed in a comfortable chair with the backrest in front of a white wall.

Electrophysiological recordings in Stages II and Stage V of the research followed a 10-interval (EEG Measurement Protocol) sequencer, in the order presented in the EEG Measurement Protocol Intervals (Table 1).

Interval 1	Interval 2	Interval 3	Interval 4	Interval 5	Interval 6	Interval 7	Interval 8			Interval 9	Interval 10
							Cold Pressure/EGS				
Base line Eyes Open (BLEO1)	Base line Eyes closed (BLEC1)	PERSONAL EXPERIENCE (PE)	Base line Eyes Open (BLEO2)	Base line Eyes closed (BLEC2)	Image Visualisation (VI PHOTO)	Base line Eyes Open (BLEO3)	Hand IN	PAIN	Hand OUT	Base line Eyes Open (BLEO4)	Base line Eyes closed (BLEC3)
2 min.	2 min.	12 min.	2 min.	2 min.	2 min.	2 min.	3 min.			2 min.	2 min.
At this stage, the subjects were asked to look at a white wall and relax, without thinking about anything in particular.	At this stage, the subjects were asked to close their eyes and relax, without thinking about anything in particular.	At this stage, the subjects were asked to proceed with the personal experience. In this phase, CG subjects were instructed to think of a person they are fond of (either from childhood or present), while SG subjects practiced, during the same interval, PCOT in a way similar to that of the experimental intervention period. Participants were instructed that the laboratory staff, who measured the EEG activity, did not know which group the subjects belonged to.	At this stage, the subjects were asked to look at a white wall and relax, without thinking about anything in particular.	In this stage the subjects were asked to close their eyes and relax, without thinking about anything in particular.	In this stage the subjects were asked to look at a photograph.	In this stage the subjects were asked to look at a white wall and relax, without thinking about anything in particular.	At this stage they were asked to insert a hand into a bowl of cold water at -4^{o} C, up to the wrist. They were told to keep their hand in the water as long as they could and to signal (by verbally announcing) when they felt pain. They were told to remove their hand from the water when the pain was unbearable.			At this stage, the subjects were asked to look at a white wall and relax, without thinking about anything in particular.	At this stage, the subjects were asked to close their eyes and relax, without thinking about anything in particular.

Table 1 EEG Measurement Protocol Intervals.

During the base line - eyes open intervals (1, 4, 7 and 9) the subjects were asked to remain relaxed, with their eyes open, without thinking about anything specific. During the base line - eyes closed intervals (2, 5, and 10), subjects were at rest with their eyes closed, instructed to remain relaxed, without thinking about anything specific.

In interval 3 (personal experience) the laboratory team, not knowing the composition of CG and SG, made no reference to PCOT. Laboratory personnel were instructed to guide subjects to settle into the personal experience without specifying its nature. The volunteers from the two groups, CG and SG, were instructed to do the following when prompted that "personal experience follows":

- CG subjects thought of a loved one/pleasant childhood experience;
- subjects from SG practiced, without written support, PCOT, without mentioning the specifics of their activity.

In interval 6 (photo), the subjects in the two groups were projected, on the white wall in front, a photograph (Photo 1), with the help of a video projector. The photograph was viewed by the subjects for 2 min. In post-testing, under similar conditions, the subjects looked at another photo for 2 minutes (Photo 2).

Photo 1 (Ahmet Sik via Getty Images)

In Stage I (pre-testing), participants from SG and CG were shown Photo 1 on a frontal white wall for 2 minutes, during which EEG recordings were made.

Photo 2 (Pixabay, 2019)

In Stage V (post-testing), participants from SG and CG were shown Photo 2 on a frontal white wall for 2 minutes, during which EEG recordings were made.

3. SELECTION OF PHOTOS

The photos were chosen from a set of six initial photos following a selection based on the following criteria:

- content without relevance to the personal life of the subjects;
- emotional valences;
- stimulation/request of empathy.

From a set of six photos with similar content, 36 people (who were not part of the CG or SG), aged between 18 and 55, gave scores on a scale of 1 (a little impressive) to 5 (very impressive). Among the evaluated images, the photos with the closest score were selected for the present research, respectively Photo 1, for the pre-test measurements and Photo 2 for the post-test measurements.

For interval 8 of the EEG Measurement Protocol (cold pressor test), a 20 cm diameter cylindrical vessel was prepared with a mixture of water and ice, being maintained at 4℃. The subjects had to put their right hand in, up to the wrist, and report when pain started; then they were to remove their hand from the water when the pain became too much. These events were marked by the technician as specific events on the electrophysiological recordings.

In all of these steps, from the EEG measurement Protocol, the subjects in the two groups were guided in the same way, by the technician, who assisted all the electrophysiological recordings.

Two sets of electrophysiological recordings, which took place in two periods: April 2019, and subsequently May-June, pre-test and, after the 8 weeks of practice of personal experience (PCOT), post-testing, were performed.

4. EEG DATA COLLECTION

For the recording and processing of brain electrical activity, we used a high-performance and precision biosignal g.USBamp amplifier (g.tec medical engineering GmbH). The device allows the recording of physiological activity from the brain, eyes, heart, including respiration, galvanic skin response, temperature and other physiological and physical parameters. Due to its technical specifications and extensive software environment, the device is widely used for neuropsychological and physiological explorations and measurements.

The device used in the research is USB-compatible and supports 16 biosignal channels sampled simultaneously with a frequency of up to 37.4 kHz at 24-bit resolution. A total of 4 independent ground ports ensure that there is no interference between recorded signals. Digital inputs and outputs allow the measurement of trigger channels along with biosignal channels to easily transmit analysis results to external devices.

The g.USBamp system offers the possibility of detecting external events ('triggers') and correlating EEG data with information from sensors (in the case of our study, the one provided for the galvanic response of the skin). The data recorded in real time were saved and later processed by means of a dedicated software, gBSanalyze.

5. PROCESSING OF RECORDED DATA

The signals taken from the biosignal amplifier g.USBamp were dealt with in advance so as to eliminate measurement noises (e.g. data filtering), but also to visually examine the recordings, to eliminate the recording fragments compromised due to noises. A paradigm is used to correlate the characteristic results extracted from the EEG signal with external events. The processing also ensured the extraction of the essential characteristics of the EEG signals in various frequency bands (exemplified, with a Simulink&Matlab program, in Fig. 2).

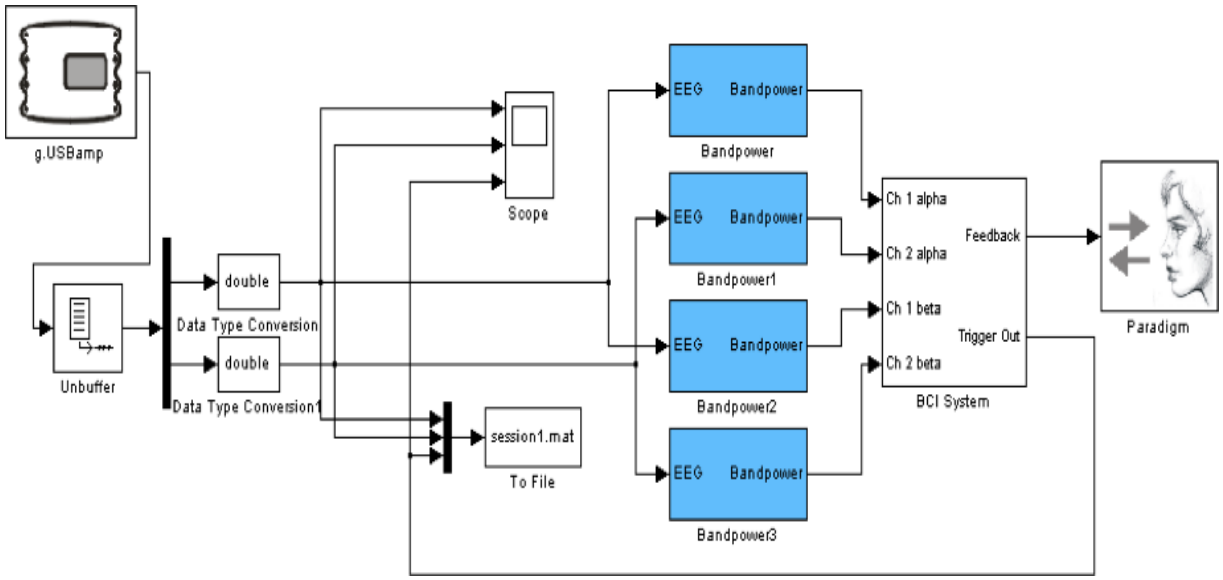

Fig. 2 Matlab Simulink program for extracting features in the field of alpha and beta frequencies.

The processing of the recorded signals was done with g.Bsanalyze (g.tec medical engineering GmbH), an interactive software for multimodal processing and analysis of biosignals in the fields of clinical research, which includes a multitude of functions, such as topographic diagrams or filters of different types (Fig. 3).

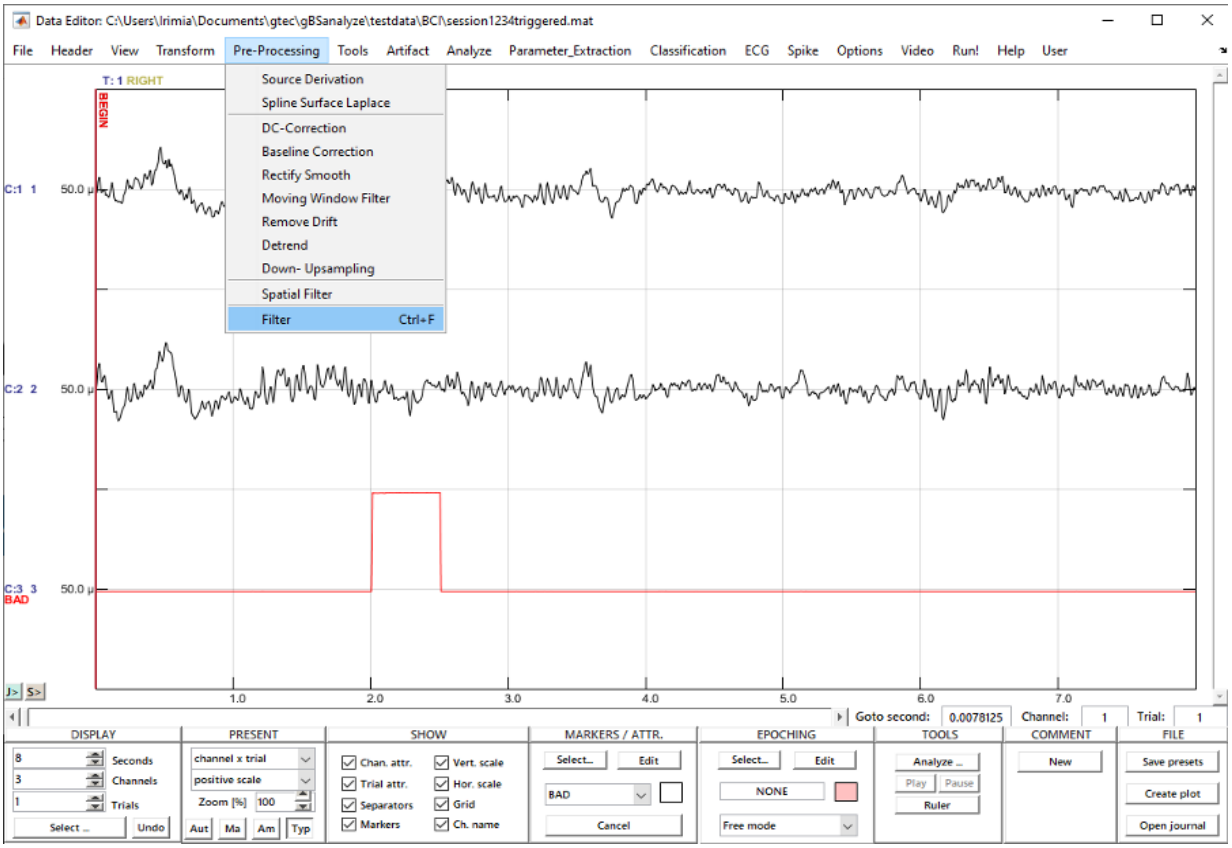

Fig. 3 The g.BSanalyze software main interface.

The files were saved in "*.hdf5" format, collecting a number of 2 files for each subject from CG and SG, with the recordings of the paradigm (EEG measurement protocol) in the Phase I of the research, pre-test, before the 8 weeks of PCOT experience, and a second post-test file after the completion of the experimental period in Phase V of the research.

For each of the 10 intervals of the paradigm (the EEG measurement protocol), "triggers" were provided to mark the beginning moment. The data were recorded working with a sampling frequency of 512 Hz. After the recordings, the acquired data were visually examined, with noise-compromised sequences removed from the final determinations (Fig. 4).

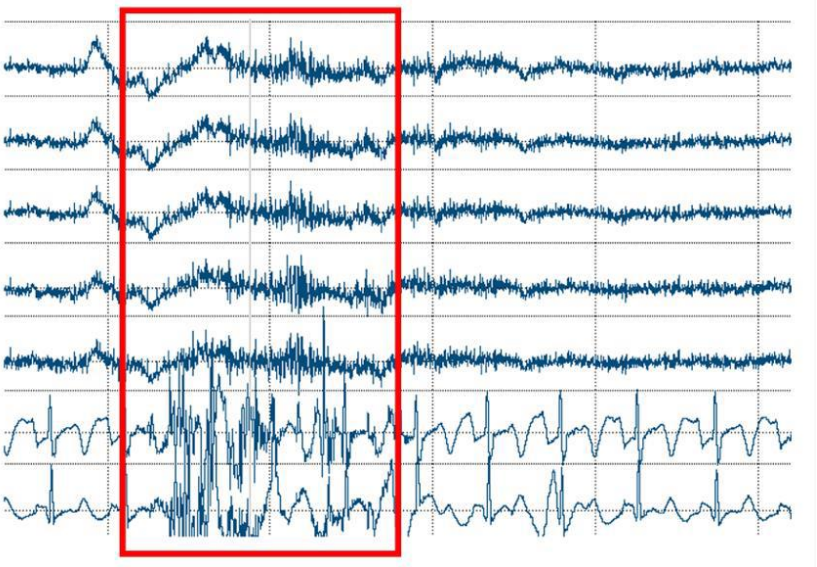

Fig. 5 Biosignal fragment affected by noise, identified by visual examination, and removed from the final

determinations.

Each file, with data acquired through EEG measurements in the 10 intervals in the paradigm, contains recordings made on the 14 channels (there is an example in Fig. 6).

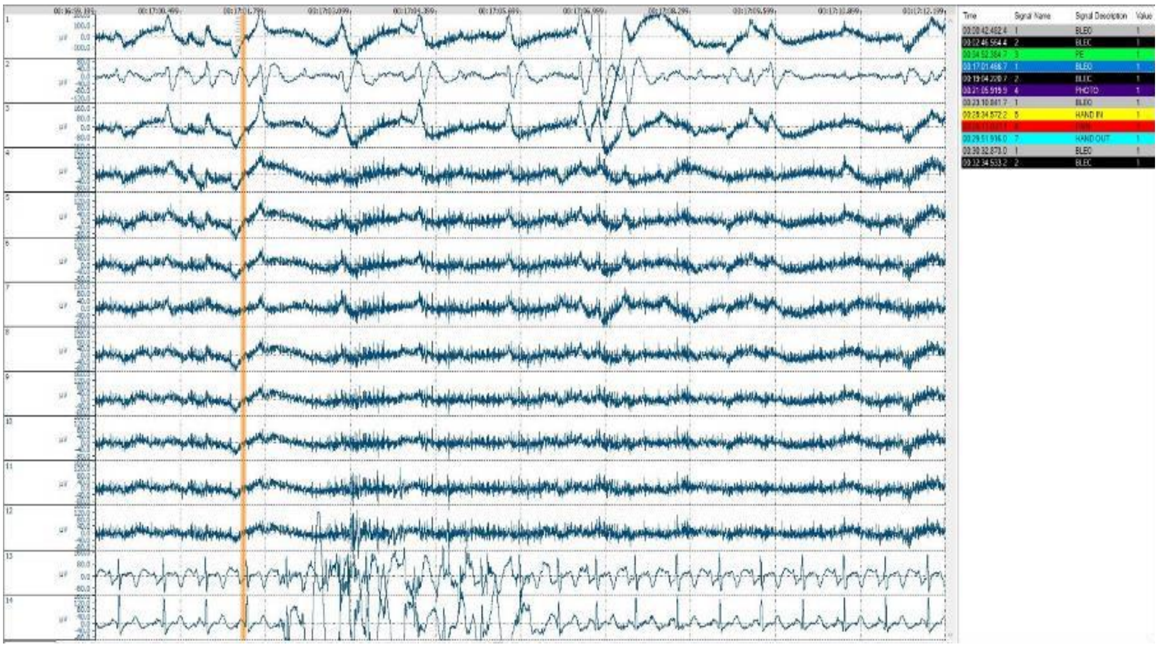

Fig. 6 Display (time segment of 13 sec.) of the 14 channels, highlighting the moments of occurrence of the triggers (on the right of the figure) that mark the activities included in the 10 stages of the paradigm.

Primary data

The processing of the recorded signals provided numerical primary data, entered in Excel tables.

Beta	Ch12	13,95170539	4,683869569	5,171
	Ch1	3,257571764	2,911450501	3,484
	Ch2	2,725716943	2,005591265	1,856
	Ch3	3,36553379	2,80694879	2,66
	Ch4	2,486052524	1,681388687	1,630
	Ch5	2,549536485	1,631414344	1,832
	Ch6	5,711809682	4,789874881	4,932
	Ch7	8,385156864	6,192530759	5,204
	Ch8	2,816874092	1,982565563	1,968
	Ch9	2,518778864	1,620793103	1,503
	Ch10	2,459850861	1,653206402	1,662
	Ch11	4,90272519	1,353404238	1,248
Gamma1	Ch12	3,214421363	1,061095882	1,098
	Ch1	5,098588183	4,587115647	5,784
	Ch2	4,441062566	3,184426978	3,541
	Ch3	5,744519192	4,761785243	4,977
	Ch4	3,802428344	2,93190946	2,484
	Ch5	3,460432495	2,569315194	2,453
	Ch6	14,85860051	12,85181894	13,09
	Ch7	24,8125077	20,01684086	19,21
	Ch8	4,385035666	3,456361506	3,241
	Ch9	3,081165689	2,271273405	2,038
	Ch10	3,730676394	2,836504244	2,631
	Ch11	4,12777894	1,931595695	1,759
Gamma2	Ch12	3,521645714	1,777710779	1,63
		BLEO1		

Fig. 7 The primary data, in the form of numerical values corresponding to the signals in the Gamma1 and Gamma2 register. The extracted fragment represents the first two sets of interval 1 (eyes open – BLEO 1), for all channels (Ch1 – Ch12 – sensors) for one of the subjects, at the time of pre-testing.

	Ch11	4,12777894	1,931595695	1,759773873	2,070363193	2,473822297	3,950078894	2,23281339	2,134340789
Gamma2	Ch12	3,521645714	1,777710779	1,63526645	2,167232272	2,851907318	5,422050453	3,321595079	2,745920536
		BLEO1				BLEC1			

Fig. 8 For each of the 10 intervals, the processing of the recorded data provided a series of numerical values (one to four). In the extracted table fragment, there are 4 numerical values corresponding to channels 11 and 12 (Ch 11 and Ch

12), during Intervals 1 (eyes open - BLEO1) and 2 (eyes closed - BLEC 1) of the Measurement Protocol, at one of the subjects, at the time of pre-testing.

6,057868529	6,371875357	7,148062192	6,183514529
8,07246002	7,764558852	6,663499085	6,272563162
9,189913998	9,247273595	10,05816569	9,127158491
PHOTO			

Fig. 9 Fragment of primary data table with 4 numerical values corresponding to the signals in the Gamma2 register, captured by sensors 11, 12 and 13, during Interval 6 of the Measurement Protocol (PHOTO), in one of the subjects, at the time of pre-testing.

26,37880455	11,40082372	58,73210054
33,65674026	18,37019707	61,26669895
HandIN	PAIN	HandOUT

Photo 7.5.4 For some of the intervals provided in the Measurement Protocol, only a single numerical value was available, which will limit the statistical analysis of the data and the comparative evaluation pre- and post-testing, intra-group and inter-group. In the extracted fragment there are the numerical values corresponding to the HAND IN, PAIN and HAND OUT subintervals of Interval 8 - Cold Pressure/EGS, for sensors 11 and 12, in one of the subjects, during pre-testing.

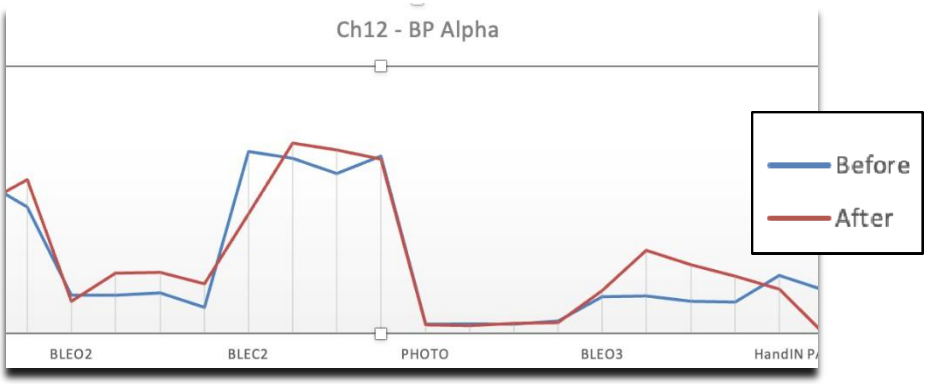

Fig. 10 In addition to the numerical values, the primary data contain graphs corresponding to these values, for each individual sensor. The extract shows a fragment of the graph corresponding to the electrical signals recorded in the alpha band, for intervals 4, 5, 6, 7, and 8 of the Measurement Protocol, for sensor 12, in one of the subjects, during pre-testing.

Such recordings were made for all 4 frequency bands (Alpha, Beta, Gamma1 and Gamma2), for all 12 channels (12 sensors), for each subject in CG and SG, throughout the 10 Intervals of the Protocol EEG measurement, pre-testing and post-testing, respectively.

6. STATISTICAL ANALYSIS TOOLS

The tools used for the statistical analysis of the primary data are non-parametric tests for the median (Wilcoxon signed-rank test), t-tests for paired data, and bar charts with S.E.M. (Standard Error of the Mean). Non-parametric tests were used for data that did not meet the normality requirement for using the corresponding parametric tests.

(a) *The median* and *the mean* are two statistical indicators of central tendency for a set of statistical data. If the observed data have a small volume (usually below 30-40), tests for the mean (called parametric tests) are not relevant, since the statistical assumptions under which they operate are not achieved. That is why, for the present situation, we used alternative tests (called non-parametric) for the median. However, the latter is a better indicator of the central tendency of the data (compared to the mean) in case of asymmetric data.

(b) *The Wilcoxon signed-rank test* is a non-parametric test for statistical hypothesis testing used to compare the locations of two populations using two matched samples.

(c) *The t-test for paired data* is a statistical technique that is used to compare two population means in the case of two samples that come in pairs.

(d) *Bar charts* are bar representations of numerical values for the levels of a category characteristic. Levels are represented on the horizontal axis of the chart and values are represented on the vertical axis. Each category value corresponds to a bar, and the height of each bar corresponds (or is proportional to) to the magnitude of the value. To allow an easy comparison of the values, the bars are represented in the same graph, of equal thicknesses (chosen by the user), without being glued together.

(e) *S.E.M.* (*Standard Error of the Mean*) is the standard deviation (or root mean square error) of the sample mean. This is a measure of the precision (or variability) for an estimated mean of a statistical population characteristic. S.E.M. value indicates how far a sample mean is likely to be from the population mean, using the original units of measurement. For a volume data set, $S.E.M. = \frac{s}{\sqrt{n}}$ where *s* is the standard deviation for a single data value.

7. STATISTICAL ANALYSIS OF EEG DATA AND INTERPRETATION OF RESULTS

EEG measurements were valid for 30 volunteers grouped into two groups (GS - 16, and GC - 14). Acquired data: 12 channels, 4 frequencies (α, β, γ_1 and γ_2), corresponding to a number of 12 moments (which include the mentioned 10 stages, to which is added the moment of inserting the hand into the water and that of withdrawing the hand from the water, within the range of cold pressor tests).

The BLEO1, BLEC1, PE, BLEO2, BLEC2, VI FOTO, BLEO3, BLEO4 and BLEC3 features have 4 values each, and the HAND IN, PAIN and HAND OUT features have a single value each (See Table 1 EEG Measurement Protocol Intervals). For this data set, there are no missing values. In all these tests, E1 - E16 represent the experimental group (SG) volunteer subjects, and N17 - N30 denote the CG subjects.

To test the working hypotheses of this study, we performed a first test, using the Wilcoxon signed-rank test, with which we compared each of the four bands, taking into account the signals recorded by all channels at once, to highlight changes in the CG and SG subjects medians, pre- and post-experience.

In this regard, we pursued an analysis of the data corresponding to each subject before the experience, in comparison with the data obtained post-experience, after the 8 weeks of PCOT practice. For each volunteer (from both groups) and for each of the α, β, γ_1 and γ_2 frequencies, the mean value of the 12 channels was calculated. Then, the Wilcoxon signed-rank test was used to check whether there were statistically significant differences in the central values corresponding to each frequency (α, β, γ_1 and γ_2) before and after the experiment[1].

The hypotheses of the Wilcoxon signed-rank test are:

(H_0): the median of the differences (for all subjects) between the two data sets is zero (or, equivalently, the two sets have the same median value).

(H_1): the median of the differences (for all subjects) between the two data sets is not zero. Table 2 shows the P-values for all these tests. P-values written in color font correspond to statistically significant differences in the median value before and after the experiment (the significance level is α = 0.05).

[1] For this stage, the paired data t-test, which compares the mean values of the matched data (data collected in pairs, usually before and after an experiment), was not chosen, as this t-test is based on the assumption that the data are normally distributed, condition which is not met here. Instead, the Wilcoxon signed-rank, non-parametric test for matched or paired data was used. This test compares the median values of two matched data sets, not their mean values. When the data are symmetrical, the median and mean values coincide.

P-values	α	β	γ_1	γ_2	P-values	α	β	γ_1	γ_2
E_1	0.2142	0.0019	0.0152	0.1849	N_{17}	0.0351	0.2301	0.0102	0.0006
E_2	0.0351	0.0016	0.0000	0.0000	N_{18}	0.2194	0.0430	0.4264	0.8233
E_3	0.6755	0.7588	0.4345	0.9001	N_{19}	0.0000	0.0000	0.0000	0.0002
E_4	0.8560	0.8342	0.8890	0.0339	N_{20}	0.1992	0.1282	0.5959	0.6154
E_5	0.0430	0.0050	0.9777	0.3869	N_{21}	0.0811	0.0003	0.0003	0.0014
E_6	0.0430	0.0005	0.0006	0.0001	N_{22}	0.0000	0.0000	0.3946	0.1318
E_7	0.0305	0.1506	0.0000	0.0001	N_{23}	0.0031	0.0001	0.0003	0.0031
E_8	0.0010	0.0275	0.0037	0.0035	N_{24}	0.0001	0.0000	0.0001	0.0011
E_9	0.5209	0.0077	0.0000	0.0001	N_{25}	1.0000	0.0003	0.0042	0.3793
E_{10}	0.0046	0.0004	0.0000	0.0000	N_{26}	0.0577	0.9001	0.8780	0.4264
E_{11}	0.0000	0.0507	0.9111	0.9777	N_{27}	0.0023	0.9777	0.3946	0.3570
E_{12}	1.0000	0.0177	0.0635	0.0295	N_{28}	0.8780	0.0001	0.0000	0.0002
E_{13}	0.4595	0.0475	0.0389	0.0559	N_{29}	0.4595	0.0913	0.0524	0.0913
E_{14}	0.1318	0.0065	0.0019	0.0028	N_{30}	0.1055	0.1391	0.2583	0.1214
E_{15}	0.0000	0.8560	0.0032	0.0000	---	---	---	---	---
E_{16}	0.0000	0.0000	0.0017	0.0316	---	---	---	---	---

Table 2 P-values for the Wilcoxon signed-rank test for the medians of each frequency. Volunteers E1-E16 are from EG, N17 - N30 are from CG.

In order to test the working hypotheses 2.1, 2.2, 2.3 and 2.4 (PCOT practiced for 30 min./day, in 8 weeks causes an increase in brain electrical activity in the alpha, beta, gamma1 and gamma2 register, in SG subjects), we used the Wilcoxon signed-rank test, searching for significant differences in median value for SG subjects occurring between pre- and post-experience time points. For each given frequency (α, β, γ_1 or γ_2), the mean value of the frequency within the SG, for all time points, was calculated. Then, it was tested whether there were significant differences in the mean value before and after the experiment. The corresponding P-values for the Wilcoxon signed-rank test are:

$$P_\alpha = 0.0001,\ P_\beta = 0.9111, \qquad P_{\gamma_1} = 0.1085,\ P_{\gamma_2} = 0.0015.$$

Significant differences (at significance level 0.05) in the medians (before and after the experiment, within the SG) are noticed for the α and γ_2 frequencies, confirming working hypotheses 2.1 and 2.4. Working hypotheses 2.2 and 2.3 are not confirmed.

Figure 11 shows the mean frequency values within the SG (at all times). Figure 12 shows the total mean values ± S.E.M. of the four frequencies [2].

[2] Here, and in the subsequent situations, total mean value is the mean of all means of the frequency group, considered in all moments.

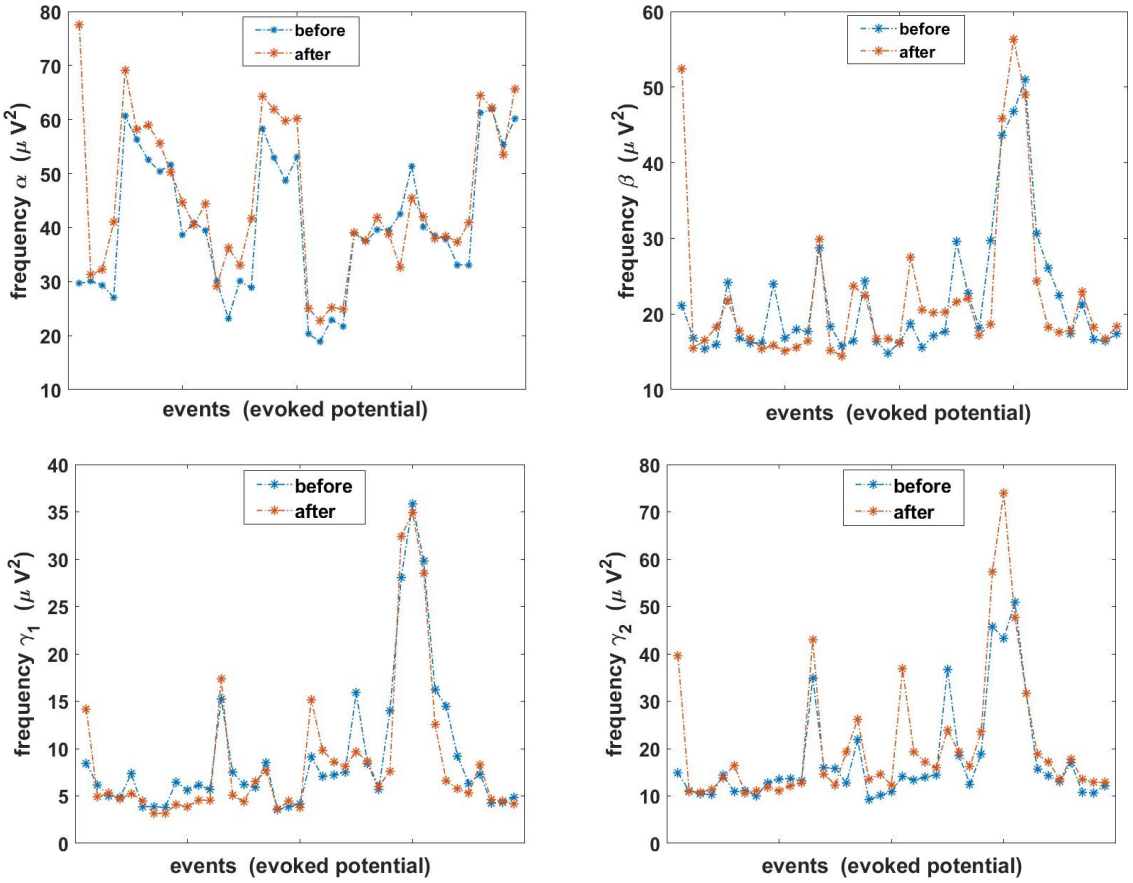

Fig. 11 Mean values for each frequency in SG before and after the experiment.

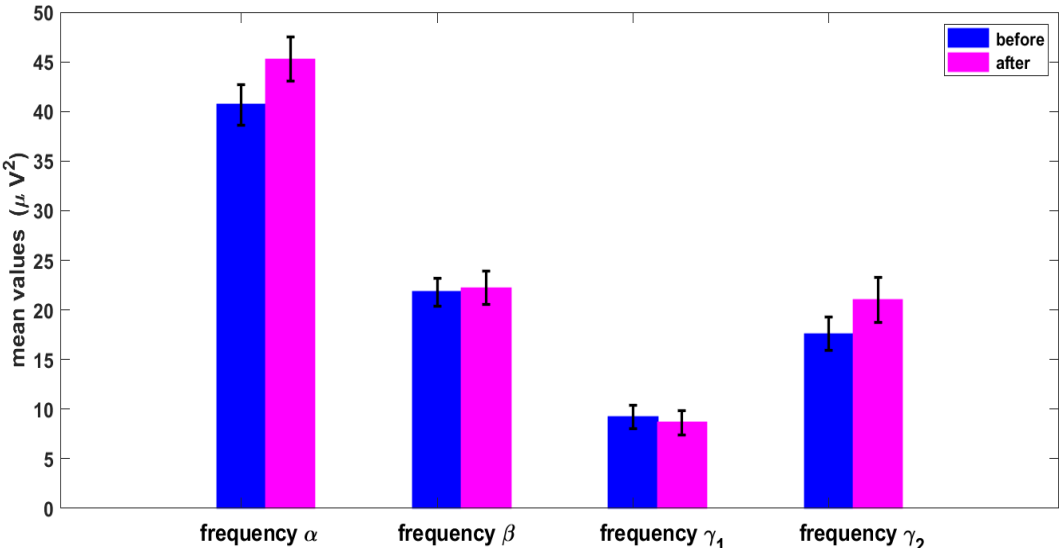

Fig. 12 Mean values ± S.E.M. of the four frequencies on all channels (SG).

Within the same hypothesis, we analysed the presence of statistically significant changes in CG as well. For this, we used the Wilcoxon signed-rank test to check for significant differences in median value in CG subjects, comparing pre/post-experience. For each given frequency (α, β, γ_1 or γ_2) measured in subjects in the Control Group, we repeated the same

procedure. We calculated the mean value of the frequency within the group, for all time points, then tested whether there were significant differences in the mean value before and after the experiment. As a result, we obtained, for the four registers, the P-value corresponding to the Wilcoxon signed-rank test:

$$P_{\alpha} = 0.0000, \qquad P_{\beta} = 0.0091, \qquad P_{\gamma_1} = 0.5300, \qquad P_{\gamma_2} = 0.2468.$$

The results show significant differences in the medians (within the CG), for the α and β frequencies, a result that suggests that the CG subjects also showed an improvement in their condition in the pre - post-testing interval, even if no experimental intervention was performed on them. These results correlate with those of Study 1 (Chapter 6), which revealed an improvement in anxiety levels (on the Hamilton scale) recorded during post-testing for CG subjects. Since the CG subjects showed an increase in electrical activity in the alpha register, it cannot be said with certainty that the increase in brain activity in the alpha register in the SG subjects was caused by PCOT. Figure 13 displays the mean frequency values within the CG (at all times).

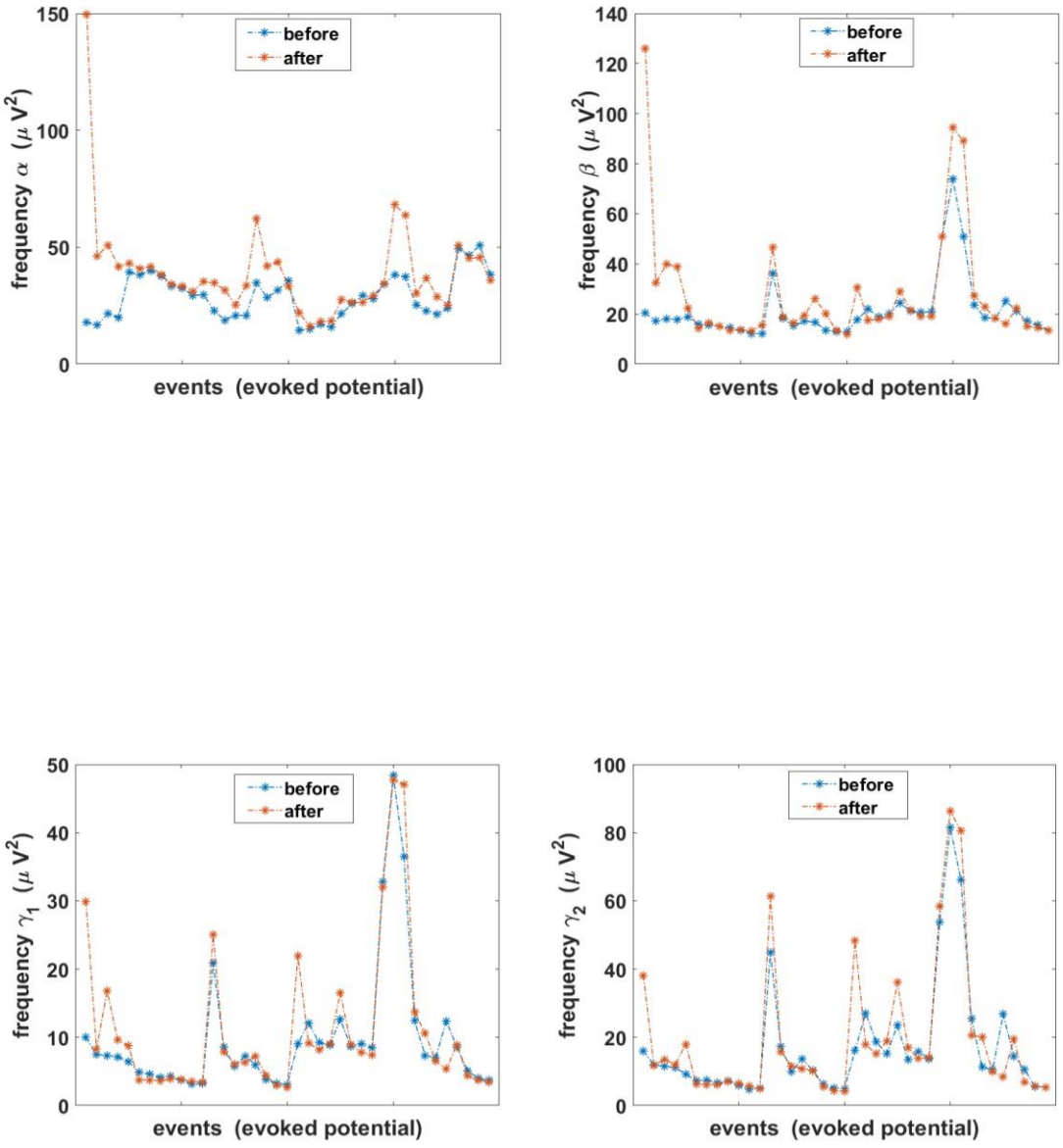

Fig. 13 Mean values for each frequency within CG, pre- and post-testing.

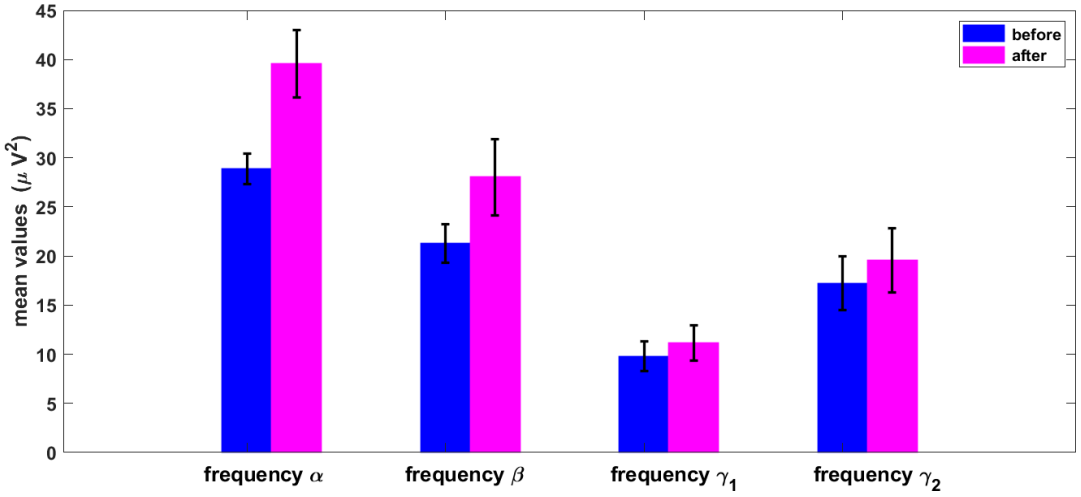

Fig. 14 Mean values ± S.E.M. of the four frequencies on all channels (CG).

In order to test the subsequent hypotheses 2.1.1, 2.2.1, 2.3.1 and 2.4.1, which regard the mean differences of the frequencies in the alpha, beta, gamma1 and gamma2 register between CG and SG, we applied the t-test - comparison, between the SG median and CG median.

Specifically, for each given frequency (α, β, γ_1 or γ_2), we calculated the mean difference (subtracting from the mean value obtained after the experimental interval, the mean value obtained in the recordings before that interval) in the frequency value, within each group, in all moments.

Whether these differences between SG and CG were statistically significant was then tested, with the P-values corresponding to the two-sample t-test are:

$$P_\alpha = 0.3274,\ P_\beta = 0.0359,\quad P_{\gamma_1} = 0.0403,\ P_{\gamma_2} = 0.1905.$$

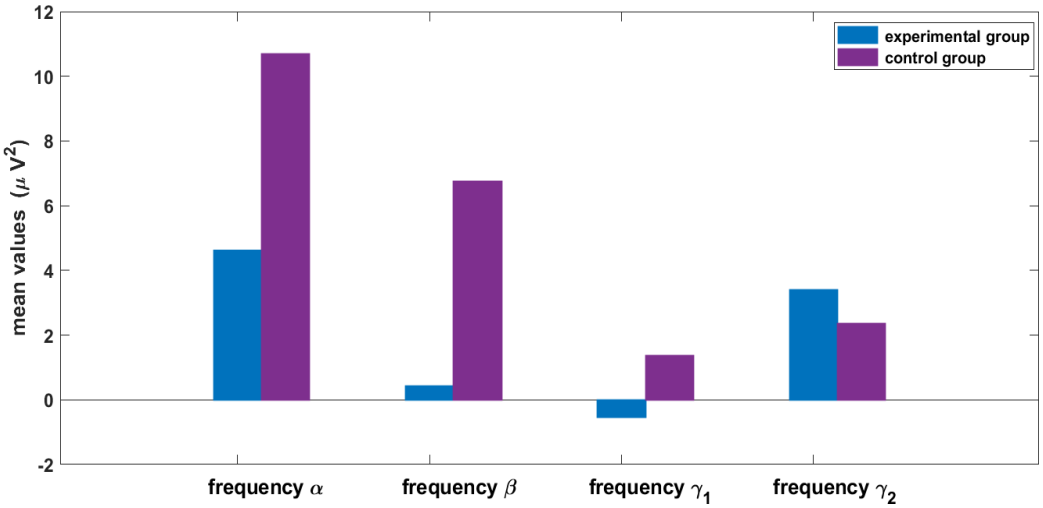

Fig. 15 Mean difference (post-experiment – before the experiment) for each frequency and each group.

Significant differences for the β and γ_1 frequencies are noticed, which confirms the subsequent hypotheses 2.21 and 2.3.1 and refutes the hypotheses 2.1.2 and 2.4.1 regarding the α and γ_2 frequencies.

For the last two hypotheses, we restrict the previous analyses to the data corresponding to the four registers, collected from the front sensors 1, 2 and 3.

For each volunteer (from both groups) and for each of the α, β, γ_1 and γ_2 frequencies, we calculated the mean value

of the first three channels. Then, we used a statistical test to check whether there were statistically significant differences in the central values corresponding to each frequency (α, β, γ_1 and γ_2) pre- and post-testing.

The assumptions of the Wilcoxon signed-rank test are:

(H0): the median of the differences (for the entire population) between the two data sets is zero (or, equivalently, the two sets have the same median value);

(H1): the median of the differences (for the entire population) between the two data sets is not zero.

Table 3 below displays the P-values for all these tests. The red P-values correspond to statistically significant differences (significance level 0.05) in the median, pre- and post-test.

P-values	α	β	γ_1	γ_2	P-values	α	β	γ_1	γ_2
E_1	0.9333	0.0787	0.1282	0.0887	N_{17}	0.9444	0.0004	0.0060	0.0295
E_2	0.7377	0.0002	0.0000	0.0000	N_{18}	0.0135	0.0229	0.0065	0.0198
E_3	0.8780	0.0001	0.0130	0.1506	N_{19}	0.0000	0.0002	0.0198	0.2194
E_4	0.2953	0.0003	0.0001	0.0000	N_{20}	0.5578	0.2142	0.7695	0.9555
E_5	0.6755	0.0037	0.0152	0.3570	N_{21}	0.0238	0.0015	0.0009	0.0238
E_6	0.0001	0.0080	0.1587	0.9444	N_{22}	0.0002	0.0000	0.0005	0.0007
E_7	0.0913	0.0001	0.0000	0.0000	N_{23}	0.2091	0.0071	0.0115	0.0416
E_8	0.0460	0.6653	0.4511	0.2703	N_{24}	0.0000	0.0000	0.0000	0.0000
E_9	0.0010	0.0507	0.0006	0.0004	N_{25}	0.5767	0.0016	0.0000	0.0001
E_{10}	0.0285	0.0060	0.0050	0.0000	N_{26}	0.4853	0.2826	0.0416	0.0002
E_{11}	0.0080	0.5959	0.2953	0.2301	N_{27}	0.0020	0.1671	0.0596	0.0940
E_{12}	0.0221	0.3644	0.0031	0.0071	N_{28}	0.0002	0.0001	0.0000	0.0000
E_{13}	0.4941	0.1214	0.0048	0.0026	N_{29}	0.0247	0.3570	0.9777	0.8560
E_{14}	0.1428	0.0005	0.0001	0.0011	N_{30}	0.3083	0.0184	0.0039	0.0010
E_{15}	0.0006	0.0475	0.0000	0.0000	---	---	---	---	---
E_{16}	0.0000	0.0001	0.0718	0.1506	---	---	---	---	---

Table 3 P-values for the Wilcoxon signed-rank test for the medians of each frequency. Volunteers E1 - E16 are from SG, and volunteers N17 - N30 are from CG.

To evaluate the last set of hypotheses, we made a comparative analysis of the data of the SG subjects with themselves, in the two moments, pre- and post-testing, corresponding to the three channels (Ch1 – PF1, Ch2 – PFz, Ch3 – PF2). We test Hypothesis 3.1: PCOT 30/8 induces changes in electrical activity, in all registers, post-testing, compared to pre-testing, in SG subjects, regarding the three frontal sensors.

Only GS is considered, for significant differences in the pre- and post-testing median value, (only regarding the first three channels), using the Wilcoxon signed-rank test. For each given frequency (α, β, γ_1 or γ_2), we calculated the mean value of the frequency within the group for the three frontal sensors at all times. Next, we tested whether there were significant differences in the mean value before and after the experiment. The corresponding P-values for the Wilcoxon signed-rank test are:

$$P_\alpha = 0.0787, \quad P_\beta = 0.5392, \quad P_{\gamma_1} = 0.0091, \quad P_{\gamma_2} = 0.5672.$$

For SG, we notice significant differences in medians (pre- and post-testing) only for the γ_1 frequency. Figure 16 shows the mean frequency values within the SG (at all times). Figure 17 shows the total mean values ± S.E.M of the four frequencies, at all moments. Here, by the total mean value we imply the mean of all the means of the frequency group, considered for all moments.

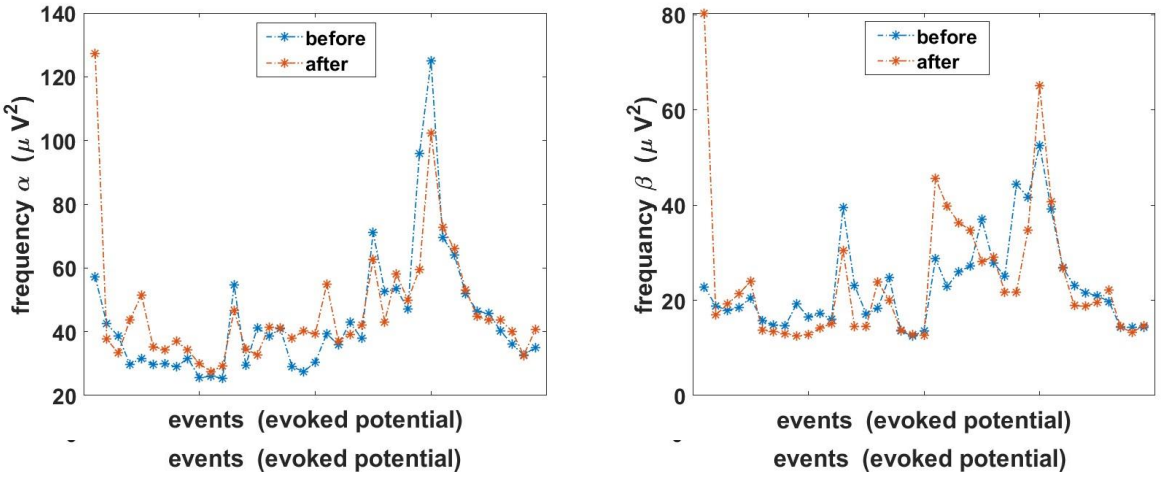

Fig. 16 Mean values for each frequency in SG subjects, pre- and post-testing.

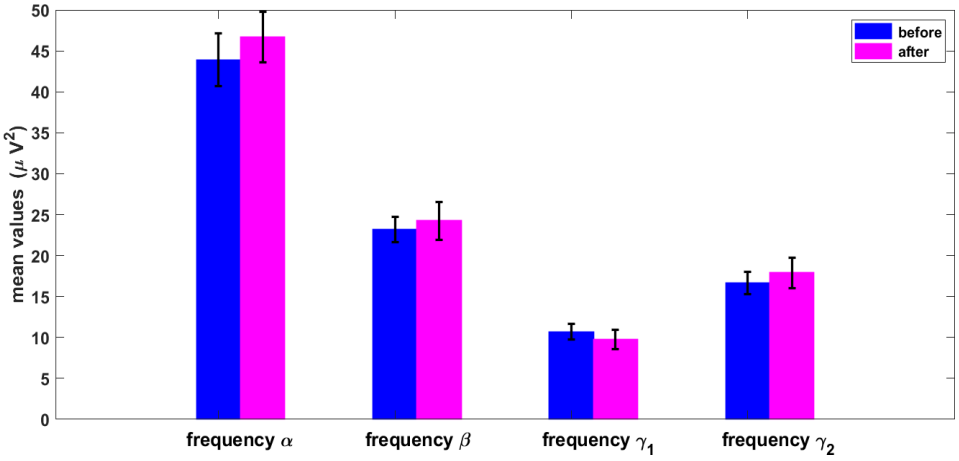

Fig. 17 Total mean values ± S.E.M. of the four frequencies, across all channels, for SG subjects.

An identical examination is carried out for the subjects of the Control Group, in order to identify significant differences in the median pre- and post-testing value, only for the first three channels, corresponding to the frontal sensors, Ch1 – PF1, Ch2 – PFz, Ch3 – PF2). We use the Wilcoxon signed-rank test to identify significant differences in pre- and post-testing median

CG values for the first three frontal channels.

For the given frequencies (α, β, γ_1 or γ_2), we calculated the mean value of the frequency within the Control Group, for the three frontal sensors, at all times, testing whether there are significant differences in the pre- and post-testing mean value. The corresponding P-values for the Wilcoxon signed-rank test, for CG subjects, are

$$P_\alpha = 0.0021, \quad P_\beta = 0.5030, \quad P_{\gamma_1} = 0.3570, \quad P_{\gamma_2} = 0.4103.$$

For CG, we notice significant differences in the medians (pre- and post-testing) only for the alpha frequency, a situation that correlates with the results obtained in Study 1, which identified statistically significant changes also in the case of CG, in the absence of an experimental intervention.

Figure 18 shows the mean frequency values within the CG (at all times). Figure 19 shows the total average values ± S.E.M of the four frequencies, for the first three channels. (By the total mean value we refer to the mean of all means of the frequency group, considered at all times.)

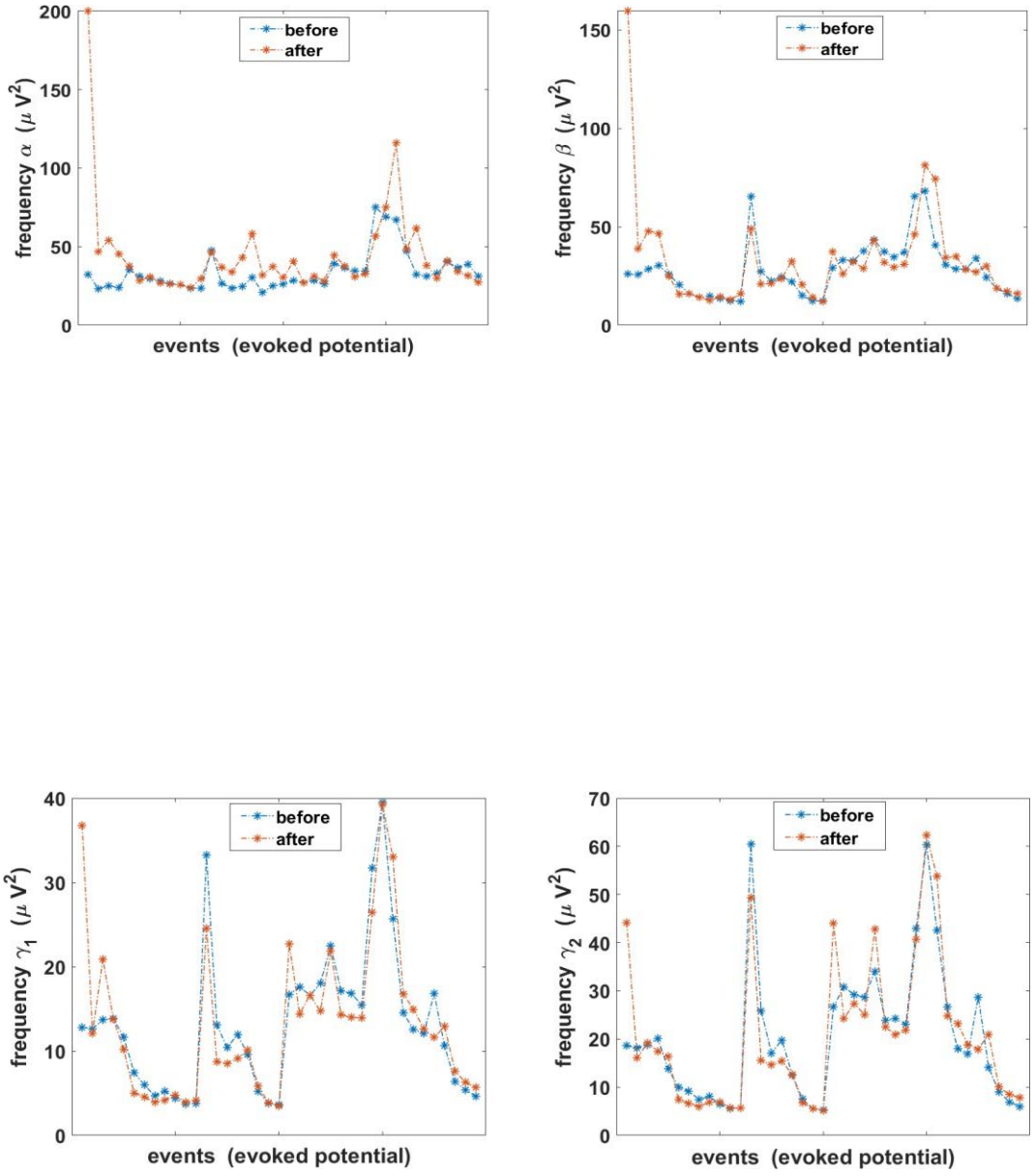

Fig. 18 Mean values for each frequency in CG subjects, pre- and post-testing.

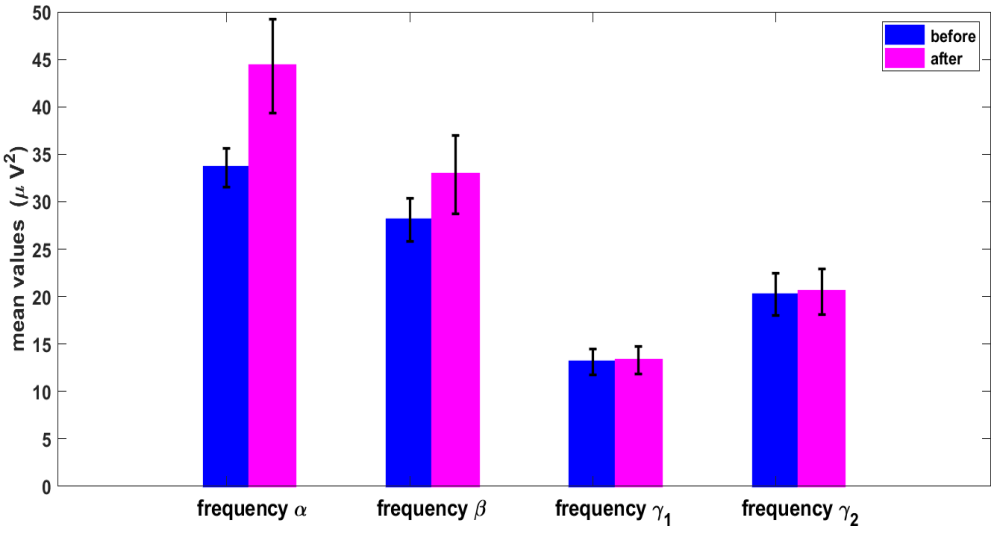

Fig. 19 Total mean values ± S.E.M. of the four frequencies, across all channels, for CG subjects.

Finally, for the last set of working hypotheses, we compare the median of the experimental group with the median obtained for the control group (only for the first three channels) (Hypothesis 3.2). We use the two-sample t-test for this. For each given frequency (α, β, γ_1 or γ_2), we calculated the mean difference (subtracting the pre-testing mean from the post-testing mean) in the frequency value within each group at all time points. Next, we tested whether these differences were significant between SG and CG. The P-values corresponding to the t-test, for the two samples, are:

$$P_\alpha = 0.1304, \quad P_\beta = 0.3816, \quad P_{\gamma_1} = 0.3172, \quad P_{\gamma_2} = 0.5805.$$

One can notice no significant differences. Some observations regarding the limitations present in the current study will be discussed in a later section within this chapter.

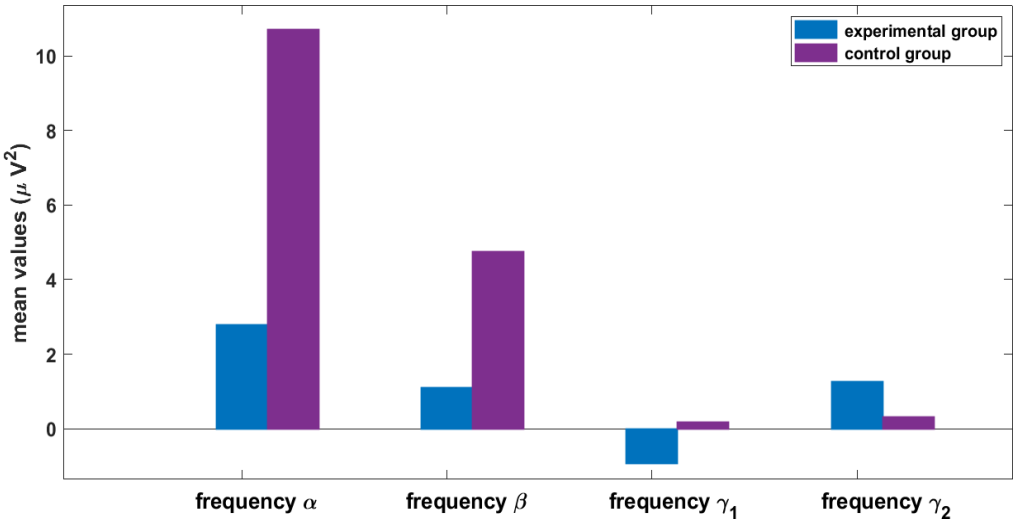

Fig. 20 To highlight the possible changes brought about by the PCOT experience, we render the mean difference (post and pre-testing), for each group and for each frequency.

8. DISCUSSIONS

Many studies highlight that S/RE trigger changes in brain electrical activity patterns [176], those focusing on Buddhist,

yoga or transcendental meditation practices being more numerous than those approaching Christian spiritual practices[3] [177].

In regard to the alpha frequency spectrum, we have seen, using the Wilcoxon signed-rank test comparitively, and evaluating the significant differences in the median value for the pre/post-experience SG subjects, statistically significant results. Testing whether there are significant differences in the median value before and after the experiment, in SG, we have identified statistically significant values of P, regarding the alpha log, respectively P_{α}= 0.0001, which suggests that the practice of PCOT could cause an increase in the intensity of electrical activity of the brain in this register.

Increases in electrical activity in the alpha register (8–12 Hz), correspond to an idling state, with reduced processing of sensory information [178], a non-directive meditation [179], but also to various stages of rest, while this state of relaxation does not mean an empty mind [179]. The intensification of the activity in the alpha band is present in some types of meditation [180] and in connection with mindfulness sessions [181] (M - technique also called open meditation OM, of non-directive monitoring of thoughts).

Enhancement of the activity in the alpha register has also been reported in the case of transcendental meditation (TM) [182, 183], in experienced practicing meditators [184, 185], but also during Zen meditation [186] and in the case of some medical assistants, participants for 8 weeks, in an MBT (Mindfulness-based treatment) intervention [187].

An intensification of electrical brain activity in the alpha register has also been reported during the Muslim Dhuha prayer. In one study, EEG recordings were made while subjects had their eyes open, under three different conditions (resting, four cycles of prayer, reciting specific verses and supplications and, finally, performing gestures and body postures specific to prayer, but without the associated recitations). The analysis of the alpha register variations showed a higher mean relative alpha power (RPa) during prostration positions (body posture in the Dhuha prayer) compared to the rest state [188]. Therefore, highlighting the intensification of electrical activity in the alpha register in SG subjects, as a result of PCOT practice (understood as interaction and dialogue with the Supreme Being) could correspond to the mentioned results.

The gamma frequency spectrum is related to the activity of the visual cortex [189], premotor, frontal and parietal regions [190]. At the same time, the electrical activity of the brain in the gamma band is also related to the unification of the perceptual field [191], which enters the debate concerning the topic of the conscience [192].

Regarding S/RE, two studies report increases in the gamma register activity in subjects practicing Buddhist meditation [193] or Vipassana, Himalayan Yoga and Isha Shoonya (in this case it is the register between 60 and 110 Hz, corresponding to the gamma2 band) [176].

Another study revealed differences in mean EEG power in the gamma register among practitioners of the Islamic ritual of Salat (a series of steps and bodily postures performed while reciting verses). The study compared subjects actually performing the ritual with other subjects only miming the execution (performing gestures without reading the verses). Recordings showed that the signal strength in the gamma register was higher (frontal and parietal regions) throughout the ritual in subjects who actually performed it compared to the level recorded in subjects who only mimicked [194]. The result suggests the contribution of cognitive and attentional processing in the S/R experience.

In the present study we have highlighted an increase in the activity in the gamma2 register, for subjects from SG, comparing pre- and post-testing, respectively $P_{\gamma_2} = 0.0015$. The fact could be significant, considering that Christian prayer in general, and Christian-Orthodox prayer in particular, is not a relaxation technique, having an important cognitive and attentional component (the text and the task of attention), as well as specific bodily postures.

The beta register is present in EEG investigations of S/RE as well. First discovered by Hans Berger, beta waves have been associated in time with various functions, such as focused attention, inhibition of movement and motor planning, maintaining the status quo, and signalling decision making [195]. It is now accepted that increased beta brain activity corresponds to anxiety, inability to relax and stress, while suppression of beta signals corresponds to ADHD, daydreaming, depression, and poor cognition [196].

Another EEG study comparing Buddhist loving kindness meditation (LKM) with Christian religious prayer is significant for the discussion of the beta register results. The study revealed that the practice of LKM corresponds to increased activity in the delta, alpha and beta register, while the practice of religious prayer is associated only with increased alpha and gamma

[3] An explanation for this fact is proposed by David P. Barash, based on the distinct manner of Buddhism, on the one hand, and of the three great Abrahamic religions (Judaism, Christianity and Islam) on the other, in relation to the results of experimental sciences (David P. Barash, Is Buddhism the Most Science-Friendly Religion?, Scientific American, February 11, 2014) [ii]. Current Buddhism quickly assimilates various results of science, without the intervention of processes of spiritual significance, while in the doctrines of Truth from the three Abrahamic religions, hermeneutic processes intervene, for the formulation of spiritual interpretations that reconcile the scientific results with the doctrine of Truth, considered immutable.

waves [197].

The result is interesting, because in the present study as well, in the EEG evaluation of the impact trained by the PCOT practice, at post-testing, the measurements performed on the SG subjects did not reveal intensifications of brain activity in the beta register, a fact that could represent a starting point for further studies.

9. LIMITS OF THE STUDY

The present study has several limitations. Some arise from the difficulties of recruiting subjects for the two groups, aspects also mentioned in the previous chapter.

Other limitations stem from the absence of EEG recordings for theta and delta.

The inclusion of the theta register in the dependent variable package in the EEG exploration of PCOT may have provided new data. A study on mindfulness, for example, found that, unlike regular relaxation, non-directive meditation sessions lead to increased electrical activity in both alpha band and theta register [179]. However, mind-wandering episodes, in addition to the decrease in amplitude and increase in frequency of alpha oscillations (8-14 Hz), also seem to induce a decrease in the frequency (increase in amplitude) of theta oscillations (4-8 Hz) [198]. An exploration of PCOT -induced changes in the theta band compared to alpha could reveal new aspects, if we also take into account a recent study that, in regard to meditation, notes inverse associations between the dynamics in the alpha and theta registers, suggesting a possible functional dissociation of the two neural signatures (alpha and theta oscillations) [199].

Also, the inclusion of the delta register could have provided new information about possible EEG peculiarities of PCOT. The comparative study mentioned above, which looked at loving kindness meditation - LKM and Christian prayer, reported the presence of activity in the delta band in the case of LKM, but not in the practice of Christian prayer [197]. Future research, targeting PCOT, could include delta band in the set of dependent variables to verify this aspect.

Other limitations of the present study stem from the insufficiency of recorded data. For example, comparison of individual CG and SG data acquired pre/post-experience for three distinct stages (BLEO1, BLEC1 and PE) was not possible due to insufficient data.

P-values	BLEO1	BLEC1	PE	BLEO2	BLEC2	PHOTO	BLEO3	BLEO4	BLEC3	All
α	0.1250	0.1250	To be filled in	To be filled in	To be filled in	To be filled in	To be filled in	To be filled in	To be filled in	To be filled in
β	0.3750	0.8750	To be filled in	To be filled in	To be filled in	To be filled in	To be filled in	To be filled in	To be filled in	To be filled in
γ_1	0.8750	0.3750	To be filled in	To be filled in	To be filled in	To be filled in	To be filled in	To be filled in	To be filled in	To be filled in
γ_2	0.2500	0.6250	To be filled in	To be filled in	To be filled in	To be filled in	To be filled in	To be filled in	To be filled in	To be filled in

Table 4 P-values for differences between pre- and post-experiment median values (for SG subjects), for three time moments, BLEO1, BLEC1 and PE.

Since the observed data have a relatively small volume (n = 16 +14), non-parametric tests (Wilcoxon tests, used to test the equality of medians) were used here to the detriment of t-tests for the equality of means. It is known that t-tests for the mean are more refined tests (in the sense that the error of accepting a false hypothesis is smaller) compared to non-parametric tests, for the situations where they are applicable.

Something similar can be found in the numerical values corresponding to the intervals in the EEG Measurement Protocol. The record provided 4 or fewer numeric values. For example:

- Interval 3 – Personal Experience (PE) – 4 numerical values;
- Interval 6 – Image view (VI) – 4 numerical values;
- Interval 8 – Cold Pressure (PAIN/HIP) – 1 numerical value.

For the 4 numerical values of the PE, a standard deviation can be calculated, therefore for the S.E.M., as well, so as to describe the variability/precision, whereas in the case of interval 8 (PAIN/HIP), for which we have only one numerical value, a standard deviation cannot be calculated, so no S.E.M. to describe the variability/precision.

For further refined studies, the number of participating subjects (SG and CG) should be higher. At the same time, for each interval provided in the EEG Measurement Protocol (e.g., personal experience, cold pressor test, etc.) several values are useful, so that a better assessment of the variability (standard deviation or S.E.M.) is possible. Thus, the number of intervals in the EEG Measurement Protocol could be reduced (from 10, as provided in the current study, to 4 or 5), with the extension of the duration of experience for each of the important intervals (PCOT, IV – image view).

Extending the range intended for PCOT (Personal Experience) for SG subjects could provide better conditions and more data for further highlighting possible differences from CG subjects, and for a more detailed analysis, selectively including channels corresponding to sensors located in certain regions of interest.

Finally, further research, which would also preserve the IV interval (Image View) could also look for possible correlations between the practice of PCOT and empathy (by applying some questionnaires), since in many existing prayers in PCOT there are parts that refer to helping other people. This change is also justified by the results of a 2015 study suggesting the existence of a distinction regarding increased activity in the beta register in the experience of empathy, discriminating between the situation in which subjects are asked to rate the emotional state of others and the situation in which they rate their own emotions arising from reporting to the condition of others [iii].

10. CONCLUSIONS

Compared to the proposed working hypotheses, the results of this study are as follows:

Hypothesis 2.1 – PCOT practised for 30 min./day, 8 weeks, causes an increase in brain electrical activity in the alpha register in SG subjects during post-testing compared to pre-testing level.

Hypothesis 2.2 - PCOT practised for 30 min./day, 8 weeks, causes an increase in brain electrical activity in the beta register in SG subjects during post-testing compared to pre-testing level.

Hypothesis 2.3 - PCOT practised for 30 min./day, for 8 weeks, causes an increase in brain electrical activity in the gamma1 register in SG subjects during post-testing compared to pre-testing level.

Hypothesis 2.4 - PCOT practised for 30 min./day, for 8 weeks, causes an increase in cerebral electrical activity in the gamma2 register in SG subjects.

RESULTS

Applying the Wilcoxon signed-rank test revealed significant differences in median value in the case of SG subjects, pre/post-experience. The intended experimental design (PCOT, 30 min./day, for 8 weeks), revealed changes only in the alpha and gamma2 registers, but not in the beta and gamma1 registers.

For each given frequency (α, β, γ_1 or γ_2), the mean value of the frequency within the SG, for all time points, was calculated. The existence of significant differences in the median values was then tested.

Corresponding to the significant differences in the median value before and after the experiment, the corresponding P-values for the Wilcoxon signed-rank test are:

$$P_{\alpha} = 0.0001,\ P_{\beta} = 0.9111,\qquad P_{\gamma_1} = 0.1085,\ P_{\gamma_2} = 0.0015.$$

The obtained values validate working hypotheses 2.1 and 2.4 (frequencies α and γ2) and invalidate working hypotheses 2.2 and 2.3.

Working hypothesis 2.1.1 - The mean differences in alpha register frequencies between SG and CG are statistically significant.

Working hypothesis 2.2.1 - The mean differences in beta register frequencies between SG and CG are statistically significant.

Working hypothesis 2.3.1 - The mean differences in gamma1 register frequencies between SG and CG are statistically significant.

Working hypothesis 2.4.1 - The mean differences in gamma2 register frequencies between SG and CG are statistically significant.

Results

The mean difference in the frequency value (α, β, γ_1 or γ_2) calculated for SG and CG and the application of the t-test revealed statistically significant differences between SG and CG. The P-values corresponding to the t-test are:

$$P_{\alpha} = 0.3274,\ P_{\beta} = 0.0359,\ P_{\gamma_1} = 0.0403,\qquad P_{\gamma_2} = 0.1905.$$

The obtained values validate the working hypotheses 2.2.1 and 2.3.1 (frequencies β and γ_1) and invalidate the working hypotheses 2.1.1 and 2.4.1 regarding the alpha and gamma register2.

Finally, the last two hypotheses, which regard possible changes induced by PCOT practice, 30 min. daily for 8 weeks, in the electrical activity in the prefrontal region in all four registers (alpha, beta, gamma1 and gamma2) among subjects in SG compared to CG evolution, the results are inconclusive. For this we compared the median SG with that of CG, for the first three channels (Ch1 – FP1, Ch2 - FPz, Ch3 – FP3), hypotheses 3.1 and 3.2 not being supported. The research did not reveal that the practice of PCOT induces changes in the electrical activity in the prefrontal region, in all registers, comparing the post-testing moment and the pre-testing moment, in the SG subjects (Hypothesis 3.1). There were no differences between the median SG and the median CG at the time of post-testing (Hypothesis 3.2), but we recorded some changes in the alpha register, in subjects from CG, changes that appeared in the experimental interval, between the pre- and post-testing phases.

As we have mentioned, it would be important for further research to improve the experimental design in order to provide sufficient primary data to allow more accurate assessments.

11. FINAL CONCLUSIONS

Together with two other previous studies [1,2], the present paper is part of a research project included in the doctoral programme completed in July 2023 with the defence of the PhD thesis entitled Neuroscience of Spiritual Life at UMPCD Bucharest. The other two previous studies aimed to highlight possible changes in some salivary markers [1], and some psychometric indicators [2] in the same SG and CG subjects, within the same experiment that had as an experimental task the practice of PCOT for 8 weeks.

The first study [1] revealed a decrease in the salivary Cortisol (SC) levels and changes in Interleukin 6 (IL-6 sal) levels in SG subjects. However, regarding SC, the comparative analysis of SG dynamics in relation to CG, pre- and post-testing, did not reveal significant differences. In addition, whether PCOT corresponds to an increase or decrease in IL-6 sal needs clarification. The second study [2] revealed post-testing differences, in SG subjects, on the Hamilton scale, regarding the a3 item ("fears/phobias"), and the 14 item ("appreciation of anxious mood at the interview"), suggesting a possible influence of the PCOT practice, in the sense of decreasing the intensity of fears/phobias and assessing the anxious mood. On the other hand, using the COPE test, higher means were revealed in SG subjects compared to CG subjects, post-testing, regarding e pos ("positive interpretation and growth") and e rel ("religious approach/religious coping").

Finally, in the present study, the third of the research project, we noticed that the application of the Wilcoxon signed-rank test revealed significant differences in the median value in the case of SG subjects, pre/post-testing in the alpha and gamma2 register. These results suggest that it is reasonable to consider that PCOT practice induces electro-physiological and psychometric changes, an issue that requires closer examination. Regarding the results obtained in these three studies, further research is needed to more rigorously evaluate possible correlations between variations in salivary markers, psychometric measurements, and electrical activity in the alpha and gamma2 band. For this, improvements are necessary. The use of salivary markers requires protocols with multiple sampling times throughout the day to account for variations introduced by the circadian rhythm. EEG measurements must allow more data to be collected for more rigorous statistical evaluations. On the other hand, the experimental design should provide for longer experimental intervals to allow subjects in SG to adapt to the complex experimental tasks. This is because S/RE in general, and PCOT practice in particular, present complex configurations, which aim at cognitive-emotional, behavioural and spiritual aspects.

All in all, transversal approaches and cross-evaluations are needed so as to allow the possibility of comparing psychometric measurements with electro-physiological and imaging data. In more general terms, for future research, methodological clarifications are needed, regarding how the demands of the scientific study and the specifics of S/RE can be reconciled. Rigour is essential in exploring S/RE, considering not only the many fundamental questions or epistemological challenges surrounding the relationship between science and religion, but also the therapeutic potential of these practices.

REFERENCES

[1] Mihalache, A.S., Zăgrean A-M, Bălan, D.G. et al.: Possible physiological changes induced by the practice of Prayer in the Christian-Orthodox Tradition. Physiology. 2023 1(104), 28-46.

[2] Mihalache, A.S.; Vicu, O-M, Zăgrean, L: Evaluation of possible psychometric changes induced by the practice of Prayer in the Orthodox Christian Tradition. Physiology. 2023 2(105), 75-46.

[1] Mihalache, A.S., Zăgrean A-M, Bălan, D.G. et al.: Possible physiological changes induced by the practice of Prayer in the Christian-Orthodox Tradition. Physiology. 2023 1(104), 28-46.

[2] Mihalache, A.S.; Vicu, O-M, Zăgrean, L: Evaluation of possible psychometric changes induced by the practice of Prayer in the Orthodox Christian Tradition. Physiology. 2023 2(105), 75-46.

[176] Braboszcz C., Cahn, B.R., Levy, J., et al.: Increased Gamma Brainwave Amplitude Compared to Control in Three Different Meditation Traditions. PLoS One. 2017 Jan 24;12(1):e0170647. doi: 10.1371/journal.pone.0170647. PMID:

28118405; PMCID: PMC5261734.

[177] Gao, J., Fan. J., Wu, B.W. et al.: Repetitive Religious Chanting Modulates the Late-Stage Brain Response to Fear- and Stress-Provoking Pictures. Front Psychol. 2017 Jan 10;7:2055. doi: 10.3389/fpsyg.2016.02055. PMID: 28119651; PMCID: PMC5223166.

[178] Pfurtscheller, G., Stancák, A.Jr., Neuper C.: Event-related synchronization (ERS) in the alpha band—an electrophysiological correlate of cortical idling: a review. Int J Psychophysiol. 1996 Nov;24(1-2):39-46. doi: 10.1016/s0167-8760(96)00066-9. PMID: 8978434.

[179] Lagopoulos, J., Xu, J., Rasmussen I. al.: Increased theta and alpha EEG activity during nondirective meditation. J Altern Complement Med. 2009 Nov;15(11):1187-92. doi: 10.1089/acm.2009.0113. PMID: 19922249.

[179] Lagopoulos, J., Xu, J., Rasmussen I. al.: Increased theta and alpha EEG activity during nondirective meditation. J Altern Complement Med. 2009 Nov;15(11):1187-92. doi: 10.1089/acm.2009.0113. PMID: 19922249.

[180] Cahn, B.R., Polich, J.: Meditation states and traits: EEG, ERP, and neuroimaging studies. Psychology of Consciousness: Theory, Research, and Practice, 2013;1(S):48–96. https://doi.org/10.1037/2326-5523.1.S.48.

[181] Lomas, T., Ivtzan, I., Fu CH.: A systematic review of the neurophysiology of mindfulness on EEG oscillations. Neurosci Biobehav Rev. 2015 Oct;57:401-10. doi: 10.1016/j.neubiorev.2015.09.018. Epub 2015 Oct 9. PMID: 26441373.

[182] Mason, L.I., Alexander, C.N., Travis, F.T. et al.: Electrophysio- logical correlates of higher states of consciousness during sleep in long-term practitioners of the Transcendental Meditation program. Sleep. 1997;20:102–110.

[183] Travis F.: Autonomic and EEG patterns distinguish transcending from other experiences during Transcendental Meditation practice. Int J Psychophysiol. 2001;42:1–9.

[184] Gaylord, C., Orme-Johnson, D., Travis F.: The effects of the transcendental mediation technique and progressive muscle relaxation on EEG coherence, stress reactivity, and mental health in black adults. Int J Neurosci. 1989;46:77–86.

[185] Travis, F., Wallace, R.K.: Autonomic and EEG patterns during eyes-closed rest and transcendental meditation (TM) practice: The basis for a neural model of TM practice. Conscious Cogn. 1999;8:302–318.

[186] Takahashi, T., Murata, T., Hamada T. et al.: Changes in EEG and autonomic nervous activity during meditation and their association with personality traits. Int J Psychophysiol. 2005 Feb;55(2):199-207. doi: 10.1016/j.ijpsycho.2004.07.004. PMID: 15649551.

[187] Wong, K.F., Teng, J., Chee. M.W.L. et al.: Positive Effects of Mindfulness-Based Training on Energy Maintenance and the EEG Correlates of Sustained Attention in a Cohort of Nurses. Front Hum Neurosci. 2018 Mar 1;12:80. doi: 10.3389/fnhum.2018.00080. PMID: 29545746; PMCID: PMC5838011.

[188] Doufesh, H., Faisal, T., Lim, K.S. et al.: EEG spectral analysis on Muslim prayers. Appl Psychophysiol Biofeedback. 2012 Mar;37(1):11-8. doi: 10.1007/s10484-011-9170-1. PMID: 21965118.

[189] Muthukumaraswamy, S.D., Singh, K.D.: Spatiotemporal frequency tuning of BOLD and gamma band MEG responses compared in primary visual cortex. NeuroImage. 2008;40(4):1552–1560. doi:10.1016/j.neuroimage.2008.01.052. PMID

18337125. S2CID 2166982.

[190] Kort, N., Cuesta, P. Houde, J.F. et al.: Bihemispheric network dynamics coordinating vocal feedback control. Human Brain Mapping. 2016;37(4): 1474–1485. doi:10.1002/hbm.23114. PMC 6867418. PMID 26917046.

[191] Singer, W., Gray, C.M.: Visual feature integration and the temporal correlation hypothesis. Annual Review of Neuroscience. 1995;18:555–586. doi:10.1146/annurev.ne.18.030195.003011. PMID 7605074

[192] Treccani, B.: The Neuropsychology of Feature Binding and Conscious Perception. Front Psychol. 2018 Dec 21;9:2606. doi: 10.3389/fpsyg.2018.02606. PMID: 30619008; PMCID: PMC6308126.

[193] Lutz, A., Greischar, L.L, Rawlings, N.B. et al.: Long-term meditators self-induce high-amplitude gamma synchrony during mental practice. Proc Natl Acad Sci U S A. 2004 Nov 16;101(46):16369-73. doi: 10.1073/pnas.0407401101.

Epub 2004 Nov 8. PMID: 15534199; PMCID: PMC526201.

[176] Braboszcz C., Cahn, B.R., Levy, J., et al.: Increased Gamma Brainwave Amplitude Compared to Control in Three Different Meditation Traditions. PLoS One. 2017 Jan 24;12(1):e0170647. doi: 10.1371/journal.pone.0170647. PMID: 28118405; PMCID: PMC5261734.

[194] Doufesh, H., Ibrahim, F., Safari, M.: Effects of Muslims praying (Salat) on EEG gamma activity. Complement Ther Clin Pract. 2016 Aug;24:6-10. doi: 10.1016/j.ctcp.2016.04.004. Epub 2016 Apr 21. PMID: 27502795.

[195] Kropotov, J.D.: Chapter 2.3 - Beta and Gamma Rhythms. In Kropotov, J.D. (Ed.): *Functional Neuromarkers for Psychiatry*. Academic Press, 2016, pp. 107-119, ISBN 9780124105133. https://doi.org/10.1016/B978-0-12-410513-3.00009-7.

[196] Abhang, P.A., Gawali, B.W., Mehrotra, S.C.: Chapter 3 -Technical Aspects of Brain Rhythms and Speech Parameters. In Abhang, P.A., Gawali, B.W., Mehrotra, S.C. (Eds.): *Introduction to EEG and Speech-Based Emotion Recognition*. Academic Press, 2016, pp. 51-79, ISBN 9780128044902. https://doi.org/10.1016/B978-0-12-804490-2.00003-8.

[ii] Barash, D.: Is Buddhism the Most Science-Friendly Religion?. Scientific American, February 11, 2014. Retrieved April 24, 2024 from https://bloGS.scientificamerican.com/guest-blog/is-buddhism-the-most-sciencefriendly-religion.

[197] Faber, E.S.L.: The neural correlates of two forms of spiritual love: an EEG study. BioRxiv. 2016: https://doi.org/10.1101/045898.

[179] Lagopoulos, J., Xu, J., Rasmussen I. et al.: Increased theta and alpha EEG activity during nondirective meditation. J Altern Complement Med. 2009 Nov;15(11):1187-92. doi: 10.1089/acm.2009.0113. PMID: 19922249.

[198] Rodriguez-Larios, J., Alaerts, K.: EEG alpha-theta dynamics during mind wandering in the context of breath focus meditation: An experience sampling approach with novice meditation practitioners. Eur J Neurosci. 2021 Mar;53(6):1855-1868. doi: 10.1111/ejn.15073. Epub 2020 Dec 18. PMID: 33289167.

[199] Katyal. S., Goldin. P.: Alpha and theta oscillations are inversely related to progressive levels of meditation depth. Neurosci Conscious. 2021 Nov 29;2021(1):niab042. doi: 10.1093/nc/niab042. PMID: 34858638; PMCID: PMC8633885.

[197] Faber, E.S.L.: The neural correlates of two forms of spiritual love: an EEG study. BioRxiv. 2016: https://doi.org/10.1101/045898.

[iii] Woodruff, C.C.: Neuroscience of Empathy and Compassion Lab. Northern Arizona University. Retrieved April 24 from https://nau.edu/psychological-sciences/nec/

[1] Mihalache, A.S., Zăgrean A-M, Bălan, D.G. et al.: Possible physiological changes induced by the practice of Prayer in the Christian-Orthodox Tradition. Physiology. 2023 1(104), 28-46.

[2] Mihalache, A.S.; Vicu, O-M, Zăgrean, L: Evaluation of possible psychometric changes induced by the practice of Prayer in the Orthodox Christian Tradition. Physiology. 2023 2(105), 75-46.

[1] Mihalache, A.S., Zăgrean A-M, Bălan, D.G. et al.: Possible physiological changes induced by the practice of Prayer in the Christian-Orthodox Tradition. Physiology. 2023 1(104), 28-46.

[2] Mihalache, A.S.; Vicu, O-M, Zăgrean, L: Evaluation of possible psychometric changes induced by the practice of Prayer in the Orthodox Christian Tradition. Physiology. 2023 2(105), 75-46.

[1] Mihalache, A.S., Zăgrean A-M, Bălan, D.G. et al.: Possible physiological changes induced by the practice of Prayer in the Christian-Orthodox Tradition. Physiology. 2023 1(104), 28-46.

[2] Mihalache, A.S.; Vicu, O-M, Zăgrean, L: Evaluation of possible psychometric changes induced by the practice of Prayer in the Orthodox Christian Tradition. Physiology. 2023 2(105), 75-46.

POSIBILE MODIFICĂRI ELECTROFIZIOLOGICE INDUSE DE PRACTICAREA RUGĂCIUNII ÎN TRADIȚIA CREȘTINĂ ORTODOXĂ

REZUMAT

Studiul de față își propune să evidențieze posibilele modificări pe care practica rugăciunii (în tradiția creștin-ortodoxă) - PCOT - după un model de 30 de minute de practică zilnică, timp de 8 săptămâni - le poate induce în activitatea electrică a creierului. Participanții (n=33) au fost împărțiți în două grupuri: Grupul de studiu (SG), n=16, cu o vârstă medie de 39,2 ani și Grupul de control (CG) n=17, cu o vârstă medie de 38,6 ani). Grupul de studiu a inclus credincioși creștini ortodocși care nu se roagă zilnic, fiind instruiți în cadrul unei sesiuni de 3 ore cu privire la specificul psiho-emoțional, comportamental și spiritual al PCOT. Nu s-a efectuat nicio intervenție asupra subiecților din Grupul de control. Studiul a inclus, înainte și după perioada de 8 săptămâni de practică zilnică a PCOT, măsurători EEG conform unui protocol de măsurare. Aplicarea testului Wilcoxon signed rank a relevat diferențe semnificative în ceea ce privește valoarea mediană în cazul subiecților SG, înainte/post-experiență, în registrele alfa și gamma2, dar nu și în registrele beta și gamma1. Sunt necesare cercetări suplimentare și modificări ale designului experimental, astfel încât să permită evaluări mai precise. Rezultatele sunt discutate în contextul unor studii similare, evidențiind unele limitări specifice ale studiilor care evaluează modificările fiziologice induse de experiențele spirituale/religioase, în special ale celor care utilizează EEG, formulând în același timp și câteva recomandări pentru creșterea calității metodologice a studiilor viitoare.

Cuvinte cheie: "Experiențe spirituale": Creștinismul ortodox

ANTIPLATELET MONOTHERAPY VERSUS ANTIPLATELET AND ANTICOAGULANT THERAPY IN REDUCING THE RISK OF PREECLAMPSIA AND FETAL INTRAUTERINE GROWTH RESTRICTION

ANGHEL SAVCIU LOREDANA[1], PATRU CIPRIAN LAURENTIU[2], PANA RAZVAN COSMIN,[2] BALACEANU DOBROMIR CRISTINA[1],CERNEA NICOLAE[2]

Clinical Emergency County Hospital Craiova, Obstetric and Gynecology Departament , St Tabaci nr.1,Craiova,200642
Departament of Obstetrics and Gynecolog ,University of Medicine and Pharmacy,Craiova,St.Petru Rares, nr 2-4,200433
Correspondence PATRU CIPRIAN LAURENTIU , patru_ciprian@yahoo.com, 0761632298

ABSTRACT

Preeclampsia is a major cause of increased maternal and perinatal morbidity and mortality with an incidence between 2% and 8% of all pregnancies. The association of preeclampsia with fetal intrauterine growth restriction and prematurity often leads to long-term consequences. Administration of low molecular weight heparin (LWMH) may improve placental development and inhibit the reactive pathways involved in pre-eclampsia and intrauterine growth restriction (IUGR).

We conducted a retrospective observational study, over a 12-month period, in a third-degree maternity in the Clinical Emergency County Hospital from Craiova. The study included a number of 1200 patients examined starting with the first trimester of pregnancy. A combined screening algorithm was applied to these patients. This algorithm included: maternal history of preeclampsia, mean blood pressure values, Doppler assessment of the uterine arteries and serum level of the placental growth factor (PIGF). During this screening we identified a number of 82 patients at high risk of preeclampsia.

The objective of the study was to evaluate the impact of the antiplatelet therapy compared to combined antiplatelet and anticoagulant therapy in the occurrence of preeclampsia and intrauterine growth restriction.

The results of the study showed an outcome improvement by reducing the risk of preeclampsia and IUGR in patients who were treated with combined therapy vs monotherapy.

Keywords: preeclampsia, IUGR, aspirin, LMWH

INTRODUCTION

Preeclampsia is defined as elevated blood pressure values above 140/90 mmHg with onset after 20 weeks of gestation accompanied by proteinuria or other signs of target organ damage. It is also an important cause of increased maternal and perinatal morbidity and mortality. Although many studies aimed to identify preventive measures for preeclampsia, the incidence of this condition has been relatively unchanged in the recent decades because the pathophysiology of this disease is not fully understood. There is increasing evidence suggesting that suboptimal trophoblastic invasion causes an imbalance of angiogenic and antiangiogenic proteins, ultimately leading to widespread inflammation and endothelial damage, increased platelet aggregation and thrombotic events with placental infarctions. [1]

The incidence of this disease ranges from 2% to 8% of all pregnancies and is a significant cause of maternal and perinatal morbidity and mortality. [2],[3] The association of preeclampsia with IUGR and prematurity often leads to long-term consequences, including increased risk of cerebral palsy and neurodevelopmental delay, respiratory disorders, hypertension, renal dysfunction, insulin resistance, obesity, cardiovascular disease and reduced work capacity. [4],[5]

Cases diagnosed with preeclampsia are also 2 to 5 times more likely to develop hypertension and long-term cardiovascular and cerebrovascular disease [6],[7]

Aspirin belongs to the class of non-steroidal anti-inflammatory drugs and its analgesic, antipyretic and anti-inflammatory effects are due to the inactivation of the cyclooxygenase enzymes COX-1 and COX-2 which leads to the suppression of prostaglandin and thromboxane production. This reduction of thromboxane also leads to inhibition of platelet aggregation, producing an antithrombotic effect [8],[9]

Low molecular weight heparin (LMWH) has been suggested as an intervention to improve placental function by increasing blood flow [10], differentiation and invasion of trophoblasts in vivo [11] preventing monocyte adhesion, inhibiting tumor necrosis factor [12] and decreasing vascular resistance and endothelial function. [13] Therefore, it could improve placental development and inhibit reactive pathways involved in preeclampsia and intrauterine growth restriction [14],[15],[16]. Although studies have failed to demonstrate a benefit of low molecular weight heparin in patients at risk, its effect in preventing such conditions is likely to be greater than previously observed when high-risk groups are selected or if heparin treatment is combined with aspirin [17],[18].

METHOD

We conducted a retrospective observational study over a 12-month period between October 2022 and September 2023, in a third-degree maternity in the Clinical Emergency County Hospital from Craiova. A group of 1200 pregnancies were examined and subject to a combined screening algorithm that included: history of preeclampsia, blood pressure values, Doppler velocities of the uterine arteries, serum level of placental growth factor (PIGF). From this group we identified 82 pregnancies at high risk of preeclampsia.

Our primary objective was to assess the impact of the antiplatelet therapy compared to combined antiplatelet and

anticoagulant therapy in the occurrence of preeclampsia in pregnancies at high risk of developing this condition.

The secondary objectives were to assess the impact of these two treatment options on preterm birth; to assess the impact on the fetal growth and intrauterine growth restriction; to assess the number of days spent in the neonatal intensive care unit; to assess the number of the intrauterine fetal deaths. Informed consent was obtained from all patients included in the study.

Inclusion criteria for the study group were: age over 18 years; pregnancy between 11-13 weeks; history of preeclampsia/uterine artery Doppler changes (pulsatility index) and elevated serum PIGF values.

The exclusion criteria were: maternal age over 36 years, body mass index (BMI) >25 kg/m2; fetal chromosomal or morphological abnormalities.

Pregnancies identified at high risk of developing preeclampsia were divided into two equal groups of 41 patients each. The first group received 150 mg aspirin and the second group received a combined treatment with 75 mg aspirin and 1mg/kg body low molecular weight heparin.

Patients were enrolled in the study in the first trimester at a gestational age between 11-13 weeks during the genetic and morphological screening program. In the cases identified at risk of developing preeclampsia the antiplatelet and anticoagulant treatment was administered. Subsequently, the enrolled patients were monitored for the fetal growth curve, Doppler velocities of both uterine arteries, umbilical artery velocities and fetal well-being criteria. Fetal assessments were performed at successive intervals of approximately 4 weeks. Maternal biological parameters were also evaluated (blood pressure, proteinuria/24 hours, hemoleukogram, uric acid, serum transaminases, lactate dehydrogenase). Depending on the pregnancy outcome, the maternal-fetal evaluation intervals were adapted to each specific pathology (presence of early/late IUGR, persistently elevated BP values, altered platelet, liver and kidney function values).

RESULTS

According to our study results we detected in the study group 35 cases with preeclampsia. According to the pregnancy onset of this disease these cases were distributed as follows: 27 cases (65.8%) between 34-37 weeks of gestation, 5 cases (12.19%) between 28-34 weeks of gestation and 3 cases (7.31%) between 24-28 weeks of gestation (Table 1).

In the second group, 29 cases of preeclampsia were diagnosed, also distributed according to gestational age: 24 cases (58.5%) between 34-37 weeks of gestation, 4 cases (9.75%) between 28-34 weeks of gestation and 1 case (2.43%) between 24-28 weeks of gestation (Table 1).

We identified a number of 23 cases (56%) that developed intrauterine growth restriction in the first group and 18 cases (43.9%) in the second group. Thus, in the first group, we had a number of 17 (41.4%) newborns with birth weight below the 10th percentile, 5 (12.19%) newborns with birth weight below the 5th percentile and 2 (4.87%) newborns with birth weight below the 3rd percentile (Table 1). In the second group we had 15 (36.5%) newborns with birth weight below the 10th percentile, 2 (4.87%) newborns with birth weight below the 5th percentile and 1 (2.43%) newborn with birth weight below the 3rd percentile.

Regarding the number of days spent in the neonatal intensive care unit, in the first group we identified 6 newborns that required more than 14 days and 2 cases were identified in the second group.

We identified 3 intrauterine fetal deaths. Of these, 2 cases were identified in the first study group and 1 in the other group. One of the fetal deaths identified in the first group was of a fetus diagnosed with early intrauterine growth restriction below the 3rd percentile; in this case, the diagnosis of preeclampsia was made at a gestational age of 26 weeks.

The second case identified with intrauterine fetal death was also from the first study group and occurred at a gestational age of 29-weeks. This patient was admitted through the emergency department with a uteroplacental apoplexy diagnosis.

In the second group we identified one intrapartum fetal death in a patient with a history of hereditary thrombophilia who developed severe HELLP syndrome at 32 weeks of gestation. Emergency Caesarean section was performed and still the fetus died before extraction.

We also recorded a postnatal fetal death in a 30-week pregnancy diagnosed with severe preeclampsia that required elective extraction. This case was identified in the first study group. Fetal death occurred because of intestinal necrosis due to vascular redistribution and intestinal ischemia. The diagnosis was immediately established and the newborn was transferred to the pediatric surgery clinic where emergency surgery was performed with an unfavorable outcome.

	First group- Aspirin 150mg	Second group -Aspirin 75mg +LMWH 1mg/kgc
EP between 34-37 weeks	27	24
EP between 28-34 weeks	5	4
EP between 24-28 weeks	3	1
IUGR <10 percentile	17	15
IUGR< 5th percentile	5	2
IUGR< 3rd percentile	2	1
Neonatal Intensive Care Unit >14 days	6	2
Fetal deaths	2	1

Table 1. Distribution of the preeclampsia and IUGR cases according to the specific treatment, gestational age, number of days spent in the intensive unit and perinatal deaths

Maternal biomarkers were no significant different in the two groups in terms of maximum blood pressure values. Still increased values of proteinuria were identified in 18 cases (43.5%) the first group vs 15 (36.5) in the second group, increased values of uric acid in 6 cases (14.3%) in the first group vs 4 cases (9.75%) in the second. Changes in liver function were detected in only one case in the second group (case with HELLP syndrome) (Table 2).

	First group - Aspirin 150 mg	Second group -Aspirin 75 mg +LMWH 1mg/kg.
BP values (systolic/diastolic)	170/100 mmhg	165/95 mmhg
Proteinuria/24h >300mg	18	15
Uric acid > 6 mg/dl	6	4
Platelets no<150000/mm3	0	1
Liver enzyme >50 UI/L	0	1
LDH>225 U/L	0	1

Table 2. Maternal biomarkers values in the two groups

DISCUSSIONS

Due to pathophysiology not yet fully understood, the management of preeclampsia has remained significantly unchanged. Correct management involves 3 directions - prevention, early detection and treatment. In order to identify and correct these risk factors, susceptible patients should be referred for preconceptual counselling.

The most effective screening model for identifying women at increased risk of developing PE is to combine maternal factor analysis, blood pressure measurement, Doppler velocities of the uterine arteries and PIGF levels at a gestational age between 11-13 weeks. [19]

In our study, using this screening algorithm we identified 82 high-risk patients who developed preeclampsia before 37 weeks of gestation (62%). This result is similar to a study conducted by Nikos et al. who identified approximately 75% of cases of preterm preeclampsia (birth before 37 weeks gestational age). [1]

In the ASPRE study, 1776 women at high risk of developing PE, identified on the basis of combined first trimester screening, were randomized to either aspirin (150 mg per day before bedtime) or placebo from 11-14 weeks to 36 weeks gestation. According to this study results, aspirin reduced the risk of PE before 37 weeks by 62% (from 4.3% to 1.6%) [19]. In our study. monotherapy with 150 mg Aspirin reduced the risk of preeclampsia before 37 weeks in 27 cases (65%).

The beneficial effect of aspirin appears to depend on the degree of compliance, with a major decrease of the observed risk in patients with ≥ 90% compliance. [19]

Studies show that LMWH transcends anticoagulant properties by promoting differentiation and trophoblast invasion in vivo [11], preventing monocyte adhesion, inhibiting tumor necrosis factor [12] and decreasing vascular resistance and endothelial function [13]. In addition to these effects, LMWH could have a favorable effect on endothelial function and angiogenesis [14]. Therefore, LMWH administration could improve placental development and inhibit reactive pathways involved in preeclampsia and IUGR.

Also, 2 randomized trials in high-risk patients showed that adding enoxaparin to standard treatment did not reduce the risk of recurrence of preeclampsia and IUGR. [17],[18]

However, the effect of heparin in preventing such conditions is likely to be greater than previously observed if specific groups of high-risk women are selected or if heparin is combined with low-dose aspirin. [17],[18]

In our study, combined treatment with aspirin 75 mg and LWMH 1 mg/kg decreased the risk of developing preeclampsia to 58.5% vs 65.8% (aspirin in monotherapy) between 34-37 weeks, 9.75% vs 12.19% between 28-34 weeks and 2.43% vs 7.31% between 24-28 weeks of gestation.

According to some studies early IUGR has a prevalence of 1-2% and is associated with preeclampsia in more than 50% of patients. [20] Doppler abnormalities of the uterine arteries, characteristic of cases associating IUGR and preeclampsia [21] was addressed by Trudinger et al. in a randomized double-blind clinical trial involving aspirin at a dose of 150 mg daily. [21] The results demonstrated an increase in birth weight of 516 g as well as an increase in placental weight.

Leitich et al. conducted a meta-analysis based on 13 clinical trials to study the effects of prophylactic aspirin treatment. [22] He concluded that aspirin treatment at doses of 100-150 mg daily from at least 17 weeks of gestation decreased the occurrence rate of intrauterine growth restriction by approximately 65%, while the perinatal mortality rate decreased by approximately 60%.

In our study we demonstrated the efficacy of combined treatment with LWMH vs aspirin as monotherapy in reducing the incidence of IUGR as follows: 43.9% vs 56% overall; 36.5% vs 41.4% newborns below the 10th percentile, 4.87% vs 12.19% newborns below the 5th percentile and 2.43% vs 4.87% newborns below the 3rd percentile. [23],[24],[25],[26]

We also recorded a reduction in the number of days spent in the neonatal intensive care unit in patients receiving combined therapy.

CONCLUSIONS

Although aspirin as monotherapy as well as combined therapy with aspirin and heparin are widely used in the prevention of preeclampsia and IUGR and their efficacy has been proven by meta-analyses, there is still no consensus on the onset of this therapy or the doses needed or when to replace aspirin with LMWH in specific cases. Thus, further studies are needed to discover new treatments and prophylaxis methods for preeclampsia and IUGR.

According to our data, we can conclude that combined therapy before 16 weeks of gestation to patients at high risk of developing preeclampsia decreases the recurrence of this disease, decreases the risk of developing intrauterine fetal growth restriction and the risks for intrauterine fetal death compared to aspirin 150 mg alone.

REFERENCES

1. Daniel L. Rolnik, Kypros H. Nicolaides ,Liona C. Poon Prevention of preeclampsia with aspirin *American Journal of Obstetrics &* GynecologyVol. 226Issue 2SupplementS1108-S1119Published online: August 21, 202 0
2. Duley L. The global impact of pre-eclampsia and eclampsia. Semin Perinatol 2009;33:130-7
3. Stevens W, Shih T, Incerti D, et al. Short-term costs of preeclampsia to the United States health care system. Am J Obstet Gynecol 2017;217:237-48.e16.
4. Irving RJ, Belton NR, Elton RA, Walker BR. Adult cardiovascular risk factors in premature infants. Lancet 2000;355:2135-6
5. Moster D, Lie RT, Markestad T. Long-term medical and social consequences of preterm birth. N Engl J Med 2008;359:262-73.
6. Wu P, Haththotuwa R, Kwok CS, et al. Pre eclampsia and future cardiovascular health: a systematic review and meta-analysis. Circ Car diovasc Qual Outcomes 2017;10:e003497.
7. Lykke JA, Langhoff-Roos J, Sibai BM, Funai EF, Triche EW, Paidas MJ. Hypertensive pregnancy disorders and subsequent cardio vascular morbidity and type 2 diabetes mellitus in the mother. Hypertension 2009;53:944-51.
8. Vane JR, Botting RM. The mechanism of action of aspirin. Thromb Res 2003;110:255-8.
9. Tóth L, Muszbek L, Komáromi I. Mechanism of the irreversible inhibition of human cyclooxygenase-1 by aspirin as predicted by QM/MM calculations J Mol Graph Model 2013;40:99-109.
10. Kingdom JC, Drewlo S. Is heparin a placental anticoagulant in high-risk pregnancies? Blood 2011;118:4780-8.
11. Quenby S, Mountfield S, Cartwright JE, Whitley GS, Vince G. Effects of low-molecularweight and unfractionated heparin on trophoblast function. Obstet Gynecol 2004;104: 354-61.
12. Manduteanu I, Dragomir E, Voinea M, Capraru M, Simionescu M. Enoxaparin reduces H2O2-induced activation of human endothelial cells by a mechanism involving cell adhesion molecules and nuclear transcription factors. Pharmacology 2007;79:154-62.
13. Torricelli M, Reis FM, Florio P, et al. Low-molecular-weight heparin improves the performance of uterine artery Doppler velocimetry to predict preeclampsia and small-for-gestational age infant in women with gestational hypertension. Ultrasound Med Biol 2006;32:1431-5.
14. Yinon Y, Ben Meir E, Margolis L, et al. Low molecular weight heparin therapy during pregnancy is associated with elevated circulatory levels of placental growth factor. Placenta 2015;36:121-4.
15. Grandone E, Brancaccio V, Colaizzo D, et al. Preventing adverse obstetric outcomes in women with genetic thrombophilia. Fertil Steril 2002;78:371-5.
16. Rai R, Cohen H, Dave M, Regan L. Rando mised controlled trial of aspirin and aspirin plus heparin in pregnant women with recurrent miscarriage associated with phospholipid antibodies (or antiphospholipid antibodies). BMJ 1997;314:253-7.
17. Llurba E, Bella M, Burgos J, et al. Early prophylactic enoxaparin for the prevention of preeclampsia and intrauterine growth restriction: a randomized trial. Fetal Diagn Ther 2020;47: 1-10.
18. Roberge S, Demers S, Nicolaides KH, Bureau M, Côté S, Bujold E. Prevention of preeclampsia by low-molecular-weight heparin in addition to aspirin: a meta-analysis. Ultrasound Obstet Gynecol 2016;47:548-53. 25. Cumpston M, Li T, Page MJ, et al. Updat.
19. ISUOG Medical Practice Guidelines: The role of ultrasound in screening and monitoring pre-eclampsia
20. Crovetto F.et al.Performance of firt-trimester integrated screening for early and small for gestational age newborns.Ultrasound Obstet Gynecol 2013
21. Trudinger BJ, Cook CM, Thompson RS, et al. Low-dose aspirin therapy improves fetal weight in umbilical placental insufficiency. Am J Obstet Gynecol. Sep 1988;159(3):681-5. [Medline].
22. Leitich H, Egarter C, Husslein P, et al. A meta-analysis of low dose aspirin for the prevention of intrauterine growth retardation. Br J Obstet Gynaecol. Apr 1997;104(4):450-9. [Medline].
23. Sinkey, R.G.; Battarbee, A.N.; Bello, N.A.; Ives, C.W.; Oparil, S .; Tita, A.T.N. Prevention, diagnosis and management of hypertensive disorders of pregnancy: a comparison of international guidelines. Curr. Hypertens. Rep. 2020, 22, 66.

[CrossRef]

24. Hamulyák, E.N.; Scheres, L.J.; Marijnen, M.C.; Goddijn, M.; Middeldorp, S. Aspirin or heparin or both for improving pregnancy outcomes in women with persistent antiphospholipid antibodies and recurrent pregnancy loss. Cochrane Database Syst. Rev. 2020, 5, CD012852. [CrossRef]

25. Cruz-Lemini, M.; Vázquez, J.C.; Ullmo, J.; Llurba, E. Low-molecular-weight heparin for prevention of preeclampsia and other placenta-mediated complications: A systematic review and meta-analysis. Am. J. Obstet. Gynecol. 2022, 226, S1126-S1144.e17. [CrossRef]

26. Wu, C.; Li, L.; Zhang, J.; Song, Y. Efficacy and safety of low-dose aspirin combined with low-molecular-weight heparin in treatment of preeclampsia: A meta-analysis and systematic review. Arch. Med. Sci. 2021, 18, 1525-1534. [CrossRef] [PubMed]

MONOTERAPIA ANTIAGREGANTA VERSUS TERAPIA COMBINATA CU HEPARINA CU GREUTATE MOLECULARA MICA IN REDUCEREA RISCULUI DE APARITIE A PREECLAMPSIEI SI A RESTRICTIEI DE CRESTERE FETALA INTRAUTERINA

REZUMAT

Preeclampsia reprezinta o cauză importanta de crestere a morbidității și mortalității materne și perinatale, cu o incidenta cuprinsa intre 2% până la 8% din toate sarcinile. Asocierea preeclampsiei cu restricția de creștere fetală intrauterina și prematuritatea duce adesea la consecințe pe termen lung. Administrarea de heparina cu greutate moleculara mica (LWMH) ar putea îmbunătăți dezvoltarea placentei și inhiba căile reactive implicate în preeclampsie și restrictia de crestere intrauterina (RCIU).

Am realizat un studiu retrospectiv observational, pe o perioada de 12 luni , intr-o maternitate de grad 3 din cadrul spitalului Cllinic De Urgenta Craiova ,ce a inclus un numar de 1200 paciente examinate incepand cu primul trimestru de sarcina. La aceste paciente, s-a aplicat un algoritm de screening combinat ce a inclus : istoric de preeclampsie, valori ale tensiunii arteriale medii , Doppler la nivelul arterelor uterine, nivelul seric al factorului de crestere placentara (PIGF). Dintre pacientele screenate am identificat un numar de 82 cu risc crescut de preeclampsie.

Obiectivul studiului a fost evaluarea impactului tratamentului antiagregant plachetar comparativ cu tratamentul combinat antiagregant si anticoagulant asupra aparitiei preclampsiei, si a restrictiei de crestere intrauterine(RCIU).

Rezultatele studiului arata o imbunatatire a outcome-ului prin reducerea riscului de aparitie a preeclampsiei si a RCIU la pacientele la care s-a administrat tratament combinat vs aspirina ca monoterapie.

Cuvinte cheie: preeclampsie, RCIU, aspirina, LMWH

IMPLICATIONS OF HEREDITARY THROMBOPHILIA IN DEVELOPMENT OF FETAL INTRAUTERINE GROWTH RESTRICTION OF UNKNOWN ORIGIN

ANGHEL SAVCIU LOREDANA[1], PATRU CIPRIAN LAURENTIU[2], POPA ADELINA[1], BALACEANU DOBROMIR CRISTINA[1], CERNEA NICOLAE[2]

[1] Clinical Emergency County Hospital Craiova, Obstetrics and Gynecology Department, St Tabaci nr.1, Craiova,200642
[2] Department of Obstetrics and Gynecology, University of Medicine and Pharmacy, Craiova, St. Petru Rares, nr 2-4,200433
Correspondence PATRU CIPRIAN LAURENTIU, patru_ciprian@yahoo.com, 0761632298

ABSTRACT

Intrauterine growth restriction (IUGR) is defined as a fetal failure to reach the genetic potential for intrauterine growth. IUGR complicates up to 10% of pregnancies, representing a primary cause of morbidity and mortality. Hereditary thrombophilia has been detected in about 65% of pregnancies and because of the association with IUGR, preeclampsia, uteroplacental apoplexy, recurrent miscarriage and fetal intrauterine death, prenatal testing is recommended.

Our study included a number of 122 patients without pre-existing pregnancy pathology (study group) who were compared with a control group that included 122 patients with normal birth weight fetuses. Patients were evaluated at about 6-7 weeks postnatally when we tried to correlate the intrauterine growth restriction with the profile of hereditary thrombophilia (determination of factor II gene mutations, factor V Leiden, MTHFR gene, PAI gene, factor XIII mutation, antithrombin III, protein C, protein S).

The results of the study showed the presence of hereditary thrombophilia in 82 cases (67.2%) in the study group and in 21 cases (17.21%) in the control group. Among the genetic analyses performed we found a predominance of PAI-1 gene as well as a positive association with intrauterine growth restriction in case of concomitant presence of factor V Leiden and PAI-1 gene or MTHFR gene.

Key words: hereditary thrombophilia, IUGR, MTHFR, PAI-1

INTRODUCTION

Intrauterine growth restriction (IUGR) is defined as a fetal failure to reach the genetic potential for intrauterine growth. This may be due to fetal, maternal or placental factors. [1]

Chromosomal abnormalities (most commonly trisomy 13, 18, 21), structural abnormalities, intrauterine infections (cytomegalovirus, rubella virus, varicella-zoster virus infection, toxoplasma infection) can be implicated as fetal causes. [1]

Of the maternal factors, the most frequently implicated may be: hypertension, insulin-dependent diabetes mellitus, kidney disease, autoimmune diseases (systemic lupus erythematosus, collagenases), severe anemia, inherited or acquired thrombophilia, chronic malnutrition, drug use (tobacco, heroin, cocaine, alcohol), use of teratogenic drugs, depression and high stress levels. [1],[2],[3]

Placental factors include placental insufficiency, uteroplacental infarction or apoplexy, placental hemangioma or chorioangioma, umbilical cord abnormalities (marginal or velamentous umbilical cord insertion, single umbilical artery). [4],[5],[6],[7]

IUGR complicates up to 10% of pregnancies and is a primary cause of morbidity and mortality. [8] These cases may face postnatal increased risk of hypoglycemia, hypothermia, hyperbilirubinemia, necrotizing enterocolitis, intraventricular hemorrhage, seizures, respiratory distress syndrome, sepsis, and neonatal death. [9]

In the long term, cognitive or neurological deficits may be associated, as well as cardiovascular (stroke, coronary heart disease) and endocrinological disorders (dyslipidemia, diabetes mellitus). [4],[10]

Thrombophilia may be associated with IUGR, PE, uteroplacental apoplexy, recurrent miscarriage, MIUF, due to impaired maternal-fetal circulation including damage to the decidua and spiral arteries also causing a decrease in placental weight; hypercoagulable state and secondary thrombosis may cause placental infarction through an increased number of syncytial nodes and "accelerated villous maturation". [11],[12],[13],[14],[15],[16]

Because of identification in 65% of pregnancies [4], testing for hereditary thrombophilia associated with IUGR is recommended by the American College of Obstetrics and Gynecology (ACOG) [17]

METHOD

We conducted a retrospective observational study over a 1-year period in the Obstetrics and Gynecology Clinic of the Emergency Clinical County Hospital from Craiova between February 2022 and January 2023.

In our study, we initially extracted from the total number of births completed in the Clinic (3820 births), the cases resulted with IUGR (400 cases). From these cases we selected a group of 122 patients without pre-existing pregnancy pathologies and compared with the control group which included 122 normal birth weight fetuses. Patients from the selected cases were evaluated at 6 weeks postnatally when we tried to correlate the intrauterine growth restriction with the profile of hereditary thrombophilia. We used a protocol that included determination of mutations of factor II (prothrombin), factor V Leiden, MTHFR

gene, PAI gene, factor XIII mutation, antithrombin III, protein C, protein S.

The patients selected in the study group presented the following inclusion criteria: age between 18 and 35 years, primiparous patients, non-smokers and who presented a first trimester ultrasound pregnancy dating scan, patients without a preexisting pathology (diabetes mellitus, hypertension, preeclampsia, systemic lupus erythematosus, antiphospholipid syndrome).

During the study, fetal monitoring was performed according to the study protocol approved by the Romanian Society of Obstetrics and Gynecology. This included a detailed morphological scan at the end of the first trimester that assessed the fetal skull (choroid plexuses, thalamus, median septum), thorax and fetal heart (lung areas, diaphragm, 4-chamber view, cardiac situs and cardiac area, ejection tracts of the great vessels, confluence of the arches to the left of the spine), abdomen (presence of stomach, bowel, integrity of the anterior abdominal wall, presence of the bladder and confirmation of the paravesical vessels) and assessment of the upper and lower limbs (evidence of trisegmented limbs, assessment of the fingers and toes); assessment of resistivity index of both uterine arteries. Ater the morphological scan, patients were genetically screened by maternal serum determination of PAPA and HCG. From the patients screened by this first trimester protocol, we selected those who met the study inclusion criteria mentioned above.

Subsequently, these patients were evaluated at a 4-week interval. Depending on the time of onset of complications (onset of IUGR related to the gestational age), this study interval was modified and applied to each patient. Pregnancy follow-up referred to a morphological reassessment scan in the second trimester (20-22 weeks of gestation), fetal growth curve monitoring, assessment of the fetal intrauterine wellbeing criteria (Manning score) and resistivity index in both uterine arteries and umbilical artery.

RESULTS

400 births were complicated by intrauterine fetal growth restriction. Of these, 122 cases fulfilled our study inclusion criteria.

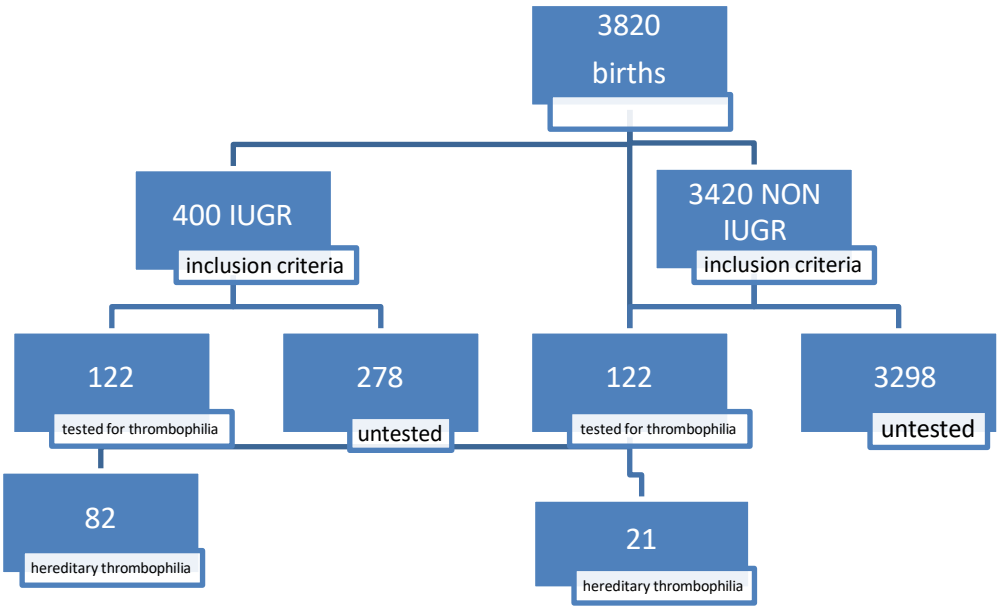

Figure 1 Patients sampling.

According to the gestational age we identified a distribution of IUGR as follows: between 30-34 weeks of gestation we identified a number of 31 cases, between 34-36 weeks of gestation we identified a number of 73 cases and over 36 weeks of gestation we identified a number of 18 cases (Figure 2).

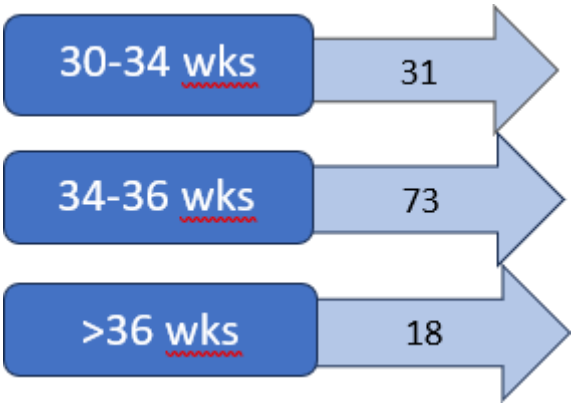

Figure 2 Distribution of IUGR cases according to gestational age

Genetic and biological analysis for hereditary thrombophilia was performed at 6 weeks postpartum. Following these results, we identified that hereditary thrombophilia was present in 82 cases (67.2%) in the group that developed intrauterine growth restriction and in 21 cases (17.21%) in the group with normal weight newborns.

Among the genetic analyses we found the predominance of the PAI-1 gene (polymorphic variant 4G/5/G) which was found in 58 cases in the group with restriction and in 24 cases in the group with normal-weight newborns. We also found a significant association of the MTHFR gene in 55 cases in the first group and in 15 cases in the second group. Homozygous factor V Leiden was present in 36 cases in the first group and in 4 cases in the second group, while the heterozygous variant was present in 32 cases in the first group and in 30 cases in the second group.

As for multiple thrombophilia (presence of more than one thrombophilic factor) a positive association with intrauterine growth restriction was detected in the case of concomitance between factor V Leiden and the PAI-1 gene or the MTHFR gene. (Table I)

	Group I(IUGR)	Group II (normal weight)
PAI-1 GENE	58 (48%)	24 (20%)
MTHFR GENE	55 (45%)	15 (12%)
FACTOR V LEIDEN HOMOZYGOUS TYPE	36 (30%)	4 (5%)
FACTOR V LEYDEN HETEROSYGOT TYPE	32 (26%)	30(24,5%)
FACTOR V LEYDEN + PAI -1 GENE	85 (69%)	12 (9,8)
FACTOR V LEIDEN + MTHFR GENE	80 (65%)	10 (8,1%)
PROTEIN S	2	0
PROTEIN C	1	0

Table I Distribution of thrombophilic mutation

DISCUSSION

Thrombophilia is a group of conditions that increase the risk of thromboembolic disease in the general population.[18] The risk increases in pregnant women due to physiological hypercoagulability caused by certain changes in clotting factors. [19] This state of hypercoagulability and secondary thrombosis can lead to changes in maternal-fetal circulation resulting in adverse pregnancy outcomes.

IUGR is a frequent cause of increased intrauterine fetal deaths, perinatal morbidity and mortality and long-term consequences, but in most cases its etiology remains unknown. [20]

In the current literature there is no consensus on the strongest association between the type of thrombophilia and IUGR. Differences could result from the ethnic heterogeneity of the groups included in the study (for example, factor V Leiden is the most common thrombophilia mutation in Europe; in the United States the prevalence is between 3% and 8%, while in Asia it is a rare mutation [21], [22] and also from the types of thrombophilia tested in each study.

Identification of the type of thrombophilia is opportune in order to diagnose a pregnancy at risk of IUGR, as it could minimize or avoid maternal-fetal complications including decreasing the risk of antepartum fetal death.

In the study group, we identified 82 (67.2%) patients with IUGR fetuses without pre-existing maternal-fetal pathologies,

while in the control group we identified 21 (17.21%) patients with normal weight fetuses who had hereditary thrombophilia. This result is similar to a study conducted by Dugalic et al [23] who also found that 69.68% cases with IUGR of unknown origin and 18.88% of cases with normal fetal growth had associated hereditary thrombophilia. Also, the results of our study are in agreement with Jamal et al and Kupforminc et al who demonstrated a significant association between IUGR and thrombophilia. [24],[25]

Depending on the subtype of the tested thrombophilia, we found a predominance of PAI-1(4G/5/G phenotype) and MTHFR (C677T, A1298C variants) gene mutations. Thus, in the IUGR group we had 58 cases (48%) with PAI-1 gene mutation and in the control group we identified 24 cases (20%). In the study group, we identified 55 patients (45%) with MTHFR gene mutations and 15 patients (12%) in the control group.

The results of a study by Mirzaei et al [26] BUC show a prevalence of thrombophilia of 32% in the control group and 68% in the IUGR group. A statistically significant association between types of hereditary thrombophilia and IUGR was present in cases of MTHFR mutations, (48% in the restriction group versus 20% in the control group) protein S deficiency (32% versus 8%) and multiple thrombophilia (24% versus no cases in the control group).

Dugalic S et al found these mutations present in 36% for the PAI-1 gene and 27% for the MTHFR gene in cases of IUGR of unknown origin and in 7% of cases in the control group. [23]

Mutlu et al [27] examined 204 cases with poor previous obstetric findings for thrombophilia mutations and discovered only one association with MTHFR mutation (90.9%) related to IUGR and hereditary thrombophilia.

On the other hand, there are studies that do not confirm the association of IUGR and MTHFR mutation. In a study published in 2018 that included a total of 303 participants with MTHFR and IUGR mutations, Del Gobbo et al [28], did not find an association between MTHFR 1298CC genotype and IUGR, but only found a trend of increasing MTHFR 677TT in IUGR.

In our study, the presence of factor V Leiden mutations was for the homozygous variant in 30% of the cases in the study group and 5% of the cases in the control group. The presence of factor V Leiden mutations was for the heterozygous variant was detected in 26% of the cases in the study group and in 24.5% of the cases in the control group.

We also identified various thrombophilic combinations. The most relevant was the association between factor V and the PAI gene which was identified in 69% of cases in the study group versus 9.8% in the control group. We also identified an association with the MTHFR gene present which was present in 65% of cases in the study group versus 8.1% in the control group.

A retrospective study published by Vicoveanu et al [29] in 2021, which included 179 pregnancies with inherited thrombophilia, analyzed neonatal outcomes and concluded that IUGR was statistically significantly associated with homozygous factor V Leiden mutation (33.3%) and combined MTHFR and factor V Leiden mutations (83.4%).

CONCLUSIONS

According to our study results, we can conclude that there may be a causal relationship between hereditary thrombophilia and IUGR, especially in relation to PAI, MTHFR, factor V Leiden gene mutations.

There is no consensus on the different types of thrombophilia; their classification should be made both in terms of thrombogenic risk and in terms of pregnancy risks. The most important thrombophilic risk is the development of IUGR.

The relationship between the different types of hereditary thrombophilia and IUGR is needed to be further studied in order to identify new ways of intervening to prevent recurrence.

REFERENCES

[1] L. M. M. Nardozza *et al.*, "Fetal growth restriction: current knowledge," *Archives of Gynecology and Obstetrics*, vol. 295, no. 5. Springer Verlag, pp. 1061–1077, May 01, 2017. doi: 10.1007/s00404-017-4341-9.

[2] C. I. Laire Nfante -r Ivard *et al.*, "ABSENCE OF ASSOCIATION OF THROMBOPHILIA POLYMORPHISMS WITH INTRAUTERINE GROWTH RESTRICTION A BSTRACT," 2002. [Online]. Available: www.nejm.org

[3] L. M. E. McCowan, S. Craigie, R. S. Taylor, C. Ward, C. McLintock, and R. A. North, "Inherited thrombophilias are not increased in 'idiopathic' small-for-gestational-age pregnancies," *Am J Obstet Gynecol*, vol. 188, no. 4, pp. 981–985, Apr. 2003, doi: 10.1067/mob.2003.218.

[4] "ACOG PRACTICE BULLETIN Clinical Management Guidelines for Obstetrician-Gynecologists." [Online]. Available: http://journals.lww.com/greenjournal

[5] D. Maulik, "Fetal Growth Restriction: The Etiology."

[6] R. E. Bohîlțea *et al.*, "Clinically Relevant Prenatal Ultrasound Diagnosis of Umbilical Cord Pathology," *Diagnostics*, vol. 12, no. 2, Feb. 2022, doi: 10.3390/diagnostics12020236.

[7] R. E. Bohiltea *et al.*, "The Strategy against Iatrogenic Prematurity Due to True Umbilical Knot: From Prenatal Diagnosis Challenges to the Favorable Fetal Outcome," *J Clin Med*, vol. 11, no. 3, Feb. 2022, doi: 10.3390/jcm11030818.

[8] J. G. Martins, J. R. Biggio, and A. Abuhamad, "Society for Maternal-Fetal Medicine Consult Series #52: Diagnosis and management of fetal growth restriction."

[9] A. W. Shand, J. Hornbuckle, E. Nathan, J. E. Dickinson, and N. P. French, "Small for gestational age preterm infants and

relationship of abnormal umbilical artery Doppler blood flow to perinatal mortality and neurodevelopmental outcomes," *Australian and New Zealand Journal of Obstetrics and Gynaecology*, vol. 49, no. 1, pp. 52–58, Feb. 2009, doi: 10.1111/j.1479- 828X.2008.00941.x.

[10] Y. Leitner *et al.*, "Neurodevelopmental outcome of children with intrauterine growth retardation: A longitudinal, 10-Year prospective study," *J Child Neurol*, vol. 22, no. 5, pp. 580–587, May 2007, doi: 10.1177/0883073807302605.

[11] "Editorials T HE A MERICAN H EALTH C ARE S YSTEM R EVISITED-A N EW S ERIES T HE E VOLVING T ECHNOLOGY
OF V ENOUS A CCESS," 1999.

[12] B. Brenner, "Thrombophilia and Adverse Pregnancy Outcome," *Obstetrics and Gynecology Clinics of North America*, vol. 33, no. 3. pp. 443–456, Sep. 2006. doi: 10.1016/j.ogc.2006.05.010.

[13] I. D. Walker, "Thrombophilia in pregnancy," 2000. [Online]. Available: www.jclinpath.com

[14] H. Pinar, C. J. Sung, C. E. Oyer, and D. 6 Singer, "REFERENCE VALUES FOR SINGLETON AND TWIN PLACENTAL WEIGHTS."

[15] B. B. Rogers *et al.*, "Avascular villi, increased syncytial knots, and hypervascular villi are associated with pregnancies complicated by factor V leiden mutation," *Pediatric and Developmental Pathology*, vol. 13, no. 5, pp. 341–347, Sep. 2010, doi: 10.2350/09-05-0657-OA.1.

[16] R. W. Redline, "Thrombophilia and Placental Pathology."

[17] "Prevalence of Common Inherited Thrombophilias Factor V Leiden."

[18] A. Dautaj *et al.*, "Hereditary thrombophilia," *Acta Biomedica*, vol. 90. Mattioli 1885, pp. 44–46, Oct. 02, 2019. doi: 10.23750/abm.v90i10-S.8758.

[19] M. J. Paidas, D. H. W. Ku, and Y. S. Arkel, "Screening and management of inherited thrombophilias in the setting of adverse pregnancy outcome," *Clinics in Perinatology*, vol. 31, no. 4. pp. 783–805, Dec. 2004. doi: 10.1016/j.clp.2004.07.002.

[20] H. L. Galan, E. Ferrazzi, and J. C. Hobbins, "Intrauterine growth restriction (IUGR): Biometric and Doppler assessment," *Prenat Diagn*, vol. 22, no. 4, pp. 331–337, 2002, doi: 10.1002/pd.311.

[21] M. J. Paidas, *Hemostasis and thrombosis in obstetrics & gynecology*. Wiley-Blackwell, 2011.

[22] J. L. Kujovich, "Factor v Leiden thrombophilia," *Genetics in Medicine*, vol. 13, no. 1. Nature Publishing Group, pp. 1–16, 2011. doi: 10.1097/GIM.0b013e3181faa0f2.

[23] S. Dugalić *et al.*, "The association between IUGR and maternal inherited thrombophilias A case-control study," *Medicine (United States)*, vol. 97, no. 41, Oct. 2018, doi: 10.1097/MD.0000000000012799.

[24] J. E. Jones, J. A. Jurgens, S. A. Evans, R. C. Ennis, V. A. M. Villar, and P. A. Jose, "Mechanisms of Fetal Programming in Hypertension," *Int J Pediatr*, vol. 2012, pp. 1–7, 2012, doi: 10.1155/2012/584831.

[25] C. L. S. Turner *et al.*, "Methylation analysis of 79 patients with growth restriction reveals novel patterns of methylation change at imprinted loci," *European Journal of Human Genetics*, vol. 18, no. 6, pp. 648–655, Jun. 2010, doi: 10.1038/ejhg.2009.246.

[26] F. Mirzaei and Z. Farzad-Mahajeri, "Association of hereditary thrombophilia with intrauterine growth restriction," 2013.

[27] I. Mutlu, M. F. Mutlu, A. Biri, B. Bulut, M. Erdem, and A. Erdem, "Effects of anticoagulant therapy on pregnancy outcomes in patients with thrombophilia and previous poor obstetric history," *Blood Coagulation and Fibrinolysis*, vol. 26, no. 3, pp. 267– 273, Apr. 2015, doi: 10.1097/MBC.0000000000000219.

[28] G. F. Del Gobbo, E. M. Price, C. W. Hanna, and W. P. Robinson, "No evidence for association of MTHFR 677C>T and 1298A>C variants with placental DNA methylation," *Clin Epigenetics*, vol. 10, no. 1, Mar. 2018, doi: 10.1186/s13148-018-0468-1.

[29] P. Vicoveanu, "The association between factor V Leiden, MTHFR C667t/A1298c polymorphisms and pregnancy outcomes,"
Revista Medico-Chirurgicala, vol. 125, no. 4, pp. 563–569, Dec. 2021, doi: 10.22551/MSJ.2021.04.11.

IMPLICAREA TROMBOFILIEI EREDITARE IN RESTRICTIA DE CRESTERE INTRAUTERINA DE ETIOLOGIE NECUNOSCUTA REZUMAT

Restricția de creștere intrauterina(RCIU) este definita ca o incapacitate fetala de atingere a potentialului genetic de crestere intrauterina. RCIU complică până la 10% din sarcini, reprezentând o cauză primară de morbiditate și mortalitate Datorita identificarii intr-un procent de 65% dintre sarcini si a asocierii cu RCIU, preclampsie, apoplexie utero-placentara, avorturi recurente si moarte fetala in utero, se recomanda testarea trombofiliilor ereditare associate RCIU.

Studiul nostru a inclus un numar de 122 de paciente fara patologii asociate preexistente sarcinii (lotul de studiu) care au fost comparate cu un lot martor ca a inclus 122 paciente cu feti cu greutate normala la nastere. Pacientele au fost evaluate la controlul de 6 saptamani postpartum pentru a corobora restrictia de crestere intrauterina cu profilul de trombofilie

ereditara (determinarea mutatiilor genelor factorului II, a factorului V Leiden, a genei MTHFR , a genei PAI, mutatia factorului XIII , antitrombina III, proteina C, proteina S.

Rezultatele studiului au aratat prezenta trombofiliei ereditare intr-un numar de 82 de cazuri (67,2%) in lotul se studiu si la 21 de cazuri (17,21%) in lotul martor. Dintre analizele genetice efectuate am constatat predominanta genei PAI-1 cat si o asociere pozitiva cu restrictia de crestere intrauterina in cazul concomitentei prezentei factorul V Leiden si a genei PAI-1 sau gena MTHFR.

Cuvinte cheie: trombofilie ereditara, RCIU, MTHFR, PAI-1

A FOCUSED REVIEW OF THE IMMUNE RESPONSE IN ELECTROCHEMOTHERAPY

Mircea Bogdan Matei[1,2*], Christien Oktaviani Matei[2,3], Ali Sibel[2], Leon Zăgrean[1], Mihaela Georgeta Moisescu[2,3]

[1]Physiology and Neuroscience Division., University of Medicine and Pharmacy Carol Davila, Bucharest, Romania

[2]Biophysics and Cellular Biotechnology Division., University of Medicine and Pharmacy Carol Davila, Bucharest, Romania

[3]Excellence Center for Research in Biophysics and Cellular Biotechnology, University of Medicine and Pharmacy Carol Davila, Bucharest, Romania

* Corresponding author

Mircea Bogdan Matei, Physiology and Neuroscience Division and Biophysics and Cellular Biotechnology Division,

University of Medicine and Pharmacy Carol Davila

Bucharest, Romania

e-mail: bogdan.matei@umfcd.ro

Abstract

Electrochemotherapy has been established since 2018 as an mainstream major cancer treatment. Electrochemotherapy is based on reversible electroporation and concomitant low-dose chemotherapy administration to target both cutaneous and subcutaneous tumor types . Standardized protocols, including the revised ESOPE (2018)[1] and NICE (2014)[2] guidelines, support electrochemotherapy (ECT), which is practiced in over 150 medical centers across Europe. The Insp-ECT (International Network for Sharing Practices on Electrochemotherapy) study[3] reported an average 80% objective response rate for multiple cutaneous tumor types following ECT treatment. The emergence of checkpoint inhibitors in immunotherapy, such as PD-L1 molecules, has highlighted the immune system's role in combating malignancy[4]. Consequently, the immune system's contribution to ECT's effectiveness, including impacts on untreated distant tumors, has garnered interest. Some studies attribute the lack of local recurrence after ECT to immunological mechanisms involving DAMPs molecules like calreticulin and HMGB1, while others argue that this response is insufficient for a systemic abscopal effect[5]. Ongoing research explores combining ECT with immuno-stimulants (including gene electro-transfer of immune molecules) to enhance therapeutic outcomes[6]. This review summarizes reports on the immune response's role in ECT's clinical efficacy and recent electro/immune therapy combinations.

Keywords: electrochemotherapy, abscopal effect, gene electrotransfer, electroporation

Overview

Electrochemotherapy (ECT) is a local procedure that combines reversible electroporation (EP) of cellular membrane with low-dose chemotherapy. The intrinsic cytotoxicity of a non-permeant or poorly permeant chemotherapeutic drug delivered intravenously or injected intratumorally, is highly increased by the exposure of cells to controlled electric pulses which permeabilize the cell membrane and allow an increased diffusion of the drug inside the cell[7]. To be treated efficiently, the whole tumor must be exposed to the drug molecules and simultaneously to electric field pulses having an intensity above a specific threshold value which reversibly permeabilize the cytoplasmic membrane. The steps of an ECT

procedure are presented in Fig 1.

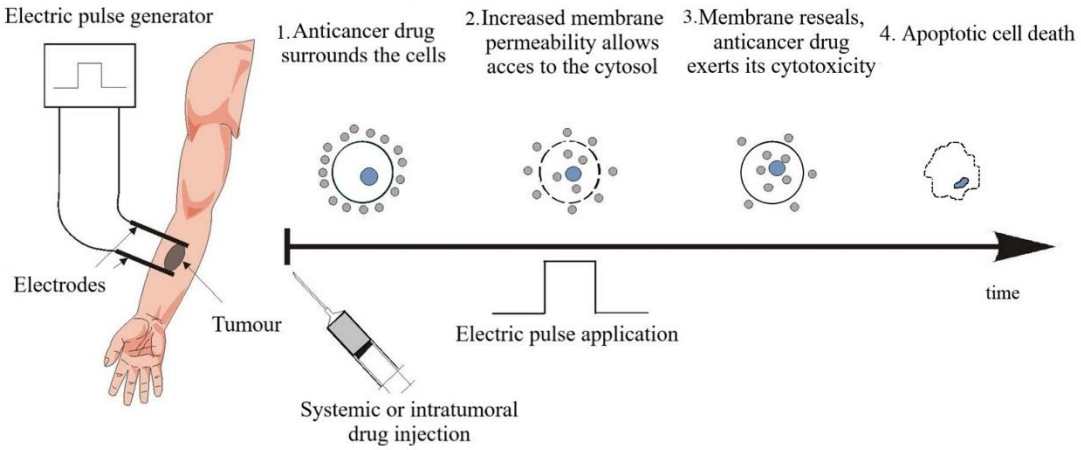

Fig 1 Schematic representation of ECT procedure: the drug is injected in bolus, after a waiting period of 20 minutes electroporation is performed on one or multiple nodules, after the cell membrane reseals, the drug exerts the cytotoxic effect ending with the apoptotic/mitotic cell death. (Adapted after Miklavcic, D.,- 2012) [8]

ECT is an effective treatment approach for a wide range of tumor histologies as malignant melanoma, non-melanoma skin cancers, breast cancer, cervical leiomyosarcoma, basal cell and Merkel cell carcinoma, Kaposi sarcoma and skin metastases of any histology which are symptomatic due to bleeding or pain. One unique advantage of ECT over conventional surgery or other ablation therapies is the possibility to treat inoperable primary cancers or metastases like those found near major neuro-vascular pathways [9]. As a therapeutic method for cutaneous tumors, ECT is accepted as a standardized procedure by ESOPE (European Standard Operating Procedures on Electrochemotherapy) and included in National Institute for Health and Care Excellence (NICE) guidelines. This standardized treatment requires the use of medical approved devices (like CliniporatorTM, IGEA [10]) which ensure a minimal invasiveness, a fast application of electric field, and a simple and clear usability. The method became more widely used after the recent reports from Insp-ECT (International Network for Sharing Practices on Electrochemotherapy) about the remarkable efficiency of ECT in large cohorts of patients: 80% objective response rate in the case of all oncological histologies, and 60–70% complete remission rate following only one treatment[11].

Some of the major benefits of ECT include: the scarce chance of drug resistance occurrence in case of repeated treatments, a reduction of chemotherapy dosage and the subsequently increased quality of life index.

During EP pulses application the cells within the targeted tumor area are subjected to transient structural changes which can be modulated by using electric pulses with precisely controlled parameters (number, shape, duration, and repetition frequency, direction of the electric field), electrode geometry, and electrode position with respect to the tumor. The pulsing procedure given in ESOPE consists in 8 square wave pulses of 100 µs, resulting in an electric field of 1000V/cm between electrodes at adequate distances, with variations in protocol depending on tumor size, drug administration pathway, electrode type and the CliniporatorTM machine used[11]. When choosing the geometry and positioning of electrodes one must consider that the whole tumor should be exposed to an electric field above the permeabilizing threshold and as homogenously as possible[8]. The normal tissue around the tumor exposed to ECT is less affected since the division rate of healthy cells is slower compared to cancer cells and the membrane repair capacity is better preserved[12].

During ECT, therapeutic drug concentrations are obtained in tumor cells, resulting in a several fold increased cytotoxicity[13].This allows the use of lower dosages of bleomycin and cisplatin, compared to standard chemotherapy, enabling to repeat the procedure several times and avoiding the risk of occurrence of major side effects of the drugs (for bleomycin: nausea and vomiting, pneumonia, pulmonary fibrosis, hematological toxicity, skin reactions; for cisplatin: nausea and vomiting, hair loss,

impeded wound healing, temporary vision loss, infections, hematological toxicity).
The implications of immune activity during ECT administration have been investigated through various in vitro, in vivo, and clinical studies, which indicate that the response to ECT differs significantly between immunodeficient and immunocompetent cases. Additionally, the role of the immune system in the progression of various solid tumors following combined ECT-immunotherapy treatment is being increasingly studied, with positive outcomes such as the absence of local recurrence being observed.[14].

ECT and immune response

A series of studies have demonstrated that electrochemotherapy induces immunogenic cell death markers, such as adenosine triphosphate, calreticulin, heat-shock proteins, and high-mobility group box-1, which are crucial for generating tumor-specific cytotoxic T cells[15, 16]. The CD8+ T cells involved are specifically generated and can potentially target cancer cells that are resistant to other treatments. Studies on ECT in immunodeficient mice also support the immune response theory: the oedema and tumor regression after ECT delivery was significantly reduced in T lymphocyte-deficient mice compared to immunocompetent ones. ECT-induced local oedema encourages the infiltration of dendritic cells and lymphocytes into the affected area [17], which are found in all tumors treated with electrochemotherapy post-therapy. Furthermore, electrochemotherapy aids in the maturation of existing Langerhans cells within the tumor, prompting their movement to the tumor-draining lymph nodes and triggering a robust peripheral release of anti-tumor monocytes. It was previously thought that electrochemotherapy only provoked a localized anti-tumor immune response and had no effect on distant untreated nodules, indicating that the immunogenic cell death induced by electrochemotherapy was not strong enough to eradicate distant tumors. However, recent findings indicate that combining ECT with immunostimulants like IL-2-based immunotherapy can potentially treat both ECT-targeted and distant nodules18.

Inflammatory responses

Reversible electroporation (EP) alone, without the addition of chemotherapy, does not result in significant cell death or non-thermal tumor ablation[14]. However, it does induce immunological effects. The secretion of pro-inflammatory mediators, such as TNF-α, IL-1β, and other cytokines from the electropermeabilized cells, drives the recruitment of immune cells to the electroporated regions. This results in an inflammatory microenvironment in the treated area [17], characterized by a high inflammatory cellular infiltration (such as macrophages, dendritic cells, and polymorphonuclear leukocytes). Additionally, the presence of antigen-presenting cells in the electroporated area leads to the upregulation of APC maturation markers such as the F4/80 antigen or molecules of the type II major histocompatibility complex class. Interestingly, studies have shown that APC and PMN infiltration also occurs when electroporation is combined with DNA injection[18], enhancing immunization in DNA vaccination contexts. Additionally, the release of ATP following EP supports the hypothesis that EP promotes the chemoattraction of DCs and their precursors, facilitating their differentiation and maturation into antigen-presenting DCs[17]. Another pro-immunological effect of EP is observed at the vascular level, where acute vasoconstriction of blood vessels[14], particularly prolonged in tumor capillaries, facilitates the extravasation of immune cells and erythrocytes.

Induced immunogenic cell death

The pathway of cell death triggered by a treatment is crucial for its therapeutic success, as it influences the effectiveness of the systemic anti-tumor immune response. The way in which tumoral cells die due to electrochemotherapy depends on the specific mechanism of action of the chemotherapy. In this course of actions the host's immune response is vital in overcoming tumor resistance [14]. Four main types of cell death have been classified based on the tumor type and chemotherapeutic drug used: (i) mitotic cell death (with bleomycin), (ii) apoptotic cell death (with bleomycin), (iii) necroptosis (with bleomycin, cisplatin, and oxaliplatin), and (iv) pyroptosis-like immunogenic cell death (with bleomycin) [19].
One apoptosis type generated by various oncological treatments (such as chemotherapeutic drugs, oncolytic viruses, physicochemical therapies (cryotherapy), photodynamic therapy or radiotherapy) is the immunogenic cell death (ICD) [20, 21]. The ICD main mechanism of action is based on the release of damage-associated molecular patterns (DAMPs) from affected tumor cells. Critically during immunogenic cell death, the increase of reactive oxygen species and the subsequent stress in the endoplasmic reticulum (ER) leads to the increased level of (DAMPs). These DAMPs include the cell surface display of calreticulin (CRT) and heat-shock proteins (HSP70 and HSP90), as well as the extracellular release of molecules such as adenosine triphosphate (ATP), high-mobility group box-1 (HMGB1), type I interferons (IFNs), C-X-C motif chemokine ligand 10 (CXCL10), and members of the interleukin-1 (IL-1) cytokine family.)[22]. These molecules act as activators and thus are able to boost tumor-specific immune

responses. ECT-released DAMPs bound on a series of risk-detecting receptors (or pattern recognition receptors (PRRs) such as toll-like receptors (TLRs) or NOD-like receptors (NLRs)[23]. These receptors are constitutive found on innate immune cells (such as dendritic cells (DCs), monocytes, and macrophages), and their activation leads to the activation of T lymphocytes that are thus able to eliminate tumor cells via phagocytosis. These processes may be supported and further enhanced by additional molecular events, such as the exposure of other ER chaperones on the cancer cell surface (including HSP90), and the secretion of various immunostimulatory cytokines like IL-1β and IL-17 by different immune cell types, thus facilitating DC recruitment into the tumor bed (also stimulated by ATP), tumor antigen engulfment by DCs (also stimulated by calreticuline), and optimal antigen presentation to T cells (also stimulated by HMGB1) [15]. ECT-treated melanoma patients have shown dendritic cell infiltration as a local response to the oncological treatment [24].

This ICD process discussed above can be complementary described as a balance between calreticulin (CRT) and CD47 upregulation on the tumor cell membrane. The CD47 is a widely expressed cell surface protein that regulates phagocytosis by innate immune cells, acts as a non- phagocytosis main signal addressed to macrophages and opposes the CRT which acts here as one of the phagocytosis main signal, as seen in Fig 2. [25].

To conclude, electrochemotherapy (ECT) induces mitotic death in the regions with both electric field and drug concentration coverage, with the apoptosis cascade triggered by tumor-associated antigens release from electroporated cells. The balance between calreticulin and CD47, as a crucial role/ and/or key mechanism of action played in the immune response should be a focus of future studies on this ECT driven immunogenic cell death. It is worth noted that/Notably, cells that receive suboptimal ECT, such as surviving cancer stem cells or chemo-resistant cells, are later identified and eliminated by the cellular immune system, specifically by primed effector T cells p(via their earlier exposure to TAAs)[6]. These findings highlight the activation of the immune system following ECT, which may explain the absence of local recurrence and support the rationale for combining ECT with immunotherapy.

Emerging co-therapies applied with ECT

Although electrochemotherapy has an efficient direct effect for solid tumors, the anti-tumor immune response it elicits is insufficient to eradicate distant tumors. Emerging combination treatments, including checkpoint inhibitors and immunomodulators, are now being employed to enhance the immunological response induced by ECT, thereby promoting a systemic anti-tumor effect.

ECT addresses immune evasion mechanisms when combined with immunotherapy

While immunogenic cell death (ICD) induced by electrochemotherapy (ECT) promotes a beneficial immune response, tumors also have developed immune evasion mechanisms that are crucial for cancer progression.

Studies have highlighted the role of tumor neoantigens in the immune recognition of cancer cells. Tumor cells that present specific mutant antigens or fail to express antigens can evade immune detection. Immune editing shape tumor cell antigenicity during tumor attacks and reductions creating surviving resistant cells that contribute to the development of new cancer cell sub-populations.

Among several strategies employed by the tumoral cells to silence the immune response : (i) reducing the expression of MHC-1 to prevent recognition by immune cells, (ii) diminishing NK cell attacks by lowering the expression of NK cell receptors and activators, (iii) immune suppressor release that create an immunosuppressive microenvironment, iv) immunoediting ability of immunocompetent T cells creating cancerous resistant cell sub-populations[18, 27]. Examples of mechanisms by which tumor cells escape immune detection are illustrated in Fig. 3.

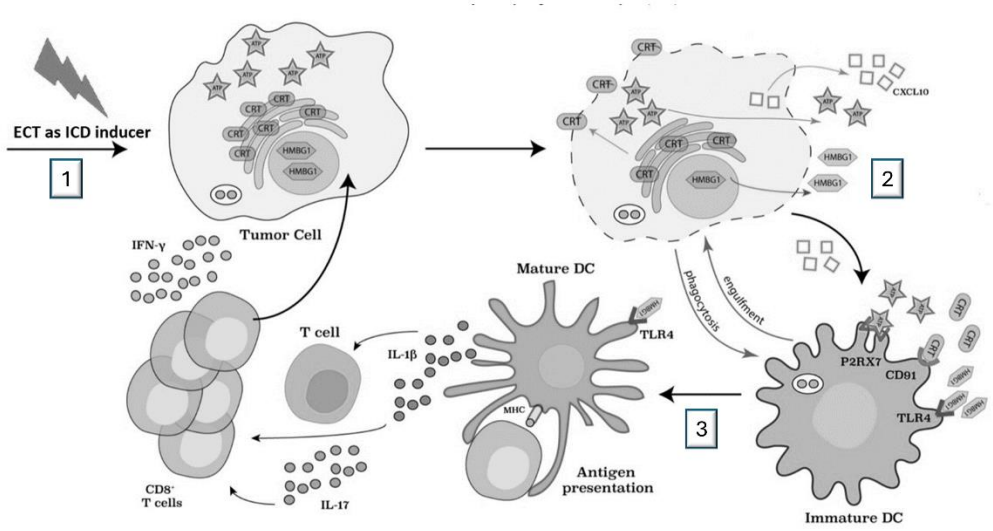

Fig. 2 Schematic representation of ECT as an ICD inducer in the micro-tumoral environment and the complex process of generation of tumor-specific cytotoxic T cells : 1) ECT application; 2) alterations in the tumor cell membrane inducing a specific immune reaction followed by the subsequent release of soluble mediators into the tumor microenvironment which in turn are bounding on dedicated receptors expressed by APC such as dendritic cells, and 3) presentation of tumor-associated antigens, leading to activation and proliferation of type T cytotoxic lymphocytes (CD8+)Note: the number of various immune cells types in place at the time of electric pulses application influences the impact of ECT in efficient removal of tumor cells. (Adapted after Terenzi et al., Journal of Inorg. Biochem. 2016[26])

The immunosuppressive microenvironment is realized mainly by altering the induction of immune checkpoint receptors (example given CTLA-4, PD-L1) and secretion of anti-inflammatory cytokines by tumoral cells (such as interleukins (IL-10) or metabolic enzymes like indoleamine 2,3-dioxygenase (IDO) [28]). A weak antitumor T cell activity is thus created which promotes the expansion of regulatory T cells (Treg) and myeloid-derived suppressor cells (MDSCs). Furthermore, macrophages are polarized towards the tumor-promoting M2 phenotype, also known as tumor-associated macrophages (TAMs).).[28]. Therefore, treatments aimed at enhancing the immune response have become a promising approach in the oncology field.

Recent advances in immunotherapy have shown promising results in cancer treatment. By combining immunotherapy with electrochemotherapy (ECT) new possibilities have been offered for long-term cancer eradication by enhancing and sustaining anti-tumor immunity.[29]. Immunotherapy has recently become one of the primary treatment options for melanoma. Most of the data on the efficacy of combining immunotherapy with other treatments have been gathered from patients with this low-survival-rate disease[30].

In a case report, combining BLM-ECT with ipilimumab, a monoclonal antibody targeting cytotoxic T lymphocyte-associated protein 4 led to a complete clinical response in a patient with multiple cutaneous melanoma metastases. Additionally, the appearance of vitiligo-like lesions specifically around the ECT treatment sites indicated that ipilimumab enhanced the immune activation initially triggered by ECT [11].

In another case report, the combination of BLM-ECT with nivolumab, an anti-programmed cell death protein 1 (PD-1) inhibitor, used as a fifth-line treatment, showed no evidence of cutaneous or visceral disease at a 4-year follow-up. This resulted in an extended remission period for a patient with advanced metastatic melanoma[31].

In a retrospective analysis patients treated with both ipilimumab and BLM-ECT, an objective response was observed in 67% of them (n=15), with 27% achieving a complete response and 40% a partial response. However, this study's limitation was the lack of a control group receiving only ipilimumab[32].

Another retrospective trial compared the effectiveness of BLM-ECT combined with ipilimumab to BLM-ECT combined with PD-1 inhibitors (pembrolizumab or nivolumab) in treating unresectable or metastatic melanoma. The ipilimumab group showed a systemic overall response rate (ORR) of 19.2%, while the anti-PD-1 group exhibited a systemic ORR of 40%. The study concluded that ECT combined with PD-1 inhibitors was more effective than ECT with ipilimumab in terms of overall response[33]. These findings are promising for the treatment of malignant melanoma, highlighting the need for more prospective trials to fully assess this combination's potential. Currently, a phase II interventional trial of ECT combined with pembrolizumab is underway[34]

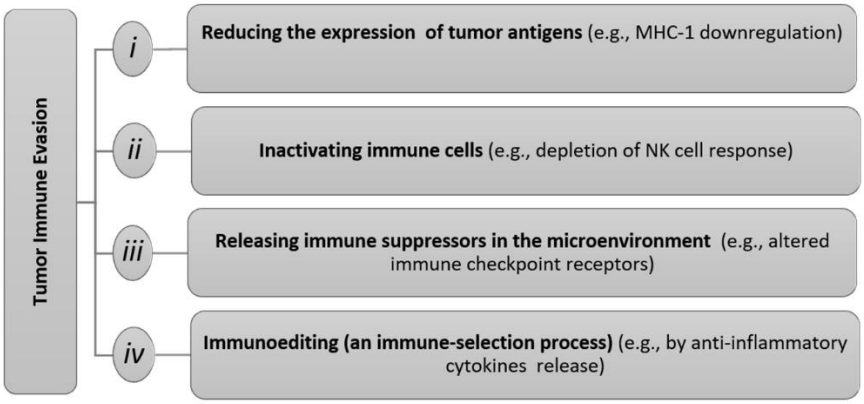

Fig. 3 Schematic representation of the ways in which tumor cells escape the immune system detection. (Abbreviations: NK, natural killer T lymphocyte; MHC-1, major histocompatibility complex molecules)

ECT and electrogene therapy

DNA vaccination and cytokine-based anti-cancer therapies represent the most advanced strategies of gene electrotransfer (GET), also known as electrogenetherapy (EGT), which aims to stimulate anti-tumor immunity. GET involves delivering plasmid DNA (pDNA) or small interfering RNA (siRNA) molecules to various tissues, including tumors, through electroporation. This process allows for the transfer of therapeutic genetic material, enabling gene therapy to restore specific cellular functions and instruct cells to produce therapeutic or immunogenic proteins endogenously[35].

GET, which can be administered either intratumorally or peritumorally into the skin, involves in vivo gene electrotransfer of plasmid DNAs (pDNAs) encoding immunomodulatory molecules like cytokines, chemokines, and adjuvant sequences. Additionally, DNA vaccines carrying tumor-specific or tumor-associated antigens (TAAs) can be used alone or combined with chemotherapeutics for tumor treatment. The choice of approach depends on the immunogenicity of the tumors and the immune status of the organism[36, 37].

Plasmids up to 15 kilobases, edited with a Kozak sequence, are used for electrotransfer-based gene treatments in eukaryotic cells. Gene expression is regulated by environmental and developmental factors, with regulatory elements located at various distances from the gene. In gene therapy, coding sequences must be minimized. Tissue-specific promoters, which limit expression to specific tissues and reduce off-target effects, are commonly used in clinical trials, though their expression levels are typically lower than those of viral promoters. Cell-specific targeting is also achievable through nuclear import sequences[38]. Regulable promoters, which can be controlled by an external factor, have significant potential but should be designed for inducible rather than repressible expression to minimize patient exposure to the inducing agent.

Electrotransfer of mRNA is commonly used to engineer antigen-presenting cells in vitro, inducing antitumor activity when injected into a patient. RNA interference can suppress gene expression after direct electroporation-mediated delivery of sequence-targeted small RNAs. Double-stranded small interfering RNA and stem-loop containing microRNA, derived from endogenous RNAs, are 20–30 base pair oligonucleotides that are processed in the cytoplasm to cleave and degrade specific target mRNAs. Since ubiquitous and resilient ribonucleases degrade cytoplasmic RNA, this must be considered when

using electroporation as a delivery method. Pattern recognition receptors identify specific pathogen components, such as bacterial endotoxin and nucleic acids, triggering an inflammatory response and/or cell death. Gene therapies, including those involving viruses, plasmids, and oligonucleotides, can be detected by these receptors and may be mistaken for pathogen invasion, leading to unregulated inflammatory responses.[36].

Immune stimulation through EGT has shown significant promise for cancer treatment due to its safe administration [39], enhanced DNA uptake, and adjuvant effects. The stress condition induced by EGT stimulates local production of inflammatory cytokines, activating the innate immune response and recruiting M1 macrophages with anti-tumor activity. It also enhances adaptive immunity by attracting lymphocytes and inflammatory cells to the electroporated areas [27].

One of the most studied applications of EGT is the transfer of an immune gene coding for IL-12, which promotes the cytotoxicity of immune cells in both the innate and adaptive immune systems, fostering an antitumor type 1 cytokine environment. IL-12 promotes the secretion of IFN-γ from NK cells and T lymphocytes, enhancing the function of antigen-presenting cells by increasing class I and II MHC molecule expression. IL-12 also has anti-angiogenic properties[27]. Although recombinant IL-12 has shown systemic toxicity during clinical testing, the first clinical trial of GET with a plasmid encoding IL-12 in 2008 proved this method is safe and controlled. Studies using IL-2 or IL-12 have demonstrated antitumor effectiveness on distant untreated tumors and long-term anti-tumor memory [40].

Combining ECT (electrochemotherapy) with immunostimulatory EGT offers a promising strategy to enhance local antitumor response and induce an abscopal effect. Recent studies [36] have focused on combining BLM-ECT with peritumorally administered IL-12 GET. A study on three murine tumor models showed that IL-12 GET enhances the antitumor effect of ECT in poorly immunogenic B16F10 melanoma, while ECT alone is more effective in achieving an abscopal effect and long-term immunity in more immunogenic 4 T1 and CT26 tumors[41].

Investigating the immune response associated with ECT and immunomodulatory GET should include examining regulatory T cells (Tregs). In the tumor environment, Treg-induced immune suppression significantly hinders anticancer responses targeted by immunotherapeutic strategies[39] . Recent findings suggest that combining Treg depletion with immunotherapy based GET in the B16F10 melanoma model could reduce systemic metastasis and improve survival rates[41].

Short interfering RNA (siRNA) is also being explored as a viable oncological treatment. For example, siRNA targeting VEGF, an angiogenic factor, has been used to suppress tumor growth[42]. Similarly, siRNA targeting cyclin B1 has shown promising effects in inhibiting tumor cell proliferation and could be clinically validated in combination with other strategies, such as T cell targeting and downregulation of PD-1 or CTLA-4 [43].

ECT and calcium electroporation

Calcium electroporation (Ca EP) is a safe, cost-effective cancer treatment that introduces high calcium concentrations into cells via electroporation, causing ATP depletion and cancer cell death. A randomized double-blind phase II study showed its safety and efficacy in treating cutaneous metastases and recurrent head and neck cancer[44]. The efficacy is comparable to BLM-ECT for small tumor metastases, with 84% objective response for BLM-ECT and 72% for Ca EP, with no statistical difference at a one-year follow-up. Further clinical trials are needed to validate these findings[7].

Although primarily a local therapy, calcium electroporation (Ca-EP) has been shown to trigger a systemic immune response. In vivo studies revealed that Ca-EP treatment of colon cancer tumors in immunocompetent mice led to a complete response and long-lasting anti-tumor effects, while immunocompromised mice did not exhibit the same response. Additionally, in vivo Ca-EP increased the systemic release of pro-inflammatory cytokines, and in vitro Ca-EP elevated the release of High Mobility Group Box 1 protein (HMGB1), an important DAMP associated with immunogenic cell death (ICD)[45].

These findings indicate that Ca-EP can activate immune stimulators and induce a systemic immune response. Another in vivo study showed that combining calcium with irreversible electroporation (which permanently permeabilizes cell membranes with high-intensity electric fields) resulted in more T-cells and fewer suppressor cells[46]. Furthermore, a case report documented a systemic response following treatment with BLM-ECT and Ca-EP in a patient with disseminated malignant melanoma[47].

These studies suggest that Ca-EP can induce a systemic immune response, either alone or in

combination with ECT. However, further research is necessary to understand the mechanisms of immune activation and to explore the potential of Ca-EP and immunotherapy combinations.

Conclusions

The immune system plays a crucial role in cancer progression and treatment response, making therapies that activate the immune response a promising approach in oncology. EP-based therapies have gained attention in recent years due to their high efficacy rates and lack of severe side effects, showing local immune activation and markers of systemic response. However, there is no consensus on the abscopal effect of immune activation from ECT.

Various immunotherapies have been recognized as effective treatments for many solid tumors, including melanoma. Both immunotherapy and ECT have achieved efficacy levels that warrant their inclusion in the standardized anti-tumor treatment panel. Consequently, combining immunotherapy with ECT requires more attention to further improve patient clinical response, quality of life, long-term local and systemic remission, and life expectancy.

The combination of ECT with gene electrotransfer (GET) of immunomodulatory molecules is currently under study and showing encouraging results. Promising in vitro, in vivo, and clinical case reports indicate the potential of calcium electroporation (Ca-EP) to stimulate the release of specific molecules that trigger immunogenic cell death (ICD).

Despite these advances, the complex mechanisms behind the systemic immune response implications in ECT and Ca-EP are not yet fully understood, necessitating further research to determine their long-term impact on patient clinical outcomes.

Bibliography

1. Gehl, J., et al., Updated standard operating procedures for electrochemotherapy of cutaneous tumours and skin metastases. Acta Oncol, 2018. **57**(7): p. 874-882.
2. NICE, Interventional procedure guidance on electrochemotherapy for metastases in the skin from tumours of nonskin origin and melanoma. National Institute for Health and Care Excellence, 2013.
3. Kunte, C., et al., Electrochemotherapy in the treatment of metastatic malignant melanoma: a prospective cohort study by InspECT. Br J Dermatol, 2017. **176**(6): p. 1475-1485.
4. Larkin, J., et al., *Five-Year Survival with Combined Nivolumab and Ipilimumab in Advanced Melanoma.* New England Journal of Medicine, 2019. **381**(16): p. 1535-1546.
5. Justesen, T.F., et al., Electroporation and Immunotherapy-Unleashing the Abscopal Effect. Cancers (Basel), 2022. **14**(12).
6. Kamensek, U., S. Kos, and G. Sersa, *Adjuvant Immunotherapy as a Tool to Boost Effectiveness of Electrochemotherapy*, in *Handbook of Electroporation*, D. Miklavcic, Editor. 2016, Springer International Publishing: Cham. p. 1-16.
7. Cucu, C.I., et al., Electrochemotherapy and Other Clinical Applications of Electroporation for the Targeted Therapy of Metastatic Melanoma. Materials, 2021. **14**(14).
8. Sersa, G., et al., *Electrochemotherapy in treatment of tumours.* Eur J Surg Oncol, 2008. **34**(2): p. 232-40.
9. Tafuto, S., et al., Electrochemotherapy as a new approach on pancreatic cancer and on liver metastases. Int J Surg, 2015. **21 Suppl 1**: p. S78-82.
10. Bertacchini, C., *Cliniporator: Medical Electroporation of Tumors*, in *Handbook of Electroporation*, D. Miklavcic, Editor. 2017, Springer International Publishing: Cham. p. 1-36.
11. Brizio, M., et al., International Network for Sharing Practices on Electrochemotherapy (InspECT): An Integrative Patients Treatment Consortium, in Handbook of Electroporation, D. Miklavcic, Editor. 2017, Springer International Publishing: Cham. p. 1-18.
12. Frandsen, S.K., et al., Difference in Membrane Repair Capacity Between Cancer Cell Lines and a Normal Cell Line. J Membr Biol, 2016. **249**(4): p. 569-76.
13. Falk, H., et al., Calcium electroporation for treatment of cutaneous metastases; a randomized double-blinded phase II study, comparing the effect of calcium electroporation with electrochemotherapy. Acta Oncol, 2018. **57**(3): p. 311-319.
14. Mir, L.M. and S. Orlowski, *Mechanisms of electrochemotherapy.* Adv Drug Deliv Rev, 1999. **35**(1): p. 107-118.
15. Kroemer, G., et al., *Immunogenic cell death in cancer therapy.* Annu Rev Immunol, 2013. **31**: p. 51-72.

16. O'Brien, M.A., et al., Local tumour ablative therapies: opportunities for maximising immune engagement and activation. Biochim Biophys Acta, 2014. **1846**(2): p. 510-23.
17. Calvet, C.Y. and L.M. Mir, *The promising alliance of anti-cancer electrochemotherapy with immunotherapy.* Cancer Metastasis Rev, 2016. **35**(2): p. 165-77.
18. Liu, J., et al., Recruitment of antigen-presenting cells to the site of inoculation and augmentation of human immunodeficiency virus type 1 DNA vaccine immunogenicity by in vivo electroporation. J Virol, 2008. **82**(11): p. 5643-9.
19. Brock, R.M., et al., Starting a Fire Without Flame: The Induction of Cell Death and Inflammation in Electroporation-Based Tumor Ablation Strategies. Frontiers in Oncology, 2020. **10**(1235).
20. Troitskaya, O.S., et al., *Immunogenic Cell Death in Cancer Therapy.* Acta Naturae, 2022. **14**(1): p. 40-53.
21. Krysko, D.V., et al., *Immunogenic cell death and DAMPs in cancer therapy.* Nat Rev Cancer, 2012. **12**(12): p. 860-75.
22. Rufo, N., A.D. Garg, and P. Agostinis, *The Unfolded Protein Response in Immunogenic Cell Death and Cancer Immunotherapy.* Trends Cancer, 2017. **3**(9): p. 643-658.
23. Ahmed, A. and S.W.G. Tait, *Targeting immunogenic cell death in cancer.* Mol Oncol, 2020. **14**(12): p. 2994-3006.
24. Gerlini, G., P. Di Gennaro, and L. Borgognoni, Enhancing anti-melanoma immunity by electrochemotherapy and in vivo dendritic-cell activation. Oncoimmunology, 2012. **1**(9): p. 1655-1657.
25. Keisari, Y., Tumor abolition and antitumor immunostimulation by physico-chemical tumor ablation. Frontiers in Bioscience,, 2017. **Landmark**(22): p. 310-347.
26. Terenzi, A., et al., *Anticancer metal drugs and immunogenic cell death.* J Inorg Biochem, 2016. **165**: p. 71-79.
27. Lampreht Tratar, U., et al., Gene Electrotransfer of Plasmid-Encoding IL-12 Recruits the M1 Macrophages and Antigen-Presenting Cells Inducing the Eradication of Aggressive B16F10 Murine Melanoma. Mediators Inflamm, 2017. **2017**: p. 5285890.
28. Becker, J.C., et al., *Immune-suppressive properties of the tumor microenvironment.* Cancer Immunol Immunother, 2013. **62**(7): p. 1137-48.
29. Longo, F., et al., Boosting the Immune Response with the Combination of Electrochemotherapy and Immunotherapy: A New Weapon for Squamous Cell Carcinoma of the Head and Neck? Cancers (Basel), 2020. **12**(10).
30. Spain, L., J. Larkin, and S. Turajlic, *New survival standards for advanced melanoma.* Br J Cancer, 2020. **122**(9): p. 1275-1276.
31. Karaca, B., et al., Electrochemotherapy with anti-PD-1 treatment induced durable complete response in heavily pretreated metastatic melanoma patient. Anticancer Drugs, 2018. **29**(2): p. 190-196.
32. Mozzillo, N., et al., Assessing a novel immuno-oncology-based combination therapy: Ipilimumab plus electrochemotherapy. Oncoimmunology, 2015. **4**(6): p. e1008842.
33. Heppt, M.V., et al., Immune checkpoint blockade with concurrent electrochemotherapy in advanced melanoma: a retrospective multicenter analysis. Cancer Immunol Immunother, 2016. **65**(8): p. 951-9.
34. MD, P.F.F., ECT-Pembrolizumab in Patients With Unresectable Melanoma With Superficial or Superficial and Visceral Metastases. [Internet]. [cited 2024 March 16th].
35. Mir, L.M., Nucleic acids electrotransfer-based gene therapy (electrogenetherapy): past, current, and future. Mol Biotechnol, 2009. **43**(2): p. 167-76.
36. Ursic, K., et al., Potentiation of electrochemotherapy effectiveness by immunostimulation with IL-12 gene electrotransfer in mice is dependent on tumor immune status. J Control Release, 2021. **332**: p. 623-635.
37. Cemazar, M. and G. Sersa, *Electrotransfer of therapeutic molecules into tissues.* Curr Opin Mol Ther, 2007. **9**(6): p. 554-62.
38. Dean, D.A., Cell-specific targeting strategies for electroporation-mediated gene delivery in cells and animals. J Membr Biol, 2013. **246**(10): p. 737-44.
39. Whelan, M.C., et al., Effective immunotherapy of weakly immunogenic solid tumours using a combined immunogene therapy and regulatory T-cell inactivation. Cancer Gene Therapy, 2010. **17**(7): p. 501-511.
40. Sersa, G., et al., Electrochemotherapy of tumors as in situ vaccination boosted by immunogene electrotransfer. Cancer Immunol Immunother, 2015. **64**(10): p. 1315-27.
41. Forde, P.F., et al., Enhancement of electroporation facilitated immunogene therapy via T-reg depletion. Cancer Gene Ther, 2014. **21**(8): p. 349-54.
42. Takei, Y., *Electroporation-mediated siRNA delivery into tumors.* Methods Mol Biol, 2014. **1121**: p. 131-8.
43. Paganin-Gioanni, A., et al., Cyclin B1 knockdown mediated by clinically approved pulsed electric fields siRNA delivery induces tumor regression in murine melanoma. Int J Pharm, 2020. **573**: p. 118732.
44. Frandsen, S.K., M. Vissing, and J. Gehl, A Comprehensive Review of Calcium Electroporation—A Novel Cancer Treatment Modality. Cancers, 2020. **12**(2): p. 290.
45. Falk, H., et al., Calcium electroporation induces tumor eradication, long-lasting immunity and cytokine responses in the CT26 colon cancer mouse model. Oncoimmunology, 2017. **6**(5): p. e1301332.

46. Novickij, V., et al., Antitumor Response and Immunomodulatory Effects of Sub-Microsecond Irreversible Electroporation and Its Combination with Calcium Electroporation. Cancers (Basel), 2019. **11**(11).
47. Falk, H., et al., Electrochemotherapy and calcium electroporation inducing a systemic immune response with local and distant remission of tumors in a patient with malignant melanoma - a case report. Acta Oncol, 2017. **56**(8): p. 1126-1131.

RĂSPUNSUL IMUN ÎN ELECTROCHIMIOTERAPIE. SCURTĂ SINTEZĂ

REZUMAT
Electrochimioterapia (ECT) a fost stabilită din 2018 ca unul din tratamentele principale împotriva cancerului. ECT se bazează pe electroporarea reversibilă a membranelor celulare și administrarea concomitentă de chimioterapie în doze mici pentru a viza atât tipurile de tumori cutanate, cât și cele subcutanate. Protocoalele standardizate, inclusiv ghidurile revizuite ESOPE (2018) și NICE (2014), susțin electrochimioterapia (ECT), care este astfel practicată în peste 150 de centre medicale din întreaga Europă. Studiul Insp-ECT (International Network for Sharing Practices on Electrochemotherapy) a raportat o rată medie de răspuns obiectiv de 80% pentru mai multe tipuri de tumori cutanate după tratamentul ECT. Apariția inhibitorilor de puncte de control în imunoterapie, cum ar fi moleculele PD-L1, a evidențiat rolul sistemului imunitar în combaterea malignității. S-a dezvoltat aşadar interesul acordat contribuției sistemului imunitar la eficacitatea ECT, inclusiv impactul acesteia asupra tumorilor îndepărtate netratate. Unele studii atribuie lipsa recurenței locale după ECT mecanismelor imunologice care implică participarea moleculelor DAMPs precum calreticulina și HMGB1, în timp ce altele susțin că acest răspuns este insuficient pentru un efect abscopal sistemic. Cercetările în curs explorează combinarea ECT cu imuno-stimulante (inclusiv electro-transferul genelor al moleculelor imune) pentru a îmbunătăţi rezultatele terapeutice. Această sinteză rezumă rapoartele privind rolul răspunsului imun în eficacitatea clinică a ECT și combinațiile recente între electrochimioterapie / imunoterapie.
Cuvinte cheie: electrochimioterapie, efect abscopal, transfer electro-genic, electroporare

EEG REACTIVITY TO EXTERNAL STIMULI IN THE IMPAIRED CONSCIOUSNESS STATES

Alexandru-Cătălin Pâslaru[1], Vlad-Petru Morozan[1], Andrei Bordeianu[1], Alexandra Mocanu[1], Mihai Stancu[1,2], Ana-Maria Zăgrean[1], Mihai Moldovan[1,3,4,5], Leon Zăgrean[1]

[1]Carol Davila University of Medicine and Pharmacy, Division of Physiology - Neuroscience, Department of Functional Sciences, Bucharest, Romania
[2]Ludwig-Maximilian University, Neurobiology, Munich, Germany
[3]University of Copenhagen, Neuroscience, Copenhagen, Denmark
[4]Rigshospitalet, Department of Neurology, Copenhagen, Denmark
[5]Rigshospitalet, Department of Clinical Neurophysiology, Copenhagen, Denmark

ABSTRACT
Electroencephalography (EEG) is an important functional assessment tool for patients with an impaired state of consciousness. Besides brain imaging, EEG brings useful information and is easier to be applied at the bedside. Sensorial stimulation of patients determines EEG changes referred to as reactivity. Visual, auditory, or somatosensory stimuli, can be used in medical practice or research to measure EEG reactivity. Reactivity might be impaired in comatose patients, and quantifying the EEG reactivity can improve the prediction of comatose patients' outcomes. However, no consensus or guidelines presently exist regarding the methodology of EEG reactivity assessment.
Key words: EEG, reactivity, coma

The electroencephalography (EEG) has long been a cornerstone in the study of brain activity, offering key insights into the neural substrates underpinning various processes and brain oscillatory rhythms [1,2]. EEG is the simple and non-invasive process of recording the brain's electrical activity and plotting it in a bidimensional time-voltage space.

Over the past four decades, significant advances in EEG technology and analytical methods have expanded our understanding of how the brain analyses and responds to external stimuli [3]. Due to novel EEG processing and analysis methods, the technique has gained more and more popularity and utility both in the clinical setting and research. In the clinical setting, EEG analysis has become an important tool used to diagnose and monitor patients suffering from sleep disorders, epilepsy, brain injuries, and coma [4].

Coma, or an impaired state of consciousness, is clinically defined as the absence of clinically relevant responses to external stimulation. A patient's level of consciousness is usually assessed using clinical scales, such as the Glasgow Coma scale (GCS), FOUR score, and Coma Recovery Scale-Revised (CRS-R), together with brain imaging techniques such as fMRI (Functional magnetic resonance imaging), CT (Computed tomography) and EEG [5–7].

However, imaging techniques may prove impractical at the bedside and there is no consensus on standardised assessment [7]. An appealing emerging field is tied to the use of EEG reactivity as a prognostic tool for patients who suffer brain lesions that alter the state of consciousness, providing vital information that can guide clinical decision-making and patient care [8].

EEG reactivity is defined as the change in the background electrical activity of the brain in response to external stimuli such as auditive, visual, nociceptive or mixed [9,10]. These changes in baseline activity may be useful in assessing the state of consciousness and the prognosis in clinical settings [7]. Moreover, the baseline activity in itself can offer clues regarding the severity of the disorder of consciousness. Some patterns are associated with worse outcomes such as spike-and-wave complexes, burst-suppression patterns, or EEG flatline [11]. Physicians might use it together with other assessment tools in order to better understand the clinical status of the patient, for example, to differentiate between the outcome of two comatose patients [6].

There are, however, problems with using EEG reactivity as a measure, or predictor, of the comatose state in the clinical setting. Despite the versatility of EEG reactivity as a measure or predictor of comatose states, the method also poses some difficulties. First and foremost, raw visual EEG interpretation in the clinic remains subjective [12]. Second, even though quantitative methods for measuring EEG reactivity in comatose patients have been described [11,13,14], there is a lack of a standardised protocol for assessing EEG reactivity: multiple non-standardised stimulus modalities exist

and there is still no consensus on what a “sufficient” reactive EEG looks like. With the advance of machine learning and computing power, there are a plethora of methods to compute the EEG reactivity measure, although few have been validated or reached clinical practice. Guidelines for standardised recording and analysis of EEG are available and in continuous update by the European Academy of Neurology, American Clinical Neurophysiology Society, and International Federation of Clinical Neurophysiology [10,15–18].

Considering the fact that patients may have impaired consciousness due to the different types of brain lesions, it is intuitive why multiple sensory modalities must exist for assessing the EEG reactivity. It is therefore essential that the stimulus reaches the brain in order for the EEG to change in response to that stimulus. One of the first aspects that must be checked when assessing the EEG reactivity is the primary response to stimuli. This can be done by triggering evoked potentials, which informs on the capacity of the receptor to react to the stimulus, the integrity of the sensory pathways and the integrity of the primary sensory cortex [19,20].

We reviewed established stimulation protocols used in assessing the EEG reactivity, and their clinical usability from the perspective of our own work. Furthermore, we reviewed novel research trends using EEG reactivity to gain insights into the brain’s default mode network.

TYPES OF EXTERNAL STIMULI

Visual stimuli

Visual stimulation used in assessing the EEG reactivity in comatose patients involves passive eye opening, or intermittent photic stimulation (e.g. simple light flashing in the eye). Event-related potentials (ERPs) such as the P300 and N170 components can be used to check if the stimulus reached the cortex. Normal evoked potentials ensure the integrity of the retina, optic pathway and the primary visual cortex. These can further trigger the changes in EEG that can be seen as reactivity. Reactivity can be falsely lower if stimuli fail to reach the cortex [21,22].

Although visual pathways are more difficult to assess in comatose patients, as compared with the auditory or somaesthetic pathways, visual stimulation can be a relevant modality for measuring EEG reactivity in comatose patients [8]. For example in [13], the authors managed to successfully use intermittent photic stimulation to assess coma severity in a small group of 5 comatose children with acquired brain injury, while in [23], the authors used IPS (intermittent photic stimulation) to assess EEG reactivity in a study with 32 patients.

Auditory stimuli

Auditory stimuli usually involve actions such as clapping or calling the patient’s own name, and it is considered more effective than visual stimulation [24]. One advantage of auditory stimulation over visual stimulation can be that auditory stimuli are delivered correspondingly even if the patient has its eyes closed or is facing away from the sound source [25]. Paradoxically, whereas visual stimulation has been cited to be used on its own as a predictor for EEG reactivity, auditory stimulation seems to be mostly used in stimulation protocols that also include other types of sensory modalities such as nociceptive or tactile stimuli [8,26].

Multiple studies which used stimulation setups that included both auditory stimuli and other types of stimuli have shown a correlation between a nonreactive EEG measure with a poor outcome in patients with impaired consciousness [24,27–29], showing that auditory stimulation should be taken into account as a significant modality when considering a stimulation protocol.

A source of difficulty and lack of reproducibility can be due to the absence of a clinical standard, as shown by the fact that auditory stimulation can involve different, slightly complex mechanisms such as clapping or calling the patient’s own name [26], which can involve different hearing ranges and auditory patterns. As such, to assess the EEG reactivity in a more stable and reproducible way, the authors from [30] used a text-to-speech synthesiser to obtain an audio recording of the subject's own name and then reversed the same recording to obtain the audio wave of the name spelt in reverse. They used both recordings as an auditory-only stimulation protocol to obtain statistically relevant results of their EEG reactivity measure when compared to controls.

In order for the stimuli to reach the cortex, all the structures involved in stimulus transduction, conduction and processing should be within physiological working parameters. These structures include the inner ear, the auditory nerve and the auditory pathway including the bulbopontine junction, lateral

lemniscus, inferior colliculus, thalamus and up to the primary auditory cortex [31]. Moreover, one can assess the auditory cortical evoked potentials to check for stimulus processes at the primary auditory cortex: the P1 with a latency of 50ms, N1 latency of 100 ms and P2 with a latency of 180 ms[32]. Along with the cortical evoked potentials, there are also brainstem auditory evoked potentials [8].

Difficulties can still arise due to lesions in the auditory pathways or cortex, and/or inner ear problems either due to age or trauma. Another source of confusion, if the reactivity measurement is done in the ICU can be the noisy baseline environment [8]. In the ICU there are machines that track the heart rate and produce rhythmic beeps as well as ventilators, aspiration devices that can produce elevated background noise levels, thus disturbing the recording setup. As mentioned previously, no consensus is in place regarding what a reactive EEG actually looks like, the main findings in a reactive EEG being amplitude and frequency changes. Unfortunately, there are still a significant number of studies that provide no definition of what a reactive EEG means, as summarised by M.M. Admiraal et al [26].

Somatosensory stimuli, nociceptive and chemical stimuli

EEG reactivity was shown to respond to somatosensory stimulation in humans both during deep anaesthesia [33], as well as during a comatose state, as the EEG reactivity to somatosensory stimulation was shown to predict the outcome of patients who are in a coma after recovering from cardiac arrest or stroke [34].

The integrity of neural pathways is a sine qua non condition to test the reactivity to these stimuli. In the case of somatosensory stimulation, the integrity of both the somatosensory pathways and the somatosensory cortex is of utmost importance.

In the clinical setting, median nerve stimulation is used together with assessment of the somatosensory evoked potentials: N9, N13, P14, N20, and P25 [8]. No standard electrical stimulation protocol exists regarding amplitude, waveform and frequency.

The nociceptive modality was proved to be the most effective method to assess the EEG reactivity [24]. Nociceptive stimuli vary greatly from nipple pinching, periosteal rub, or compression of the fingernail bed [8].

Chemical stimuli could also be used to check EEG reactivity, as for example, olfactory stimuli produce changes in the EEG [35]. The setup might prove technically more complex, although the olfactory pathway has the advantage of having the fewest synapses until it reaches the cortex.

BURST-SUPPRESSION EEG REACTIVITY

Burst-suppression (BS) is an EEG pattern that is characterised by alternating periods of electrical activity with high amplitude (burst) and periods of low voltage electrical activity (suppression) [36]. This type of activity can occur physiologically during foetal life, during coma of different aetiologies or deep anaesthesia [37,38]. This pattern of activity can be seen as an on-off electrical activity so that an index can be derived, the burst-suppression ratio. BS ratio is defined as the time spent in suppression from the total interest trial time. BS ratio varies from 0 (continuous EEG) to 1 (isoelectric line). The BS pattern present on an EEG of a patient with acquired brain injury (irrespective of the aetiology), is usually considered a negative prognostic marker, which is obviously in the absence of any sedation drugs administered beforehand [39].

Physiological burst-suppression patterns can occur during progressive deepening of anaesthesia, where the EEG evolves from continuous to BS, with suppression periods getting longer and longer until an isoelectric line is seen. The isoelectric line does not necessarily involve no brain activity [40]. This phenomenon can be completely reversible [40].

There are studies that show that BS patterns change in response to external stimuli, and this change can be used to assess EEG reactivity. After stimulations, the number of bursts usually increases, and the time when the EEG is in suppression decreases. An index can be derived using the suppression ratio during the stimulus-free period and stimulus period, and changes of this index can be used to assess EEG reactivity [33,41]. While BSR depends on the recording setup, more precisely on the distance between electrodes [42], it can be used to predict the outcome of a patient in a comatose state [13].

CONTINUOUS EEG REACTIVITY IN COMATOSE PATIENTS

EEG reactivity was proposed as a marker for patient outcome also in continuous EEG recordings, improving patient prediction outcome after cardiac arrest [43,44]. An altered reactivity can be seen after a

cardiac arrest, while the reactivity can recover slower or faster depending on the use of hypothermia as neuroprotection [44,45] as the recovery was observed to be faster in hypothermic patients [44]. As described previously, there is still no consensus on what a reactive EEG actually looks like. Visually observable changes in amplitude or frequency, or even waveforms, can be used to classify an EEG as reactive, while some studies use standard terminology for EEG assessment [15].

It is considered that an increase in activity following stimulation is a predictor of a good outcome in regards to a patient's state, while a decrease in EEG activity is a predictor of a poor outcome [24], while the alpha and theta bands of the EEG signal have a more discriminative power.

DEFAULT MODE NETWORK AND EEG REACTIVITY

The human brain has an extensive network composed of different areas that were found to have a reduction in its activity while performing different tasks [46]. Functional magnetic resonance imaging and positron emission tomography mapped these areas and named the resting state of this network "A Default Mode of Brain Function" [47] or default mode network (DMN). Structurally the default mode network, as known at this time, is composed of three major structures, the dorsal medial prefrontal cortex, the ventral medial prefrontal cortex and the posterior cingulate cortex with the adjacent precuneus and the lateral parietal cortex, the area 39 (Brodmann area) [48]. The DMN is active during introspection, self-oriented thinking, perceptual decoupling, task-irrelevant thoughts, unconscious thought, or stimulus-independent thought [49], and it is deactivated during task-oriented activity [47,50]. Studies show deactivation of DMN, a phenomenon which can be called DMN reactivity, to both visual and auditory stimulation [51].

Functional MRI studies indicate that there is a positive link between cognitive performance and the functional interconnectivity of the DMN [52–55]. Alterations of DMN functionality are seen in neuro-psychiatric diseases like Alzheimer's disease, but to this time no biomarker that strongly correlates with Alzheimer's was observed [56]. A negative correlation can be seen in the functionality of DMN in schizophrenia [57]. Disruptions in DMN connectivity as seen for dementia can be also seen in autism spectrum disorder patients [58]. EEG assessment of DMN functionality shows a correlation between DMN connectivity and social anxiety disorder [59,60]. One study also revealed, using both fMRI and EEG analysis, that out of the major structural components of the DMN, only some correlate with alpha power - the medial prefrontal cortex and the posterior cingulate cortex[61].

A method of measuring the most reactive EEG macrostate to photic stimulation (the default EEG macrostate - DEM), considered the EEG activity of DEM, demonstrated the impairment of DMN in comatose patients after stroke [23].

CONCLUSIONS AND FURTHER DIRECTIONS

The EEG is a standard assessment method used in comatose patients [62,63]. EEG reactivity is more and more used either as a standalone method or more frequently in association with other clinical tools, as stated above, to evaluate the status and assess the outcome of these patients [34,64–66]. EEG reactivity study and assessment gains more and more popularity as can be seen in Figure 1. Somatosensory reactivity seems to be a good choice over the auditory reactivity assessment especially in those with low or impaired auditory reactivity [67]. Pain stimuli are frequently used in the clinical assessment of coma patients and this can also be easily integrated into EEG reactivity [68]. Although visual reactivity is not the first to be chosen in the clinical setting, different methods of assessing the EEG reactivity to visual stimuli emerged in both children and adults with an impaired state of consciousness [13,23,69]. Somatosensory evoked potentials and EEG reactivity are good predictors of patient outcome, and combining them with other modalities such as motor response, GCS, or neuroimaging techniques, can increase the prediction accuracy [70–72].

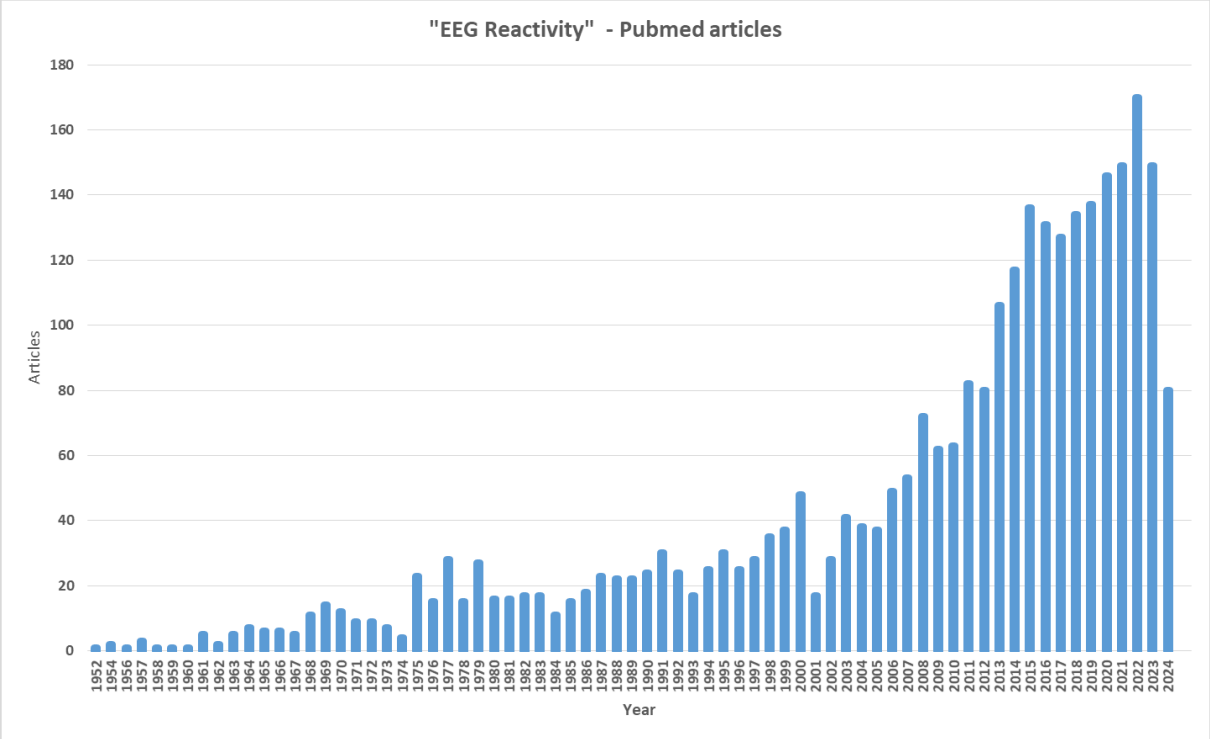

Fig 1. A total number of 2,604 articles were found in PubMed, from 1952 to July 2024 that contain "EEG reactivity"

There is high variety in how EEG reactivity data is acquired, tested, analysed, and interpreted, as we have shown that multiple simulation protocols exist, and multiple EEG reactivity measures have been developed [10]. At this time, to the best of our knowledge, a consensus for standardised practice for EEG reactivity in clinical practice has not been reached [67]. Although multiple studies indicate the effectiveness of EEG reactivity assessment in patient prognostic and the use of EEG reactivity as a prognostic marker, more profound and unified research is needed to understand the basis of reactivity and to define better protocols that can be used in clinical practice for the prognostication of patients [10,39,73].

Bibliography

1. Steriade, M. Grouping of Brain Rhythms in Corticothalamic Systems. *Neuroscience* 2006, *137*, 1087–1106.
2. Chaddad, A.; Wu, Y.; Kateb, R.; Bouridane, A. Electroencephalography Signal Processing: A Comprehensive Review and Analysis of Methods and Techniques. *Sensors* 2023, *23*, doi:10.3390/s23146434.
3. Zhang, H.; Zhou, Q.-Q.; Chen, H.; Hu, X.-Q.; Li, W.-G.; Bai, Y.; Han, J.-X.; Wang, Y.; Liang, Z.-H.; Chen, D.; et al. The Applied Principles of EEG Analysis Methods in Neuroscience and Clinical Neurology. *Mil Med Res*2023, *10*, 67.
4. Müller-Putz, G.R. Electroencephalography. *Handb. Clin. Neurol.*2020, *168*, 249–262.
5. Teasdale, G.; Maas, A.; Lecky, F.; Manley, G.; Stocchetti, N.; Murray, G. The Glasgow Coma Scale at 40 Years: Standing the Test of Time. *Lancet Neurol.*2014, *13*, 844–854.
6. Wang, J.; Huang, L.; Ma, X.; Zhao, C.; Liu, J.; Xu, D. Role of Quantitative EEG and EEG Reactivity in Traumatic Brain Injury. *Clin. EEG Neurosci.*2022, *53*, 452–459.
7. Kondziella, D.; Bender, A.; Diserens, K.; van Erp, W.; Estraneo, A.; Formisano, R.; Laureys, S.; Naccache, L.; Ozturk, S.; Rohaut, B.; et al. European Academy of Neurology Guideline on the Diagnosis of Coma and Other Disorders of Consciousness. *Eur. J. Neurol.*2020, *27*, 741–756.
8. Azabou, E.; Navarro, V.; Kubis, N.; Gavaret, M.; Heming, N.; Cariou, A.; Annane, D.; Lofaso, F.; Naccache, L.; Sharshar, T. Value and Mechanisms of EEG Reactivity in the Prognosis of Patients with Impaired

Consciousness: A Systematic Review. *Crit. Care*2018, *22*, 184.
9. Kang, X.-G.; Yang, F.; Li, W.; Ma, C.; Li, L.; Jiang, W. Predictive Value of EEG-Awakening for Behavioral Awakening from Coma. *Ann. Intensive Care*2015, *5*, 52.
10. Hwang, J.; Cho, S.-M.; Geocadin, R.; Ritzl, E.K. Methods of Evaluating EEG Reactivity in Adult Intensive Care Units: A Review. *J. Clin. Neurophysiol.*2022, 10.1097/WNP.0000000000001078.
11. Johnsen, B.; Jeppesen, J.; Duez, C.H.V. Common Patterns of EEG Reactivity in Post-Anoxic Coma Identified by Quantitative Analyses. *Clin. Neurophysiol.*2022, *142*, 143–153.
12. Foreman, B.; Claassen, J. Quantitative EEG for the Detection of Brain Ischemia. *Crit. Care*2012, *16*, 216.
13. Nita, D.A.; Moldovan, M.; Sharma, R.; Avramescu, S.; Otsubo, H.; Hahn, C.D. Burst-Suppression Is Reactive to Photic Stimulation in Comatose Children with Acquired Brain Injury. *Clin. Neurophysiol.*2016, *127*, 2921–2930.
14. Hermans, M.C.; Westover, M.B.; van Putten, M.J.A.M.; Hirsch, L.J.; Gaspard, N. Quantification of EEG Reactivity in Comatose Patients. *Clin. Neurophysiol.*2016, *127*, 571–580.
15. Sinha, S.R.; Sullivan, L.; Sabau, D.; San-Juan, D.; Dombrowski, K.E.; Halford, J.J.; Hani, A.J.; Drislane, F.W.; Stecker, M.M. American Clinical Neurophysiology Society Guideline 1: Minimum Technical Requirements for Performing Clinical Electroencephalography. *J. Clin. Neurophysiol.*2016, *33*, 303–307.
16. Rossetti, A.O.; Claassen, J.; Gaspard, N. Status Epilepticus in the ICU. *Intensive Care Med.*2024, *50*, 1–16.
17. Seeck, M.; Koessler, L.; Bast, T.; Leijten, F.; Michel, C.; Baumgartner, C.; He, B.; Beniczky, S. The Standardized EEG Electrode Array of the IFCN. *Clin. Neurophysiol.*2017, *128*, 2070–2077.
18. Nuwer, M.R.; Lehmann, D.; da Silva, F.L.; Matsuoka, S.; Sutherling, W.; Vibert, J.F. IFCN Guidelines for Topographic and Frequency Analysis of EEGs and EPs.The International Federation of Clinical Neurophysiology. *Electroencephalogr. Clin. Neurophysiol. Suppl.*1999, *52*, 15–20.
19. MacDonald, D.B.; Dong, C.C.; Uribe, A. Intraoperative Evoked Potential Techniques. *Handb. Clin. Neurol.*2022, *186*, 39–65.
20. Pruvost-Robieux, E.; Marchi, A.; Martinelli, I.; Bouchereau, E.; Gavaret, M. Evoked and Event-Related Potentials as Biomarkers of Consciousness State and Recovery. *J. Clin. Neurophysiol.*2022, *39*, 22–31.
21. Goto, Y.; Furuta, A.; Tobimatsu, S. Magnesium Deficiency Differentially Affects the Retina and Visual Cortex of Intact Rats. *J. Nutr.*2001, *131*, 2378–2381.
22. Ohlsson, M.; Westerlund, U.; Langmoen, I.A.; Svensson, M. Methylprednisolone Treatment Does Not Influence Axonal Regeneration or Degeneration Following Optic Nerve Injury in the Adult Rat. *J. Neuroophthalmol.*2004, *24*, 11–18.
23. Serban, C.-A.; Barborica, A.; Roceanu, A.-M.; Mindruta, I.; Ciurea, J.; Pâslaru, A.C.; Zăgrean, A.-M.; Zăgrean, L.; Moldovan, M. A Method to Assess the Default EEG Macrostate and Its Reactivity to Stimulation. *Clin. Neurophysiol.*2022, *134*, 50–64.
24. Johnsen, B.; Nøhr, K.B.; Duez, C.H.V.; Ebbesen, M.Q. The Nature of EEG Reactivity to Light, Sound, and Pain Stimulation in Neurosurgical Comatose Patients Evaluated by a Quantitative Method. *Clin. EEG Neurosci.*2017, *48*, 428–437.
25. Driver, J.; Spence, C. Attention and the Crossmodal Construction of Space. *Trends Cogn. Sci.*1998, *2*, 254–262.
26. Admiraal, M.M.; van Rootselaar, A.-F.; Horn, J. Electroencephalographic Reactivity Testing in Unconscious Patients: A Systematic Review of Methods and Definitions. *Eur. J. Neurol.*2017, *24*, 245–254.
27. Sivaraju, A.; Gilmore, E.J.; Wira, C.R.; Stevens, A.; Rampal, N.; Moeller, J.J.; Greer, D.M.; Hirsch, L.J.; Gaspard, N. Prognostication of Post-Cardiac Arrest Coma: Early Clinical and Electroencephalographic Predictors of Outcome. *Intensive Care Med.*2015, *41*, 1264–1272.
28. Duez, C.H.V.; Ebbesen, M.Q.; Benedek, K.; Fabricius, M.; Atkins, M.D.; Beniczky, S.; Kjaer, T.W.; Kirkegaard, H.; Johnsen, B. Large Inter-Rater Variability on EEG-Reactivity Is Improved by a Novel Quantitative Method. *Clin. Neurophysiol.*2018, *129*, 724–730.
29. Gilmore, E.J.; Gaspard, N.; Choi, H.A.; Cohen, E.; Burkart, K.M.; Chong, D.H.; Claassen, J.; Hirsch, L.J. Acute Brain Failure in Severe Sepsis: A Prospective Study in the Medical Intensive Care Unit Utilizing Continuous EEG Monitoring. *Intensive Care Med.*2015, *41*, 686–694.
30. Șerban, C.-A.; Barborică, A.; Roceanu, A.-M.; Mîndruță, I.-R.; Ciurea, J.; Stancu, M.; Pâslaru, A.C.; Zăgrean, A.-M.; Zăgrean, L.; Moldovan, M. Towards an Electroencephalographic Measure of Awareness Based on the

Reactivity of Oscillatory Macrostates to Hearing a Subject's Own Name. *Eur. J. Neurosci.*2024, *59*, 771–785.
31. Hashimoto, I. Auditory Evoked Potentials from the Human Midbrain: Slow Brain Stem Responses. *Electroencephalogr. Clin. Neurophysiol.*1982, *53*, 652–657.
32. Van Dun, B.; Kania, A.; Dillon, H. Cortical Auditory Evoked Potentials in (Un)Aided Normal-Hearing and Hearing-Impaired Adults. *Semin. Hear.*2016, *37*, 9–24.
33. Călin, A.; Kumaraswamy, V.M.; Braver, D.; Nair, D.G.; Moldovan, M.; Simon, M.V. Intraoperative Somatosensory Evoked Potential Monitoring Decreases EEG Burst Suppression Ratio during Deep General Anesthesia. *J. Clin. Neurophysiol.*2014, *31*, 133–137.
34. Liu, G.; Su, Y.; Liu, Y.; Jiang, M.; Zhang, Y.; Zhang, Y.; Gao, D. Predicting Outcome in Comatose Patients: The Role of EEG Reactivity to Quantifiable Electrical Stimuli. *Evid. Based. Complement. Alternat. Med.*2016, *2016*, 8273716.
35. Rikimaru, F.; Shiraishi, K.; Kato, T. Effect of Olfactory Stimulation on the EEG. *Nihon Bika Gakkai Kaishi (Japanese Journal of Rhinology)*2008, *47*, 8–15.
36. Swank, R.L.; Watson, C.W. Effects of Barbiturates and Ether on Spontaneous Electrical Activity of Dog Brain. *J. Neurophysiol.*1949, *12*, 137–160.
37. Amzica, F. Basic Physiology of Burst-Suppression. *Epilepsia*2009, *50 Suppl 12*, 38–39.
38. Pawar, N.; Barreto Chang, O.L. Burst Suppression During General Anesthesia and Postoperative Outcomes: Mini Review. *Front. Syst. Neurosci.*2021, *15*, 767489.
39. Azabou, E.; Fischer, C.; Guerit, J.M.; Annane, D.; Mauguiere, F.; Lofaso, F.; Sharshar, T. Neurophysiological Assessment of Brain Dysfunction in Critically Ill Patients: An Update. *Neurol. Sci.*2017, *38*, 715–726.
40. Kroeger, D.; Florea, B.; Amzica, F. Human Brain Activity Patterns beyond the Isoelectric Line of Extreme Deep Coma. *PLoS One*2013, *8*, e75257.
41. Hartikainen, K.; Rorarius, M.; Mäkelä, K.; Peräkylä, J.; Varila, E.; Jäntti, V. Visually Evoked Bursts during Isoflurane Anaesthesia. *Br. J. Anaesth.*1995, *74*, 681–685.
42. Moldovan, M.; Calin, A.; Kumaraswamy, V.M.; Braver, D.; Simon, M.V. Burst-Suppression Ratio on Electrocorticography Depends on Interelectrode Distance. *J. Clin. Neurophysiol.*2016, *33*, 127–132.
43. Admiraal, M.M.; Horn, J.; Hofmeijer, J.; Hoedemaekers, C.W.E.; van Kaam, C.R.; Keijzer, H.M.; van Putten, M.J.A.M.; Schultz, M.J.; van Rootselaar, A.-F. EEG Reactivity Testing for Prediction of Good Outcome in Patients after Cardiac Arrest. *Neurology*2020, *95*, e653–e661.
44. Zachariah, J.; Rabinstein, A.A. The Reemergence of EEG Reactivity After Cardiac Arrest. *Neurohospitalist*2017, *7*, 137–140.
45. Arrich, J.; Schütz, N.; Oppenauer, J.; Vendt, J.; Holzer, M.; Havel, C.; Herkner, H. Hypothermia for Neuroprotection in Adults after Cardiac Arrest. *Cochrane Database Syst. Rev.*2023, *5*, CD004128.
46. Shulman, G.L.; Fiez, J.A.; Corbetta, M.; Buckner, R.L.; Miezin, F.M.; Raichle, M.E.; Petersen, S.E. Common Blood Flow Changes across Visual Tasks: II. Decreases in Cerebral Cortex. *J. Cogn. Neurosci.*1997, *9*, 648–663.
47. Raichle, M.E.; MacLeod, A.M.; Snyder, A.Z.; Powers, W.J.; Gusnard, D.A.; Shulman, G.L. A Default Mode of Brain Function. *Proc. Natl. Acad. Sci. U. S. A.*2001, *98*, 676–682.
48. Raichle, M.E. The Brain's Default Mode Network. *Annu. Rev. Neurosci.*2015, *38*, 433–447.
49. Greicius, M.D.; Krasnow, B.; Reiss, A.L.; Menon, V. Functional Connectivity in the Resting Brain: A Network Analysis of the Default Mode Hypothesis. *Proc. Natl. Acad. Sci. U. S. A.*2003, *100*, 253–258.
50. Menon, V. 20 Years of the Default Mode Network: A Review and Synthesis. *Neuron*2023, *111*, 2469–2487.
51. Greicius, M.D.; Menon, V. Default-Mode Activity during a Passive Sensory Task: Uncoupled from Deactivation but Impacting Activation. *J. Cogn. Neurosci.*2004, *16*, 1484–1492.
52. Buckner, R.L.; Andrews-Hanna, J.R.; Schacter, D.L. The Brain's Default Network: Anatomy, Function, and Relevance to Disease. *Ann. N. Y. Acad. Sci.*2008, *1124*, 1–38.
53. Sormaz, M.; Murphy, C.; Wang, H.-T.; Hymers, M.; Karapanagiotidis, T.; Poerio, G.; Margulies, D.S.; Jefferies, E.; Smallwood, J. Default Mode Network Can Support the Level of Detail in Experience during Active Task States. *Proc. Natl. Acad. Sci. U. S. A.*2018, *115*, 9318–9323.
54. Persson, J.; Pudas, S.; Nilsson, L.-G.; Nyberg, L. Longitudinal Assessment of Default-Mode Brain Function in Aging. *Neurobiol. Aging*2014, *35*, 2107–2117.

55. Prakash, R.S.; Heo, S.; Voss, M.W.; Patterson, B.; Kramer, A.F. Age-Related Differences in Cortical Recruitment and Suppression: Implications for Cognitive Performance. *Behav. Brain Res.*2012, *230*, 192–200.
56. Eyler, L.T.; Elman, J.A.; Hatton, S.N.; Gough, S.; Mischel, A.K.; Hagler, D.J.; Franz, C.E.; Docherty, A.; Fennema-Notestine, C.; Gillespie, N.; et al. Resting State Abnormalities of the Default Mode Network in Mild Cognitive Impairment: A Systematic Review and Meta-Analysis. *J. Alzheimers. Dis.*2019, *70*, 107–120.
57. Hu, M.-L.; Zong, X.-F.; Mann, J.J.; Zheng, J.-J.; Liao, Y.-H.; Li, Z.-C.; He, Y.; Chen, X.-G.; Tang, J.-S. A Review of the Functional and Anatomical Default Mode Network in Schizophrenia. *Neurosci. Bull.*2017, *33*, 73–84.
58. Nair, A.; Jolliffe, M.; Lograsso, Y.S.S.; Bearden, C.E. A Review of Default Mode Network Connectivity and Its Association With Social Cognition in Adolescents With Autism Spectrum Disorder and Early-Onset Psychosis. *Front. Psychiatry*2020, *11*, 614.
59. Al-Ezzi, A.; Kamel, N.; Faye, I.; Gunaseli, E. Analysis of Default Mode Network in Social Anxiety Disorder: EEG Resting-State Effective Connectivity Study. *Sensors* 2021, *21*, doi:10.3390/s21124098.
60. Imperatori, C.; Farina, B.; Adenzato, M.; Valenti, E.M.; Murgia, C.; Marca, G.D.; Brunetti, R.; Fontana, E.; Ardito, R.B. Default Mode Network Alterations in Individuals with High-Trait-Anxiety: An EEG Functional Connectivity Study. *J. Affect. Disord.*2019, *246*, 611–618.
61. Bowman, A.D.; Griffis, J.C.; Visscher, K.M.; Dobbins, A.C.; Gawne, T.J.; DiFrancesco, M.W.; Szaflarski, J.P. Relationship Between Alpha Rhythm and the Default Mode Network: An EEG-FMRI Study. *J. Clin. Neurophysiol.*2017, *34*, 527–533.
62. Friedman, D.; Claassen, J.; Hirsch, L.J. Continuous Electroencephalogram Monitoring in the Intensive Care Unit. *Anesth. Analg.*2009, *109*, 506–523.
63. Vincent, J.-L. *Annual Update in Intensive Care and Emergency Medicine 2020*; Springer Nature, 2020; ISBN 9783030373238.
64. Thenayan, E.A.L.; Savard, M.; Sharpe, M.D.; Norton, L.; Young, B. Electroencephalogram for Prognosis after Cardiac Arrest. *J. Crit. Care*2010, *25*, 300–304.
65. Krainik, A.; Hund-Georgiadis, M.; Zysset, S.; von Cramon, D.Y. Regional Impairment of Cerebrovascular Reactivity and BOLD Signal in Adults after Stroke. *Stroke*2005, *36*, 1146–1152.
66. Logi, F.; Pasqualetti, P.; Tomaiuolo, F. Predict Recovery of Consciousness in Post-Acute Severe Brain Injury: The Role of EEG Reactivity. *Brain Inj.*2011, *25*, 972–979.
67. Tsetsou, S.; Novy, J.; Oddo, M.; Rossetti, A.O. EEG Reactivity to Pain in Comatose Patients: Importance of the Stimulus Type. *Resuscitation*2015, *97*, 34–37.
68. Wijdicks, E.F.M.; Bamlet, W.R.; Maramattom, B.V.; Manno, E.M.; McClelland, R.L. Validation of a New Coma Scale: The FOUR Score. *Ann. Neurol.*2005, *58*, 585–593.
69. Calin, A.; Kumaraswamy, V.M.; Braver, D.; Nair, D.G.; Moldovan, M.; Simon, M.V. Intraoperative Somatosensory Evoked Potential Monitoring Decreases EEG Burst Suppression Ratio During Deep General Anesthesia (Vol 31, Pg 133, 2014). *J. Clin. Neurophysiol.*2018, *35*, E7.
70. Carter, B.G.; Butt, W. Are Somatosensory Evoked Potentials the Best Predictor of Outcome after Severe Brain Injury? A Systematic Review. *Intensive Care Med.*2005, *31*, 765–775.
71. Dubowitz, D.J.; Bluml, S.; Arcinue, E.; Dietrich, R.B. MR of Hypoxic Encephalopathy in Children after near Drowning: Correlation with Quantitative Proton MR Spectroscopy and Clinical Outcome. *AJNR Am. J. Neuroradiol.*1998, *19*, 1617–1627.
72. Oddo, M.; Rossetti, A.O. Predicting Neurological Outcome after Cardiac Arrest. *Curr. Opin. Crit. Care*2011, *17*, 254–259.
73. Guérit, J.-M.; Amantini, A.; Amodio, P.; Andersen, K.V.; Butler, S.; de Weerd, A.; Facco, E.; Fischer, C.; Hantson, P.; Jäntti, V.; et al. Consensus on the Use of Neurophysiological Tests in the Intensive Care Unit (ICU): Electroencephalogram (EEG), Evoked Potentials (EP), and Electroneuromyography (ENMG). *Neurophysiologie Clinique/Clinical Neurophysiology*2009, *39*, 71–83.

Reactivitatea EEG la stimuli externi în stări de conștiență alterată

REZUMAT
Electroencefalograma (EEG) este o metodă funcțională important pentru monitorizarea pacienților a căror stare de conștiență este alterată. Alături de imagistica cerebrală, EEG adduce informații importante, fiind o metodă mai ușor de utilizat la patul pacientului. Stimularea senzorială a pacienților determină schimbări ale EEG cunoscute ca reactivitate. Stimulii vizuali, auditivi sau somatosenzoriali pot fi folosiți în clinică sau în cercetare pentru a măsura reactivitatea EEG. Reactivitatea EEG poate fi modificată la pacienții comatoși, iar cuantificarea acesteia poate oferi un prognostic mai bun la acești pacienți. La momentul actual, nu există un consens sau ghiduri în ceea ce privește metodele de evaluare a reactivității EEG.
Cuvinte cheie: EEG, reactivitate, comă